AD-A051 245 FRAUNHOFER-GESELLSCHAFT GARMISCH- PARTENKIRCHEN (WES--ETC F/G 4/1
ANALYSIS OF AEROSOL TRANSPORT AEROSOL REMOTE SENSING BY LIDAR.(U)
SEP 77 R REITER, W CARNUTH, M LITTFASS DA-ERO-75-G-077

UNCLASSIFIED NL

1 OF 2
AD
A051245

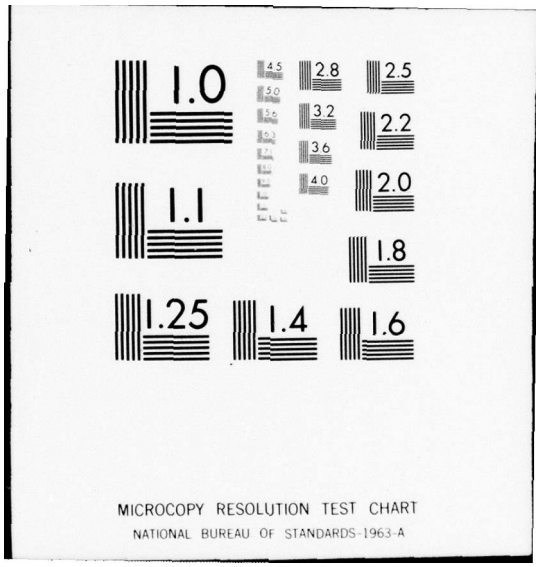
1.0
1.1
1.25
1.4
1.6
1.8
2.0
2.2
2.5
2.8
3.2
3.6
4.0
4.5
5.0
MICROCOPY RESOLUTION TEST CHART
NATIONAL BUREAU OF STANDARDS-1963-A

AD _____

ANALYSIS OF AEROSOL TRANSPORT
AEROSOL REMOTE SENSING BY LIDAR

FINAL REPORT

BY

Reinhold Reiter

Walter Carnuth

Michael Littfaß

and

Horst Jaeger

September 1977

EUROPEAN RESEARCH OFFICE
United States Army
London England

Grant Agreement No. DA-ERO-75-G-077

Institut für Atmosphärische Umweltforschung
der Fraunhofer-Gesellschaft

D-8100 Garmisch-Partenkirchen, Germany
Kreuzeckbahnstraße 19

UNCLASSIFIED

SECURITY CLASSIFICATION OF THIS PAGE (When Data Entered)

REPORT DOCUMENTATION PAGE	READ INSTRUCTIONS BEFORE COMPLETING FORM
1. REPORT NUMBER	2. GOVT ACCESSION NO. / 3. RECIPIENT'S CATALOG NUMBER
4. TITLE (and Subtitle): Analysis of Aerosol Transport Aerosol Remote Sensing by Lidar,	5. TYPE OF REPORT & PERIOD COVERED: FINAL TECHNICAL REPORT, JAN 77 - SEP 77
	6. PERFORMING ORG. REPORT NUMBER: -
7. AUTHOR(s): Reinhold/Reiter, Horst/Jaeger, Walter/Carnuth, Michael/Littfass	8. CONTRACT OR GRANT NUMBER(s): DAERO-75-G-077
9. PERFORMING ORGANIZATION NAME AND ADDRESS: Institut fur Atmospharische Umweltforschung, Garmisch, Partenkirchen, Germany	10. PROGRAM ELEMENT, PROJECT, TASK AREA & WORK UNIT NUMBERS: 6.11.02A-1T161102B52B-00-441
11. CONTROLLING OFFICE NAME AND ADDRESS: USA R&S GP (EUR), Box 65, New York, NY 09510	12. REPORT DATE: SEP 1977 / 13. NUMBER OF PAGES: 97
14. MONITORING AGENCY NAME & ADDRESS (if different from Controlling Office)	15. SECURITY CLASS. (of this report): UNCLASSIFIED / 15a. DECLASSIFICATION/DOWNGRADING SCHEDULE

16. DISTRIBUTION STATEMENT (of this Report)

Approved for Public Release, Distribution Unlimited

17. DISTRIBUTION STATEMENT (of the abstract entered in Block 20, if different from Report)

18. SUPPLEMENTARY NOTES

19. KEY WORDS (Continue on reverse side if necessary and identify by block number)

TURBULENCE: ATMOSPHERIC AEROSOLS.

20. ABSTRACT (Continue on reverse side if necessary and identify by block number)

Final report concerns primarily techniques and instrumentation adaptation (incl calibration) and trial as these relate to analysis of aerosol transport and aerosol remote sensing by Lidar. Investigator concludes that the techniques and instruments which he has investigated operated successfully.

DD FORM 1 JAN 73 1473 EDITION OF 1 NOV 65 IS OBSOLETE

AD 392 977

UNCLASSIFIED

SECURITY CLASSIFICATION OF THIS PAGE (When Data Entered)

AD_____

ANALYSIS OF AEROSOL TRANSPORT
AEROSOL REMOTE SENSING BY LIDAR

FINAL REPORT

BY

Reinhold Reiter

Walter Carnuth

Michael Littfaß

and

Horst Jaeger

September 1977

EUROPEAN RESEARCH OFFICE

United States Army

London England

Grant Agreement No. DA-ERO-75-G-077

Institut für Atmosphärische Umweltforschung
der Fraunhofer-Gesellschaft

D-8100 Garmisch-Partenkirchen, Germany
Kreuzeckbahnstrasse 19

Table of contents

ABSTRACT

The activities in the reporting period focussed attention on the following topics:

1. Final technical setup of the stationary lidar system by improvement of the electronic data processing, full automation of the measuring run via a separate computer program for tropospheric and stratospheric backscatter measurements, improvement of the photon counting system.

2. Final mechanical and electronic setup of the mobile lidar system including test run of both laser systems, completion through some technical extensions as compared to the original layout (e.g. a heater for the cooling water needed for transport of the system in winter), preparatory works for the inclusion of the primary neodymium-glass laser wavelength (1060 nm).

3. Theoretical and practical works designed to derive lidar calibration constants for the stationary lidar. This includes a) calculation of Rayleigh backscatter from air density measured by radiosondes at very weak aerosol backscatter and b) in situ measurement of the given size distribution of the aerosol particles at our mountain stations during simultaneous lidar shots, and comparison with the measured aerosol backscatter intensity.

4. Numerous lidar measuring series for remote sensing of the time variation of aerosol concentration and size distribution demonstrating the practical application have been carried out in the troposphere in the course of the day.

5. Operation of the fully developed single photon counting system permitted the recording of numerous backscatter

profiles (on the average 2 - 3 per month) in the stratosphere up to 35 km. These measurements made it possible to trace changes in the aerosol layer in the lower stratosphere with consideration of time, height range, and intensity, and they seem to indicate a second aerosol layer in the middle stratosphere which remains to be verified.

The method used in measuring the stratospheric aerosol backscatter can be considered as satisfactory and fully developed.

Work remains to be done on the calibration of the lidar system since the hitherto existing data are not yet substantiated. Further technical and theoretical improvements turned out to be necessary. These calibration procedures are to be finalized before realistic routine remote measurements of the aerosol parameters in the troposphere can be started.

I. OBJECTIVES AND BACKGROUND

The background of the investigations to be discussed in the present report can be found in the preceding reports R. REITER et al.(1975) and R. REITER et al. (1976 a, b). Our present activities are a consequent continuation of the works described in said reports.

The goals aspired to achieve in the working year can briefly be outlined as follows:

1. Completion of the technical equipment of the stationary (double-frequency lidar) system and the on-line computer aimed at a fully-automatic performance of lidar shots and data acquisition concerning both tropospheric and stratospheric (photon counting) measurements. In this connection elaboration of the necessary computer programs.

2. Technical construction of the mobile lidar system (three-frequency lidar) to the most possible extent including installation of power supply, cooling aggregate, data acquisition in the truck, and final assembly of the optical system (tiltable transmitter and receiver) on the trailer; first measurements.

3. Determination of calibration constants of the lidar systems in such a manner that through measurements of aerosol backscatter intensity in more than one wavelength the aerosol particle concentration can be determined simultaneously in different orders of magnitude. For the calibration we use a) at very weak aerosol concentration the Rayleigh backscatter, the intensity of which can be calculated from atmospheric density directly measured by means of radiosondes, and b) an in-situ calibration is made of the aerosol backscatter by

measurement of the given aerosol size distribution and particle density at our measuring stations at different levels.

4. The aerosol backscatter intensity is also to be measured in the stratosphere by means of photon counting. As the same is very weak, the Rayleigh (molecular) backscatter must be exactly known. For this reason own rawinsondes are launched from which the actual atmospheric density data can be derived.

5. Finally, measurements as regularly as possible are to be performed also in the troposphere for studying the vertical and time variations of the aerosol concentration. For this purpose the calibrated lidar systems are to be employed. As far as the calibration procedures are not finished, such measurements will be replaced by the derivation and evaluation of relative backscatter profiles.

II. STATUS OF THE LIDAR TECHNIQUE AT THE INSTITUTE FOR ATMOSPHERIC ENVIRONMENTAL RESEARCH

1. The stationary system

1.1. Parts of the system which have not been changed since 1976

In the last annual report from July 1976 a complete and detailed description of the stationary lidar system has been given. The following parts of the system have not essentially been changed in the meantime:

- the Q-switched ruby laser transmitter with 694 nm wavelength, 100 MW peak output power and 1 Hz maximum pulse repitition frequency
- the power supply for the laser and the Q-switch
- the fluorescence suppression
- the frequency doubler for generating the second transmitter wavelength (347 nm)
- the two energy monitors with peak digitizer
- the fixed vertical Cassegrain receiving telescope with 52 cm diameter
- the EMI 9618 photomultiplier tube for the detection of the backscattered light (for medium-range, analog recordings only)
- the Biomation 8100 transient recorder
- the gain switching amplifier
- the photon counter with range gating
- the preamplifier
- the on-line computer with graphic display terminal and punch tape output.

These parts are described in the 1976 annual report, pp. 7 -

18, and in the diagrams Fig. III. 1 and 2. They are once more shown in the photographs Figs. II. 5 - II. 9 of this report.

1.2. Improvements and extensions of the stationary system since July 1976

During the last year a number of improvements and extensions to the lidar system hardware have been performed which partially have been announced in the previous report (parts VI and VII). The major part of the innovations concerns the improvement of the data acquisition and the automation of the system operation, a smaller part the transmitter-receiver system.

The block scheme Fig. II.1 presents the complete stationary lidar system in its present state. For the sake of clearness not all control lines are included in the figure; they are shown completely in Fig.II.2 which will be described below. The innovations will now be described in detail:

1.2.1. Special photomultiplier for photon counting

The EMI photomultiplier tube is not specially designed for photon counting purposes. The quite low secondary emission factor at the dynodes (2 - 5 , depending on the applied voltage) causes heavy statistical fluctuations of single photon peaks. The resulting broad pulse height distribution curve renders an exact discrimination between signal and noise pulses very difficult or impossible at all. So we found a slowly decreasing background superposed on the return signals, probably due to the strong close-range signal in spite of the range-gating of the tube, if the full sensitivity of the receiver, without any attenuation by the gray wedge, was used. This background could only be eliminated by reducing the received backscattered light by a factor of 10. Further-

more, the pulse frequency resolution of the EMI 9816 tube proved to be quite low, probably due to the high number of dynodes. For these reasons, the acquisition of a complete backscatter profile from 6 to 30 km altitude required the application of a great number of different gray wedge settings in order to get sufficient counting statistics on the one hand and avoid exessive pulse overlapping on the other.

For these reasons a RCA 8852 photomultiplier tube has been provided. This tube is equipped with a gallium phosphide coated first dynode, providing a secondary emission ratio of up to 50 at this dynode and consequently a greatly improved counting statistics. First measurements revealed the performance of this new tube to be surprisingly much better than the EMI tube. Together with a new, faster photon counter input comparator, the pulse frequency range was extended by a factor of no less than 10. Furthermore, even with full receiver sensitivity no superposed background at all is observed with the return signals. Consequently, the total number of laser shots required for the measurement of a complete backscatter profile with given accuracy is now considerably reduced.

Unfortunately, at least at the time of commission of the tube no version was available with sufficient sensitivity as well for 694 nm as for 347 nm wavelength. So for the analog measurements conducted in both frequencies the EMI tube is still to be used and is to be replaced by the RCA tube for stratospheric measurements performed with 694 nm wavelength only. In order to facilitate the change of the tubes, the heavy and unhandy photomultiplier cooling box, which proved to be unnecessary, was replaced by two separate smaller conventional housings for each tube with separate sockets and voltage divider networks allowing the change of the tubes within less than a minute. Examples of stratospheric measurements with the new tube are presented in part IV of this report.

1.2.2. Polarizer for measurement of signal depolarization

With the initial single-frequency version of the system a polarizer was available in front of the photodetector. The plane of polarization was changed by turning the whole detector housing. With the onset of the two-frequency operation the polarizer was removed temporarily because the polarization plane of the 347 nm laser beam is perpendicular to that of the 694 nm beam, and the change of the transmitter frequency would have required each time the time-consuming turning of the photomultiplier case by 90 degrees. However, as the measurement of the signal depolarization is desirable for several reasons, a motor-operated turnable mount for the polarizer was fixed to the receiver, which may be controlled from inside either manual or by the computer (see below).

1.2.3. Background stop tube for the receiver

The receiver sensitivity during daytime is limited, among other things, by the skylight background level. Initially skylight bypassing the telescope secondary mirror and entering directly the photomultiplier cathode contributed very essentially to the background level. For this reason a tube T was mounted at the center hole of the primary mirror (see Fig. II.1) which reduced the background by a factor of nearly five. This resulted in a marked improvement of accuracy especially of the weaker 347 nm signals.

1.2.4. Automatic temperature control for the laser

The laser is cooled by a closed water circuit which is recooled by tap water by means of a heat exchanger. The exact wavelength of the ruby laser depends somewhat on temperature. In order to avoid unintentional tuning of the laser to one of the near-by water vapor absorption lines, a magnetic valve operated by a contact thermometer was applied to the tap water line. This valve stops the tap water flow if the temper-

ature of the secondary circuit water drops below a preset value.

1.2.5. Floppy disc memory

In addition to the 16 K core memory a floppy disc memory is now available with the on-line computer. It consists of two separate units with 300 k capacity each and avoids the necessity of intermediate punch tape output of averaged signals during a series of measurements (e.g. between a 694 nm and a 347 nm measurement). Instead of that, any number of single signals may be stored on one or more floppy discs and output on punch tape later after finishing a complete series of measurements. This device is also very convenient for storage of programs. The usage is described more detailed in part II.1.3. of this report.

1.2.6. Neutral filter wheel

Previously the receiver sensitivity attenuation was accomplished by a continuous neutral or gray wedge, remotely operated by a magslip. Because it proved to be difficult setting the wedge to a certain attenuation value with sufficient reproducibility, it has been replaced by a motor-operated filter wheel with 3 discrete neutral filters and one empty hole (zero-attenuation position).

1.2.7. Devices for complete automatic operation of the system

The Biomation 8100 transient recorder is fully externally programmable. For utilization of this possibility a special computer interface has been available for more than a year. It has already been mentioned in the July 1976 annual report and is shown in Fig. III.1, denoted as "interface 2". However, the external programming of the transient recorder only seemed quite unsatisfactory, and so it was decided to develop additional electronic circuits allowing a complete

automatic, computer-controlled operation of the whole system. This should include the following single operations:

- programming of the transient recorder
- laser start
- change of transmitter wavelength
- change of interference filter
- change of neutral filter
- setting of photomultiplier high voltage
- setting of range gate length and delay
- triggering of the data acquisition electronics for the measurement of the skylight background
- change of the polarizer position.

The control electronics which has been developed here at the institute by our co-workers (see Fig. II.2) will now be described in detail, including a modified data transfer from transient recorder and photon counter, guided by Fig. II.2.

1.2.7.1. Input/output control facilities of the computer

For the exchange of data between computer and external devices two 32-bit input/output controllers are available. The input and output lines are divided into four groups or channels à 8 bit each, which are accessed by channel select function codes from the computer. During an output transfer, the 8-bit word from the computer is loaded into the input register of the selected channel, and an output data strobe pulse is issued to the device. During an input transfer, the 8 input lines from the selected channel are scanned by an input multiplexer and the resulting input word is supplied to the computer when "data in" occurs. Additonally an external interrupt line is available with each I/O controller.

1.2.7.2. Transient recorder programming and data transfer

All front panel controls of the Biomation 8100 transient recorder may be remotely controlled without regard to the phys-

ical position of the manual buttons and knobs. The digital control is effected via bit-parallel, word-serial data exchange. The control functions of the transient recorder are divided into several groups, such as arm or trigger control groups, to which the remote control can be applied separately. Thus any control group or combination of control groups may be under remote digital control, other groups may be released for manual front panel operation.

The remote control of the recorder requires 16-bit control words, which are supplied by interface No. 2 from the computer. By means of this interface the 16-bit word is generated from two 8-bit words issued sequentially from the computer to the interface. This is shown in Fig. II.2, where heavy lines indicate a set of more than one, usually 8 or 9, individual data lines.

The digital data stored in the transient recorder are output sequentially as 8-bit words. Previously, the data of both transient recorder and photon counter/peak digitizer had been transferred to the computer via interface No. 1, as described in detail in the July '76 annual report. With the computer a single channel, 8-bit interface was used for this purpose which otherwise is destined for punch tape input and output. As with the I/O controllers sufficient input channels are available, one channel of controller No. 1 is now used for the data transfer from transient recorder and photon counter. Data from photon counter/photodiode peak digitizer are still transferred via interface 1, the transient recorder data via the new interface 2. The usage of this interface offers several advantages. First, data recording may be done in the "off" mode of the recorder, allowing the examination of the data prior to the transfer to the computer. The data transfer is initiated by the computer by issuing a special instruction word to the recorder. Furthermore, for technical reasons the data transfer is much faster than with the former interface, which allows

the transfer routine for one data word to be executed by the computer within less than 100 microseconds. Consequently, as the recorder memory made up of MOS shift registers needs refreshing between output words at read rates slower than 100 microseconds per word, the time required for the transfer of the total memory contents is reduced from 2.5 to about .2 seconds.

The usage of only one input channel for transferring both the transient recorder and photon counter data is made possible by tri-state outputs in both interfaces. An internal electronic switch operated by a computer instruction, which is not included in Fig. II.2, prevents simultaneous output from both interfaces.

1.2.7.3. External range gate control

Previously the range gate length ("gate") and delay time ("delay") had been set manually by two 4-digit decimal switches each, in increments of .1684 microseconds. The 8 digits may now be set by the computer, where for saving of output channels multiplex operation is used. The most significant 4 bits of the 8-bit word output from the computer are used as digit address, the 4 least significant bits denote the "value" of the corresponding digit, BCD-coded. Manual control of the gate and delay is still possible. The change from manual to remote operation is accomplished either via the computer again or via an external switch, which is not included in the block scheme.

1.2.7.4. High voltage control

The output voltage of the Ortec photomultiplier high voltage supply may be controlled externally by applying a DC reference voltage between 0 and 9 Volts to a special connector. This voltage is generated by an analog multiplexer, which

acts like a manual step switch on a precise voltage divider chain. The analog multiplexer is controlled by the computer via the above-mentioned multiplexer. Only hundreds and thousands of volts can be set remotely, which has been decided to be sufficient. Manual remote control of the high voltage is possible, similarly as with the range gate control. Two digits of a four-digit decimal switch are used for this purpose (cf. the photograph Fig. II.9). Precautions are made to avoid the unintentional application of a too high voltage to the photomultiplier tube. If an attempt is made to set the voltage to a value above a limit voltage either manually or by the computer, the voltage is set to zero and an error message is issued to the computer via a combined error line. Error signals from other devices are also transferred through this line. The limit voltage may be changed by a computer-operated switch from 1300 Volts for analog measuring to 2000 Volts for photon counting. After any change of the HV a certain settling time, depending on the amount of the change, is required by the PMT to attain its nominal gain. In order to prevent measurements before the gain has stabilized an error signal is output for a time interval simulated by a R-C network.

1.2.7.5. Neutral filter wheel control

As mentioned above, the previously used continuous neutral wedge has been replaced by a filter wheel containing 3 neutral filters with 7.7, 1.5, and .3 % transmissivity, respectively, and one empty hole ("no attenuation" position of the wheel). The wheel is operated by a servo motor. The position of its axis is indicated by a potentiometer connected with it. By applying a logical "1" signal to one of the four input lines (denoted by 0...3 in Fig. II.2) of the control unit by the computer, the servo motor moves the wheel to the desired position. An error signal is output as long as the motor is moving. Manual operation is possible by means of a toggle switch with positions 0 - 3 and "ext". In the latter

position only remote control is possible.

1.2.7.6. Transmitter frequency and polarizer control

As the polarization planes of the 694 and 347 nm laser beams are perpendicular to each other, the 0^{o}-position of the polarizer for 694 nm is physically the same as the 90^{o}-position for 347 nm, with the angle denoting that between the planes of the polarizer and of the polarization of the incident light. As it was desired to maintain the position of the polarizer with respect to the polarization plane of the transmitted light when the transmitter wavelength is changed, a combined control unit has been developed. A wavelength change thus requires three single operations: Shifting of the frequency doubler into the laser beam path, changing the interference filter and changing the polarizer position. The frequency doubler servo motor has hitherto been operated by a two-position switch at the operating console; the end positions of the doubler carriage have been indicated by two lamps operated by micro switches. The control has now been removed from the console switch to a computer-operated relay in the control unit. When the carriage is moving, i.e. when none of the micro switches is closed, an error signal is output to the computer.

The interference filter wheel has formerly been moved by means of magslips. As the magnetic momentum goes to zero when the wheel approaches the desired position, the positioning is not precisely reproducible. (As mentioned above, the magslip drive for the neutral wedge had been replaced by a servo motor for the same reason). The magslip has been replaced, therefore, by a rotary magnet. This device is operated from the control unit.

The polarizer drive is quite similar to that of the frequency doubler carriage. It is moved by a DC servo motor, which is

stopped by microswitches as soon as one of the two end positions is reached. The motor is operated by the frequency/ polarizer control unit which is in turn controlled from the computer via four lines which are denoted in Fig. II.2 by "R", "UV", "0^{o}", and "90^{o}". Applying a logic "one" signal to the "R" line, which means 694 nm (red), the frequency doubler is moved out of the laser beam path, the 694 nm interference filter is moved into the telescope focus and the polarizer either parallel to the polarization plane of the 694 nm incident signal if a "one" is applied to the "0^{o}" line, or normal to it if a "one" is issued to the "90^{o}" line. Accordingly, if a "one" is applied to the "UV" (ultraviolet) line, the frequency doubler is moved into the laser beam, the 347 nm filter into the focus, and the polarizer parallel to the 347 nm plane if a "one" is issued to the "0^{o}" line, or normal to the 347 plane, if a "one" is issued to the "90^{o}" line. The actual position of the polarizer depends, therefore, on both the polarizer and the frequency control signal from the computer.
The four control signals may also be issued to the control unit manually via pushbuttons.
The electronics for remote control of range gate, high voltage, filter wheels, polarizer and frequency doubler is contained in a 19" chassis. Its front panel is shown in the photograph Fig. II.9.

1.2.7.7. Automatic laser start

The laser is started by closing a normal-open contact at the laser power supply (cf. description in the previous reports). This contact may now be closed remotely by a relay operated from the computer via interface No. 2.

1.2.7.8. External clock

An external digital clock, synchronized by line frequency,

has been developed. The four digits (hours and minutes) are output in BCD code and input to the computer. Two 8-bit channels of one I/O controller are used for this purpose. The clock may be questioned by the computer and the actual time output on punch tape together with the signals, as described in detail in paragraph 1.3. Furthermore, measurements may be started automatically at any time by means of the clock.

1.2.7.9. External stop pushbutton

An easily accessible "emergency" pushbutton has been installed which gives an interrupt signal to the external interrupt input of one I/O controller. Pressing this button interrupts the current program if the computer interrupt system is enabled (see below). This is used for example when a laser shot is to be repeated because of superposed spurious pulses.

1.2.7.10. Automatic trigger and reset of photon counter

The automatic background measurement with the photon counter as well as with the transient recorder requires the computer triggering of the photon counter (in the latter case because of the needed range gate start). This is now possible via one of the data output lines from the computer. Simultaneously with the photon counter triggering a pulse is fed through a cable to one of the external trigger input connectors of the transient recorder.

Via another data output line the combined photon counter/peak digitizer unit may be reset externally. This is convenient for analog measurements as in this case the energy monitor data only are needed and the data transfer may be stopped by reset when the peak digitizer readout is completed.

1.3. The new computer programs

With the availability of the automatic control of the system the development of completely new programs was necessary. As now by means of the floppy disc memory programs can be loaded very quickly into the computer, two separate programs for analog and photon counting measurements were prepared. They will now be described briefly with the aid of Figs. II. 3 and 4.

1.3.1. The analog measuring program

The flow diagram Fig. II.3 a and b shows the program for automatic analog measurements with the transient recorder. The automatic operation of the system requires a set of control words for the transient recorder and the control devices. They are stored in a table which is included in the program and loaded into computer together with it. As like previously one complete measurement series actually consists of four single measurements, e.g. one low resolution measurement (with low photomultiplier gain) for the lower parts of the total altitude interval of interest and one high-resolution measurement for the upper parts in both transmitter wavelengths, the table of control words is divided into four groups of partially different words for the same control operations. The table contains a standard set of control words suitable for most atmospheric conditions, but it may deliberately be changed from the keyboard, for example if extremely intense backscatter requires a reduced sensitivity of the recorder, if the altitude range is to be changed and so on. Furthermore it is possible to store any number of different tables on a floppy disc and to load one of them into the computer instead of the original table.

Before starting the program the actual date is entered into the computer from the keyboard for later output on punch tape and display on the terminal screen. The program starts

with a decision whether a manual start of the measurements is desired or if an automatic start at certain times, given by the external clock, is desired. This decision is done according to the position of one of the four sense switches of the computer. In the case of automatic start, the computer checks the current time and compares it with the desired starting times, e.g. every half and full hour, and goes on if this condition is met. The program then takes the first from the four sets of control words and stores them into a "current control word buffer". The subroutine called "measure", which the computer executes subsequently, takes the control word from this buffer.
After execution of this subroutine which is described below, the program continues storing the second set of control words into that buffer, again executes the subroutine and so on until all four single measurements are completed. Finally the transient recorder and control devices are returned to front panel (manual) operation and the program goes to start location again.

The subroutine, which really represents the major part of the complete program, is shown in Fig. II.3 b. At first the control words from the current buffer are output to the devices, and all buffers for data to be entered as well as the buffer containing the current number of laser shots are set to zero. As soon as a possible error signal is reset, i.e. if all servo motors are at their correct positions and the PMT high voltage has settled, the data acquisition electronics is triggered for background measurement. The stored data is then transferred to the computer. The data transfer routines for transient recorder and photon counter/peak digitizer are quite similar to those in the former program described in the 1976 annual report and are therefore not included in the diagram. From a part of the transient recorder data the background level is calculated and added to the background buffer. The next step is firing the laser. Thereafter, the stored signal may be viewed on the screen of the

recorder display during an 1 sec. pause. The interrupt system is enabled during this pause, and by pressing the "emergency" button the last laser shot may be repeated (also the foregoing background measurement) if necessary. When the pause is over the stored data are transferred from the transient recorder to the computer and added to the signal buffer contents. Likewise the energy monitor value is transferred and added to the peak digitizer buffer contents. This is followed by incrementing the shot number and comparing it with the intended number of shots. If the current number of shots is still less than the proposed number, the background and signal measurements are repeated; otherwise, the time is again input into the computer, the background sum subtracted from the signal sum, the "net" signal multiplied by R^2, divided by the average laser energy, multiplied by a scale factor and plotted on the terminal screen together with the correct altitude scale. The current date and time, transmitter wavelength, range gate data and transient recorder input range and trigger delay are also displayed and the complete plot hardcopied if wanted. The routine is then finished by storage of the net signal on a floppy disc for later punch tape output.

1.3.2. The photon counting program

The flow diagram Fig. II.4 presents the new photon counting program. Initially the photomultiplier HV and its limit is set to 2000 Volts. Then the first set of control words for range gate neutral filter wheel and polarizer position is output from the computer. All control words are contained in a table similar to the analog measuring program. After setting the current shot number and other buffers to zero, the measurement is started by triggering the photon counter without firing the laser for background measurement. Since the computer triggering is possible we measure the background in this way instead of using the eleventh or reference channel of the counter which results in an increased

accuracy. After triggering the photon counts are transferred to and stored in the computer. Then the laser is started, the counts are again transferred to the computer and the previously measured background subtracted. The "net" counts are output on punch tape in binary format, converted to decimal numbers and displayed on the terminal screen. The net counts are added to signal buffer contents (which is zero initially) and, with the exception of the first shot, the statistical errors of the accumulated counts are calculated. Then the next measurement cycle is started with the background measurement. The series of measurements with a given range gate and neutral filter setting is stopped automatically if the average statistical error is below 4 %, if 50 single shots have been fired, or manually by means of the fourth computer sense switch. The shot number, sum of energy monitor values, range gate data and time are then output on punch tape, and the range-corrected and energy-normalized partial backscatter profile displayed on the terminal in a semi-log scale, together with the error limits.

The complete series of measurements is now repeated with the following sets of control words until the end of the table is reached. As in the case of analog measuring, the final evaluation of the data is still performed off-line on the main computer with precise plotting facilities.

In general we use a height resolution of 600 m with the photon counting measurements. The corresponding 4 microseconds gate length per counting channel is included, therefore, in the standard control word table, but may be changed deliberately via the keyboard terminal. The standard altitude intervals and neutral filter settings for the partial measuring series are the following:

Series No.	Altitude Interval (km)	Neutral Filter Attenuation
1	34.8 - 40.8	0 %
2	30.0 - 36.0	0 %
3	25.2 - 31.2	0 %
4	20.4 - 26.4	0 %
5	15.6 - 21.6	92.3 %
6	10.8 - 16.8	92.3 %
7	6.0 - 12.0	98.5 %
8	32.4 - 38.4	0 %
9	27.6 - 33.6	0 %
10	22.8 - 28.8	0 %
11	18.0 - 24.0	0 %
12	13.2 - 19.2	92.3 %
13	8.4 - 14.4	92.3 %
14	3.6 - 9.6	98.5 %

As shown in the table, the complete series of amplitude intervals consists of two parts which are shifted by 300 m with respect to each other resulting in a real height resolution of 300 instead of 600 m. Examples of backscatter profiles measured by means of the photon counting technique will be presented in part IV.2 of this report.

2. The mobile lidar system

The mobile lidar system has been described in detail in the 1976 annual report. In the meantime the electronics and auxiliary equipment as cooling system etc, has been fixed to the van. For safety reasons this work had to be done very carefully and took several months. To prevent freezing of the water in the cooling circuit during transport of the system at air temperatures below zero, a heater has been con-

structed to which the cooling water tubings can be connected and which contains a little pump to circulate the water slowly. The heating power is delivered by the vehicle battery. As well as the lasers and the electronics have been tested separately, some defects especially in the electronics have been eliminated. First testing measurements will be possible as soon as the final alignments are completed.

The mobile lidar system is shown on the photo Fig. II.10. It has been presented at the "laser 77" exhibition in June at Munich.

III. ABSOLUTE CALIBRATION OF THE LIDAR SYSTEM

1. Calibration constants

The method of absolute calibration of the monostatic double frequency ruby lidar system has been described in previous reports by REITER et al. (1975, 1976a). Several new calibration experiments have been carried out in order to determine the lidar system constants needed for the evaluation of lidar backscattering profiles with respect to aerosol concentration and size distribution.

Table III.1 contains a list of lidar system constants that have been found until now (see also Fig. III.1).

Table III.1

Date	A(694 nm)[1]	A(347 nm)[1]	fitted to [2]
05 Mar 76	$3.4\ 10^{11}$	$7.7\ 10^{10}$	Wank
05 Mar 76	$1.8\ 10^{11}$	$6.5\ 10^{10}$	Rayleigh
11 Mar 76	$2.1\ 10^{11}$	$5.1\ 10^{10}$	Wank
01 Jul 76	$2.3\ 10^{11}$	$4.2\ 10^{10}$	Wank
01 Jul 76	$2.2\ 10^{11}$	$3.5\ 10^{10}$	Rayleigh
08 Sep 76	$2.8\ 10^{11}$	$1.4\ 10^{10}$	Wank
04 Mar 77	$1.4\ 10^{11}$	$2.1\ 10^{10}$	Wank
09 Mar 77	$2.0\ 10^{11}$	$2.0\ 10^{10}$	Wank
22 Mar 77	$2.6\ 10^{11}$	$1.2\ 10^{11}$	Rayleigh
20 May 77	$2.9\ 10^{11}$	$8.5\ 10^{10}$	Wank

1) The unit of the system constant is mV J^{-1} m^3 sterad.

2) The lidar backscattering profiles were fitted to expected backscattering values computed from additional data:

Wank : combined Rayleigh and aerosol scattering based on impactor measurements of the aerosol size distribution at Wank peak (1780 m),

Rayleigh: pure Rayleigh scattering deduced from simultaneous radiosonde data during days with extreme weak aerosol backscatter.

There is a considerable spreading in the calibration constants of about 40 % at 694 nm and more than one order of magnitude at 347 nm. Of course, the larger spreading in the ultraviolet is mainly due to the higher fraction of Rayleigh scattering. But there are still other uncertainty factors that are not yet eliminated by data normalization and the fitting procedure. These uncertainty factors may

be of technical origin, or they may enter the calibration routine through the various models and assumptions that have to be made.

On 22 March 1977 the system constants were derived under rather clean air conditions. According to the impactor measurements, the aerosol concentration was less than 10 % of the "normal" concentration measured at Garmisch-Partenkirchen and at Wank peak. Under these conditions Rayleigh scattering is the predominant scattering process, which is described very well by theory. Therefore the resulting lidar calibration is not so much affected by assumptions on aerosol scattering but rather by apparative factors. The extremely high system constant at 347 nm on this special day was probably due to the fact that energy monitoring via photodiode gave too small transmitted energies. Energy normalization then leads to an additional factor contributing to the lidar calibration constant. It is planned to improve the present energy monitoring system.

On 4 March 1977 a relatively small system constant at 694 nm is found. The meteorological parameters and a characteristic visibility indicated the advection of Sahara dust. This was confirmed by aerosol samples on filters exposed at the mountain stations and by impactor measurements. The size distribution (Fig. III.2) shows an enhancement of particles in the size range 0.4 - 1.0 μm diameter. The bimodal log-normal function which we use to describe aerosol size distributions has a gap just in this size range (Fig. III.3). Since backscattering at both 694 and 347 nm is sensitive to particles of that "medium" size, any deviations from the measured particle size spectrum will alter the calibration constants considerably. Moreover, the shape of these particles, their refractive index and its humidity dependence are probably different from the mean aerosol to which our model refers. A variation of these parameters is not yet possible with this calibration routine.

Fig. III.3 shows a bimodal log-normal distribution with the same backscattering properties at 694 and 347 nm as the measured size distribution (solid line) measured on 4 Mar 77. Since we use log-normal distributions with fixed mean diameters (0.4 and 2.0 /um) and standard deviation 0.3, a size distribution with enhanced medium size particles is accounted for by higher particle concentrations in the fine and coarse particle range. This somewhat unsatisfactory model will be modified in the future to allow for broader size distributions.

The discussion of the details of the lidar calibration routine shows that the lidar system constants that have been determined so far, are valid only on the very day of their determination if high demands are placed on the method of remote aerosol sensing. Although this is not the final stage of our lidar calibration procedure, one can at least compute a sequence of aerosol concentration and size distribution profiles for a limited time interval of several hours. Sometimes, however, we found too large variations of the system constants (or better: system factors) in the course of a day maybe due to thermal shifts or to almost undetectable damages in the optical parts of the lidar system that are exposed to the high energy of the laser beam. In some cases lidar system constants had to be rejected, because vertical distortions of the backscatter signals led to inconsistent concentration profiles. These vertical distortions may be produced by poor adjustment of optical parts of the system or by considerable deviations of the atmospheric extinction from the values calculated after Mie theory. However, it seems to be promising through future improvements at the system to reduce the possible errors.

Some examples of time sequences of aerosol concentration profiles are given in chapter IV.

2. Improvements in data processing

The evaluation routine, which is used to extract aerosol concentration and size distribution profiles from calibrated lidar backscattering signals, is not much different from the calibration routine and was described by REITER et al. (1975, 1976a). Some improvements of the computer programs have facilitated the fitting of the lidar data to the impactor measurements of the aerosol size distribution at Wank peak.
These improvements are:

- the automatic calculation of a bimodal log-normal size distribution having the same backscattering properties as a given size distribution,

- an automatic fit of lidar backscatter profiles at 694 and 347 nm to given backscatter values, reduction of the fitting parameters to the lidar system constants and computation of partial concentration profiles,

- an immediate graphic display of these profiles on the computer display terminal to check the validity of the lidar data and the various parameters involved in the evaluation routine,

- an automatic computation of a regression line through the logarithmic lidar backscatter profile in a selectable range interval for comparison with Rayleigh backscatter profiles.

These new facilities help to speed up the throughput of data, a necessary condition for establishing time series of aerosol concentration and size distribution profiles.

IV. APPLICATIONS OF THE LIDAR SYSTEM

1. Tropospheric measurements

The lidar system was applied to the measurement of vertical and time variations of the aerosol content in an atmospheric column above the lidar installation. The results of some of these measurements are presented in three different ways. In the case of normalized non-calibrated backscatter signals, three-dimensional plots for both lidar wavelengths 694 and 347 nm show the qualitiative variation of the backscattering medium with altitude and time. Examples are given in Figs. IV.6a, b - 10a, b.

In some cases an absolute lidar calibration was carried out and the backscatter signals were processed further in order to establish profiles of partial aerosol concentrations for fine aerosol particles (about 0.4 /um diameter) and coarse particles (about 2.0 /um diameter) respectively. These profiles are presented either in three-dimensional plots for both size ranges (Figs. IV.4a, b - 5a, b) or, for a better understanding of the size distribution, in sequences of both partial concentration profiles in the same diagram (Figs. IV.1a, b - 3a, b).

1.1. Aerosol concentration profiles

1.1.1. Size distribution in sequences of both particle concentration profiles, basic remarks on the method

Figs. IV.1a, b - 3a, b show sequences of aerosol concentration profiles in the fine and coarse size range.
On 8 September 1976 (Fig. IV.1) radiosondes were launched in the morning, in the afternoon and in the evening in order to measure the changes of the humidity profile during

the day. If the relative humidity exceeds 70 %, many features of the lidar backscatter can be explained by particle growth and changes in the refractive index and the size distribution due to the water coating and solution of the hygroscopic and soluble fraction of the aerosol. In this case it is desirable to have many humidity profiles simultaneously with the lidar firings.

On 4 March (Fig. IV.2)and 20 May 1977 (Fig. IV.3), the aerosol layers are partly composed of Sahara dust. Although these cases are not very appropriate for an absolute lidar calibration, they are good examples of the applicability of a double frequency lidar to the measurement of particle size distributions. Moreover, the profiles on 4 March, although rather "well-behaved", show some of the typical features common to all concentration profiles calculated with our evaluation routine. The features are also inherent to the size distribution model we use, but to a high degree resulting from a combination of the given lidar wavelengths and the predominant aerosol concentrations and size distributions at our measuring site. This will be shown in the following section.

Frequently, the concentration profiles of fine and coarse particles seem to be somewhat distorted mirror images: an increase of fine aerosol is accompanied by a decreasing concentration of coarse particles. On 4 March 1977, these variations are nearly of the same order (Fig. IV.2a, b). The two partial concentrations are not independent, they are coupled through the measured scattering functions at 694 and 347 nm. Or, inversely, the laser light is backscattered by both fine and coarse particles. Contrary to the real physical situation, one usually measures two independent backscattering functions, because the two lidar wavelengths use two different paths through the lidar system (two independent calibration constants) and because lidar firings in the two wavelengths are not simultaneous.

The partial concentrations are calculated from the following set of linear equations:

$$N_1 \Phi_1^R + N_2 \Phi_2^R = f_A^R,$$

$$N_1 \Phi_1^{UV} + N_2 \Phi_2^{UV} = f_A^{UV}$$

with

N_1, N_2 : particle concentration of fine (1) and coarse (2) particles,

$\Phi_{1,2}^{R,UV}$: collective backscattering function per particle for a log-normal size distribution with mean diameters 0.4 µm (1) or 2.0 µm (2) at wavelength 694 nm (R) or 347 nm (UV),

$f_A^{R,UV}$: aerosol backscattering function per unit volume at wavelength 694 (R) or 347 nm (UV).

Collective backscattering functions derived from Mie theory are tabulated in REITER et al. (1976b). For relative humidities below 50 %, i.e. a refractive index 1.62 - 0.02i, these values are

$$\Phi_1^R = 0.52\ 10^{-14},\quad \Phi_2^R = 0.67\ 10^{-12},$$

$$\Phi_1^{UV} = 0{,}26\ 10^{-13},\quad \Phi_2^{UV} = 0{,}17\ 10^{-12}.$$

The unit is $m^2\ sterad^{-1}$.

If there is a range interval where the backscattering function f_A^R at 694 nm remains nearly constant while the backscattering function f_A^{UV} shows variations, the partial concentrations N_1 and N_2 will vary also, in opposite directions.

The relative variations are of the same order of magnitude if the size distribution in this range interval is given by the ratio

$$N_2/N_1 \approx \Phi_1^R / \Phi_2^R \approx 10^{-2}.$$

This holds on March 4, 1977 (Fig. IV.2a), where the relative variations of fine and coarse particle concentrations are indeed equal but of opposite sign.

The variation of the particle concentrations is due to a variation of the backscattering functions. As the total backscattering function is composed of aerosol and Rayleigh scattering, the relative variation of the particle concentration may be considered high. For instance, the relative variation of the fine aerosol particle concentration is related to the relative variation (or error) of the backscattering signal Y^{UV} and the system constant A^{UV} at 347 nm by the expression

$$\frac{dN_1}{N_1} \gtrapprox \frac{1}{N_1} \cdot 3 \cdot 10^8 \left(\frac{dA^{UV}}{A^{UV}} + \frac{dY^{UV}}{Y^{UV}} \right).$$

The factor $3 \cdot 10^8$ m^3 is given by $\Phi_2 \, {}^R f_m^{UV}/D$, with the Rayleigh backscattering function f_m^{UV} as a lower limit of the total backscattering function and

$$D = \left(\Phi_1^R \, \Phi_2^{UV} - \Phi_2^R \, \Phi_1^{UV} \right).$$

$f_m^{UV} \approx 8.4 \cdot 10^{-6}$ m^{-1} sterad^{-1}, $D \approx - 1.66 \cdot 10^{-26}$ m^4 sterad^{-2}.

If the fine aerosol particle concentration is $3 \cdot 10^8$, its relative variation is of the same order as the variation of the backscattering signal or the error of the calibration

constant. If this concentration is of the order 10^7, an amplification by a factor of 10 leads to large variations in the concentration profile. This kind of variation can be found in Fig. IV.1a.

The considerations on error propagation do not necessarily indicate the impossibility of an absolute calibration of the lidar system or of the computation of aerosol concentration and size distribution profiles from calibrated lidar backscattering signals. They simply show the necessity to determine all parameters involved in the calibration and evaluation as accurately as possible, to have a most realistic scattering theory and model of aerosol size distribution. Furthermore one should be very careful at interpreting the resulting concentration profiles.

1.1.2. Diurnal variations demonstrated by three-dimensional plots

Fig. IV.4 shows the diurnal variations as three-dimensional plots which were discussed before in a different way in chapter 1.1.1. (Fig. IV.2a). First a supplementary remark to Fig. IV.2a: The lidar shots at 11.35 CET have been fitted to the aerosol particle data of the station Wank (▲). However, it is satisfying to note that the aerosol concentration profiles in the coarse and fine range calculated on this basis are consistent with the aerosol particle data of the stations Zugspitze and Garmisch. Fig. IV.4a, and above all Fig. IV.4b show in the layer between 2.5 and 3.0 km agitations in the aerosol concentration. This, as well as the increase in the coarse range aerosol concentration with height in the afternoon of 4 March (Fig. IV.4b) is indicative of heterogeneous aerosol conditions and of an influx of coarser particles in the height - a behavior being typical in the case of advection of Sahara dust.

A similar behavior is particularly well demonstrated by the

fine and coarse particle profiles on 22 May 1977 (Fig. IV.5) when an exeptionally marked influx of Sahara dust occurred. In the course of the day the profile of the fine aerosol concentration (Fig. IV.5a) varies only in the usual manner: Increase in particle concentration from morning to afternoon in the lower 1.5 to 2.0 km, and slight variation between 2.5 and 3.0 km. Consequently the gradient of the decrease of the particle concentration with height becomes increasingly steeper in the course of the day. The profile of the coarse aerosol concentration shows a completely different pattern (Fig. IV.5b): Between 1.5 and 2.5 km we observe a remarkable rise with altitude the steepness of which steadily decreases from morning to afternoon, the lower boundary of the aerosol layer with the coarse particles continuously falling off. This behavior is quite characteristic of an acute influx of coarser particles into the middle troposphere. The sharpness of the layer is slowly reduced by turbulence in the course of several hours, the lower boundary of the haze layer steadily decreasing until it finally reaches the valley level.

Just these examples demonstrating the influx of Sahara dust through lidar observations clearly show the possibilities of applying a calibrated lidar system in practice although the accuracy presently achieved with regard to a quantitative evaluation is not yet satisfying to a full extent.

1.2. Diurnal variation of lidar backscattering (non-calibrated backscatter signals), three-dimensional plots

Fig. IV.6 shows the situation on 20 September 1976 in ruby light (Fig. IV.6a) and in UV-light (Fig. IV.6b).
We clearly observe, mainly in Fig. 6a, the increase of backscatter intensity in the course of the day in altitudes up to about 2.8 km and the rise of the aerosol from about 2.0

to 2.8 km and further the formation of layers with maximum backscattering in the range of the upper boundary of the exchange layer (2.8 km). This behavior is in agreement with the temperature- and humidity lapse rates of the same day. In the afternoon we find the needle-shaped peaks as a result of precondensation and of the first, yet weakly defined cloudiness, respectively. The fluctuations in higher altitudes (mainly in UV-light) are a consequence of the then too unfavorable signal/noise ratio which quite recently could essentially be improved. Nevertheless, Fig. b, too, reveals (though somewhat weaker) an increase of the backscatter intensity and rise of the aerosol in the course of the day.

Aerosol structures can rather clearly be identified in Figs. IV.7 a and b presenting the profiles of 22 Sep 76. This concerns on the one hand the smoke swathes in the forenoon, but just so the upper boundaries of haze remaining stable over longer time intervals with backscatter intensity maxima in about 2.1 and 2.5/2.6 km between 14.00 and 17.00 CET. These aerosol structures are only faintly defined in UV-light (Fig. IV.7b).

For comparison Fig. IV.7c shows the lapse rates of dry T and wet T' bulb temperature and positve air conductivity λ_+ for 16.30 CET on the same day. According to those, the upper boundary of the exchange layer is in exact agreement with the ruby laser backscatter profile (Fig. IV.7a).

Fig. IV.8 is also an instructive example (unfortunately without UV-shot due to malfunction of the instrument). It shows fairly well the agitation in the aerosol structure up to 3 km altitude as a function of time: In the morning a sharp upper boundary of haze still exists at 2.5 km which is, however, soon being dissipated. In the valley floor we have a wavelike increase of backscatter, haze layers form at various altitudes and the aerosol rises on the whole

from afternoon to the evening up to heights of about 3.5 km. The weather situation on 23 September (Fig. IV.8) can briefly be described as follows:
Autumnal anticyclonic weather, practically cloudless; strong radiation, vigorously developed mountain wind. Exchange coefficients rising in the course of the day from about 4 to 150 g cm^{-1} sec^{-1}. Visibility in the valley and at the Wank between 60 -95 km.
This means that even under quite good conditions of visibility the aerosol conditions can yet fairly well be detected by our lidar system.

This series is to be continued with another particularly instructive example (20.10.76) illustrated in Fig. IV.9. The weather conditions can be characterized as follows:
Large scale: Anticyclone above Russia, an intensifying cyclone in the western Mediterranean, flat cold air layer above Bavaria.
Local: Forenoon until afternoon only some very isolated cumulus fractus, in late afternoon trend to formation of stratus. In the course of the day, through the mountain valley wind, heavily polluted air hanging over the pre-alpine region was carried into our valley, the thickness of the haze layer steadily increasing. Vertical exchange intensity: very weak.

Visibility in km at the following times:						
CET:	10	12	14	16	18	20
Valley km:	19	14	9	6	5,5	5
Wank:	≥ 100 km					

In ruby light (Fig. IV.9a) as well as in UV-light (Fig. IV. 9b), the invasion of haze into the valley floor, the system-

atic rise of the upper boundary of haze, and the steady increase in the backscatter intensity at all levels of the haze layer is clearly to be seen. The upper boundary remains sharply defined and at heights above 1600 m the atmosphere was always free of the haze advection (cf. the above stated visibility ranges).

Fig. IV.9c shows the dry T and wet T' bulb temperature lapse rates for 15.30 CET. The inversion lies between 1150 and 1300 m in exact agreement with the lidar backscatter.

The graphical representation in Fig. 9b was cut off at 2.2 km since the UV-backscatter in the height $>$ 2.2 km could not be distinguished from the noise (extremely low aerosol concentration).

Anyhow, it should be pointed out that measurements of aerosol backscatter in ruby light are possible without difficulties also under conditions of more than 100 km visibility as can be seen from Fig. IV.9a in heights above 1.6 km.

We will conclude the series of examples with Fig. IV.10. It illustrates fairly well the relatively rapid fluctuations in the aerosol concentration as a function of time and altitude without the appearence of any stationary structures. The agitation in ruby light backscatter is conspicuously higher than in UV-light which may lead to the conclusion that the inhomogeneities concern above all the coarse part of the aerosol. Apart from that, in the basic structure good agreement is found between Figs. 10 a and b. The lapse rates of temperature and humidity neither reveal any stationary structures. This example makes it clear that a consistent description of the time-space aerosol structure can only be obtained with the aid of continuous lidar backscatter profiles recorded with high time resolution.

2. Observations of stratospheric aerosols by photon counting technique

2.1. Improvements of photon counting data

The off-line evaluation of the photon counting data remained basically unchanged since annual report R. REITER et al. (1976). However, major improvements of the whole measuring set-up of the lidar system are yielding much better data. These data are now of such a quality that certain statements regarding aerosol presence in the lower stratosphere can be made.

Since October 1976 an RCA 8852 PMT can be used instead of the EMI 9816 PMT when utilizing the photon counting facilities of the lidar system. This new PMT is distinguished by a much better time resolution resulting in a dead-time reduction to about one tenth of the previous value. The linear counting range now is considerably extended. With regard to counting statistics, however, both PMTs show similar behavior which can be expected within the range of total time resolution of the single photon pulses.

Another improvement is the installation of a filter wheel in the receiver light path holding several neutral filters and providing unrestrained light passage and light attenuation at several levels. The filter wheel replaced the gray wedge which could not be adjusted at reproducible attenuation settings. The reconstruction of the backscatter profile by computer calculations is very much simplified because fixed attenuation factors can now be incorporated in the program and tedious alignment of the profile sections as described in the last report can be ommitted.

A present backscatter profile is recorded by observing 600 m intervals per channel of the 10-channel counter and 7 successive delay settings are necessary to cover a height

interval from 7 to 40 km. Per delay setting laser returns are recorded until a 4 % standard deviation is attained but a maximum of 50 laser firings per delay is not exceeded. Up to 4 series per night averaged provide a mean profile which consists of as much as 1000 to 1200 individual laser returns.

Additional information on the nature of the scattering medium can be gained by determining the degree of depolarization of the return signal. An analyzer in the receiver light path can be adjusted parallel or perpendicular to the plane of polarization of the emitted laser pulse, the intensity ratio of the received signals indicating the change of polarization.

2.2. Rayleigh backscatter profiles

The measured total backscatter (e.g. molecular plus particulate backscatter) has to be compared with the backscatter from a purely molecular atmosphere (Rayleigh scattering). To minimize errors we try to combine measured backscatter profiles with Rayleigh profiles derived from actual atmospheric density data which are delivered by our own rawinsondes. These radiosondes are launched at the site of the institute at least within 12 hours from a lidar campaign.

In case radiosonde data cannot be made available a "standard" profile has to be taken as a reference. To check on the validity of such a "standard" profile, 37 Rayleigh profiles obtained from radiosonde data between January 75 and May 77 have been examined. This material has been investigated regarding seasonal trends and the backscatter profiles have been classified as follows: below the tropopause (height interval 0 - 8 km) and above the tropopause (height interval 20 - 30 km) the slopes of the profiles have been determined and related to the time

scale. Below the tropopause, which usually is found between 10 and 13 km, a seasonal trend of the inclination is found with a maximum in June-July and a minimum in December-January. However, the scatter of the data is in the order of the seasonal variations. Only little seasonal variations can be found above the tropopause with a scatter by far exceeding the variations. So any slope of the profile can be found at any time.

Applying a seasonal "standard" Rayleigh profile if actual radiosonde data are not available therefore is only a compromise. Deviations of the actual Rayleigh profile from a "standard" profile can be in the order of the presently measured net aerosol backscatter.

Our Rayleigh profiles have been compared with the Rayleigh profile derived from density values of the 1976 US Standard Atmosphere. Below the tropopause there is a very good agreement, the"US Rayleigh profile" showing a slope corresponding to our mean value of all evaluated profiles. Above the tropopause the "US Rayleigh profile" shows a steeper slope resulting in 3.5 % more molecular backscatter. However, the scatter of our profiles includes the slope of the "US Rayleigh profile" above the tropopause.

2.3. Measured backscatter profiles

The quality of the measured backscatter data was improved to such an extent after the introduction of the new PMT that only results obtained since October 76 will be reported. Intense instrumental maintenance now allows to make use of all clear sky periods. Unfortunately the number of nights suitably clear is rather limited and we are forced to conduct our observations during nights when cirrus clouds tend to hamper our recordings. Only during night time measurements can be performed to avoid the high background due to diffuse sky radiation. Cirrus clouds,

usually changing rapidly in density, can cause an intensity shift of the individual sections of the backscatter profile and matching of these sections with the general trend of the whole profile might then be necessary.

During the period October 76 through July 77 eleven backscatter profiles, in most cases up to 35 km, have been recorded, many of them through a more or less dense cirrus layer. These profiles are shown in Figs. IV.11 - IV.21. The polygonal curves present the measured total backscatter, the smooth curves are the calculated molecular backscatter. The horizontal bars denote 1 standard deviation of the statistical fluctuations of the photon counts.

The matching of the measured total backscatter signal with the calculated molecular return is accomplished at height levels of minimum aerosol backscatter. Suitable levels are above the tropopause around 15 km and between 20 and 25 km. Deviations from the purely molecular backscatter are generally found around the tropopause if cirrus layers are present, between 16 and 22 km, and above 25 km.

On February 14, 1977, (Fig. IV.15) the degree of depolarization of the return signal has been determined between 5 and 14 km. The cirrus clouds between 7 and 10 km could be identified as ice particle clouds as indicated by a depolarization of 60 %. For the molecular return a depolarization of 3.6 % has been derived in very good agreement with published values.

2.4. Stratospheric aerosol layer

A good means of describing particulate backscatter is the scattering ratio, e.g. the quotient of measured total backscatter to calculated molecular backscatter. Fig. IV.22 presents scattering ratios derived from the measurements

between October 76 and July 77. Each curve is the mean of several individual profiles recorded during the night of observation. The tropopause level usually is found at 10 to 12 km where in many cases cirrus clouds produce large scattering ratios.

Above the tropopause a distinct layer of increased backscatter intensity in the order of 10 to 15 % of the molecular return can be observed. During the period of observation the lower boundary of this layer is rising from about 15 to 17 km and the upper boundary from about 21 to 25 km. The maximum of backscatter however is reaching a maximum altitude at 21 km in March 77, rising from 18 km in October 76 and declining to 19 km in July 77. This layer corresponds to that described by Junge with scattering ratios reported for the pre-Fuego situation. The eruption of the volcano Fuego in Guatemala in October 1974 was the last strong major volcanic injection into the stratosphere.

Towards higher altitudes above 25 km the scattering ratio is again increasing without returning to unity at a defined altitude. Although the greater part of this deviation from unity is covered by assuming an error of 10 % (to be discussed in the following) our measurements seem to indicate a second particulate layer around 30 km. Since measurements by other groups at the same latitude (Garmisch-Partenkirchen 47.5°N) are not available, comparison and discussion of our findings regarding a second layer are presently not possible.

2.5. Error discussion

The 1 σ square root error of the photon counts amounts to about $\pm$2 % at 10 to 15 km and increases to about $\pm$7 % at 30 to 35 km. The Rayleigh profile derived from radiosonde density data will be affected by errors: Uncertainties of the radiosonde data will introduce an error, but by matching

measured and calculated backscatter profiles this error will be reduced and the remainder will not exceed 1 or 2 %. In some cases the Rayleigh profile has to be extrapolated to higher altitudes causing an error which can be regarded as of the same order. For the calculation of the Rayleigh backscatter profile a "no particulate extinction model" has been applied which meets the present stratospheric situation. The error thus introduced has been estimated applying literature values of the particulate to extinction ratio to an assumed aerosol layer between 18 and 25 km. An error of .2 % of the two-way transmission caused by this layer has been calculated and can be neglected. Thus a maximum error of about 10 % can be assumed for our measurements between 30 and 35 km.

V. CONCLUSIONS

The works under contract led to the following results or conclusions respectively:

1. Computerized, fully-automatic multi frequency lidar systems make it possible, with very high resolution regarding time and distance (resp. height) to determine aerosol structures and to study their variations.

2. If information is wanted relying not only on relative backscatter data but also comprising a discrimination of aerosol concentrations in different particle size ranges, the absolute calibration of the lidar systems is a necessary requirement. This can be done by observation of the pure molecular backscatter as well as by in situ measurements of the aerosol size distribution in the troposphere during lidar shots. These calibration procedures involve a great amount of effort and

lack in their present state, mainly in UV-light, sufficient accuracy. Therefore, further attention must be devoted to this subject.

Nevertheless some examples of absolute remote aerosol sensing show that on principle the method used is practicable and delivers satisfying results if the calibration constants are known with sufficient accuracy.

3. Further it showed up that even non-calibrated lidar measurements in the troposphere yield valuable information on interesting aerosol structures and their variations, especially with regard to convection, advection, and condensation processes. Such data can be easily obtained with the aid of fully developed automatic lidar systems.

4. The method used for single photon counting proved to be completely suitable for the performance of routine monitoring of relative aerosol backscatter in the stratosphere up to 35 km. Since October 1976 we are conducting at our Institute stratospheric aerosol monitoring. On the average we obtain 2 - 3 profiles per month during cloudless nights.

The works on the lidar systems, their calibration and practical application will be continued under contract No. DA-ERO 77-G-064.

VI. REFERENCES

/ 1 / REITER, R., CARNUTH, W., LITTFASS, M., and VARSHNEYA, N.C.:
Analysis of aerosol transport. Final Technical Report, July 1975, Grant Agreement No. DA-ERO-591-73-G0057.

/ 2 / REITER, R., CARNUTH, W., LITTFASS, M., and JAEGER, H.:
Analysis of aerosol transport, aerosol remote sensing by lidar.
Annual Report, Volume I, August 1976a,
Grant Agreement No. DA-ERO-75-G-077.

/ 3 / REITER, R., CARNUTH, W., LITTFASS, M., and JAEGER, H.:
Analysis of aerosol transport, aerosol remote sensing by lidar.
Annual Report, Volume II, August 1976b
Grant Agreement No. DA-ERO-75-G-077.

LEGENDS OF FIGURES

Fig. II.1 : Revised block scheme of the stationary lidar system

Fig. II.2 : Block scheme, remote control electronics

Fig. II.3 a and b : Flow charts of computer program for automatic analog measurements

Fig. II.4 : Flow chart of the computer program for automatic photon counting measurements

Fig. II.5 : Laser with power supply of stationary lidar system

Fig. II.6 : Receiver case with radiation shield of stationary lidar system

Fig. II.7 : Receiver case of stationary lidar system as viewed from above, showing telescope mirrors, frequency doubler, and 45 deg. mirrors

Fig. II.8 : Data acquisition electronics of the stationary lidar system, including Biomation recorder, photon counter, peak digitizer, remote control unit, and on-line computer with display terminal, hard copy, and floppy disc memory

Fig. II.9 : Front panel of remote control unit

Fig. II.10: The mobile lidar system

All other figures are described with full particulars in the text.

FIGURES

Fig. II.1

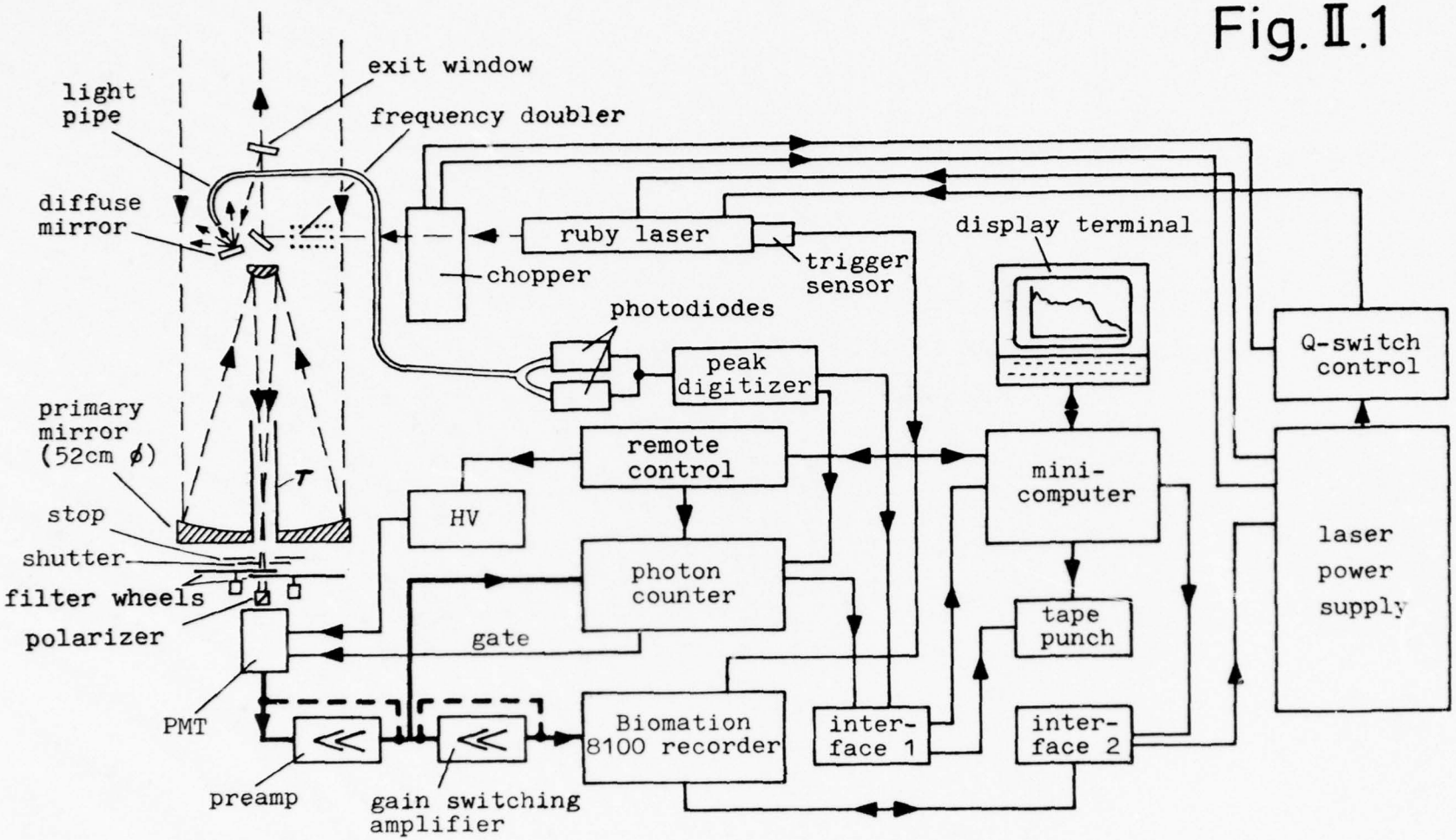
exit window
light pipe
frequency doubler
diffuse mirror
ruby laser
trigger sensor
display terminal
chopper
photodiodes
peak digitizer
Q-switch control
primary mirror (52cm ϕ)
remote control
mini-computer
stop
HV
shutter
photon counter
laser power supply
filter wheels
polarizer
gate
tape punch
PMT
Biomation 8100 recorder
inter-face 1
inter-face 2
preamp
gain switching amplifier

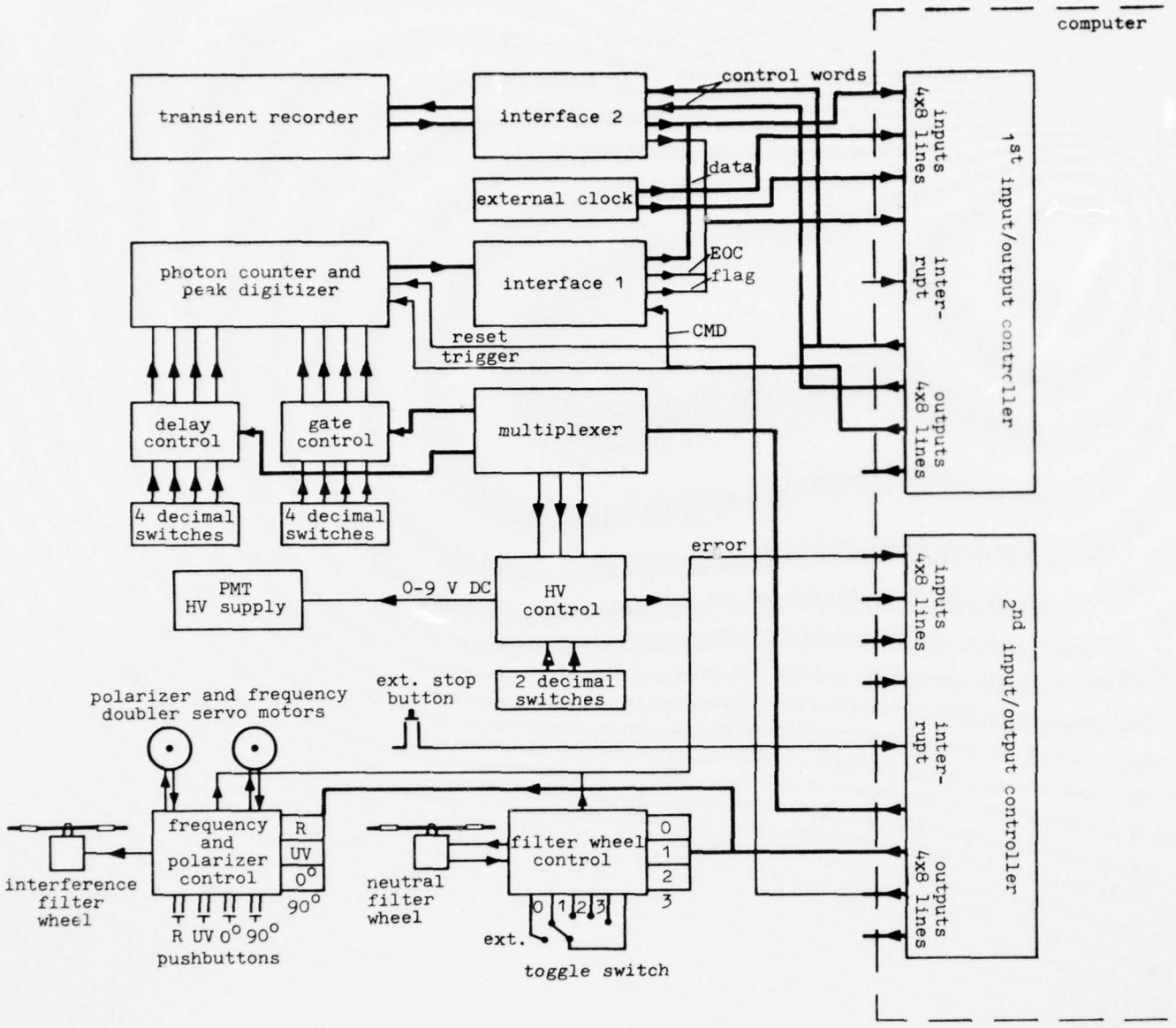
computer
transient recorder
interface 2
control words
data
external clock
photon counter and peak digitizer
interface 1
EOC
flag
CMD
reset
trigger
delay control
gate control
multiplexer
4 decimal switches
4 decimal switches
error
PMT HV supply
0-9 V DC
HV control
2 decimal switches
ext. stop button
polarizer and frequency doubler servo motors
frequency and polarizer control
R
UV
0°
90°
interference filter wheel
R UV 0° 90°
pushbuttons
neutral filter wheel
filter wheel control
0
1
2
3
ext.
toggle switch
1st input/output controller
2nd input/output controller
inputs 4x8 lines
inter-rupt
outputs 4x8 lines

Fig.II.2

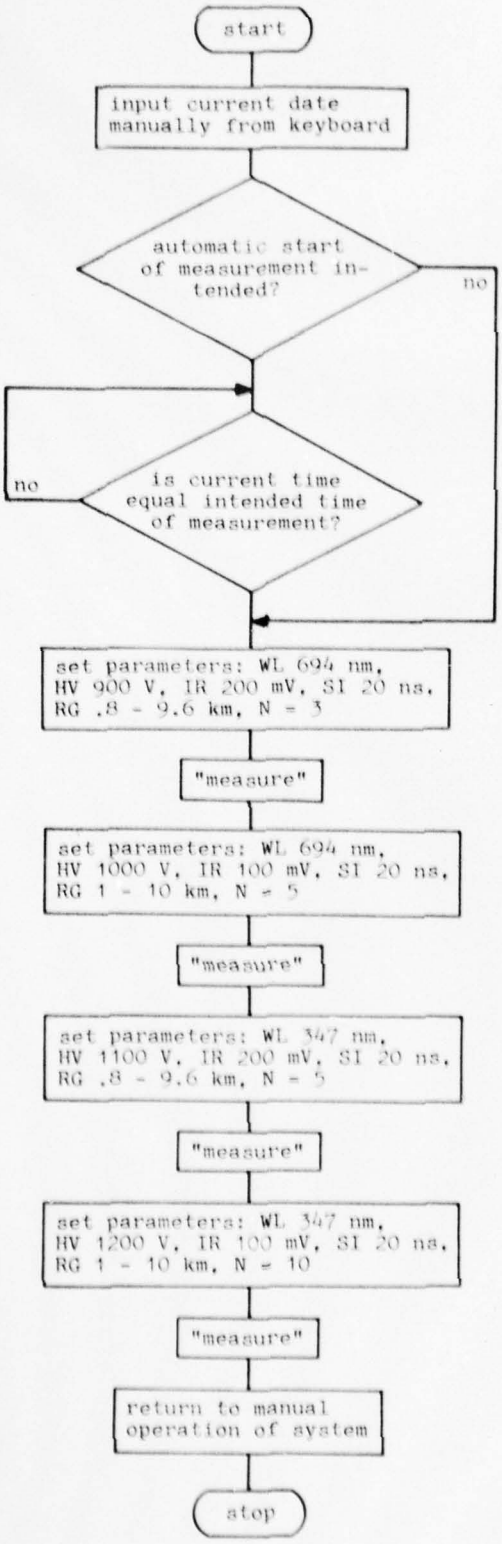

NOTE:

WL = wavelength
HV = photomultiplier high voltage
IR = input range of transient recorder
SI = sample interval of recorder (20 ns = 6 km tot.)
RG = range gate interval
N = intended number of shots

Fig.II.3a

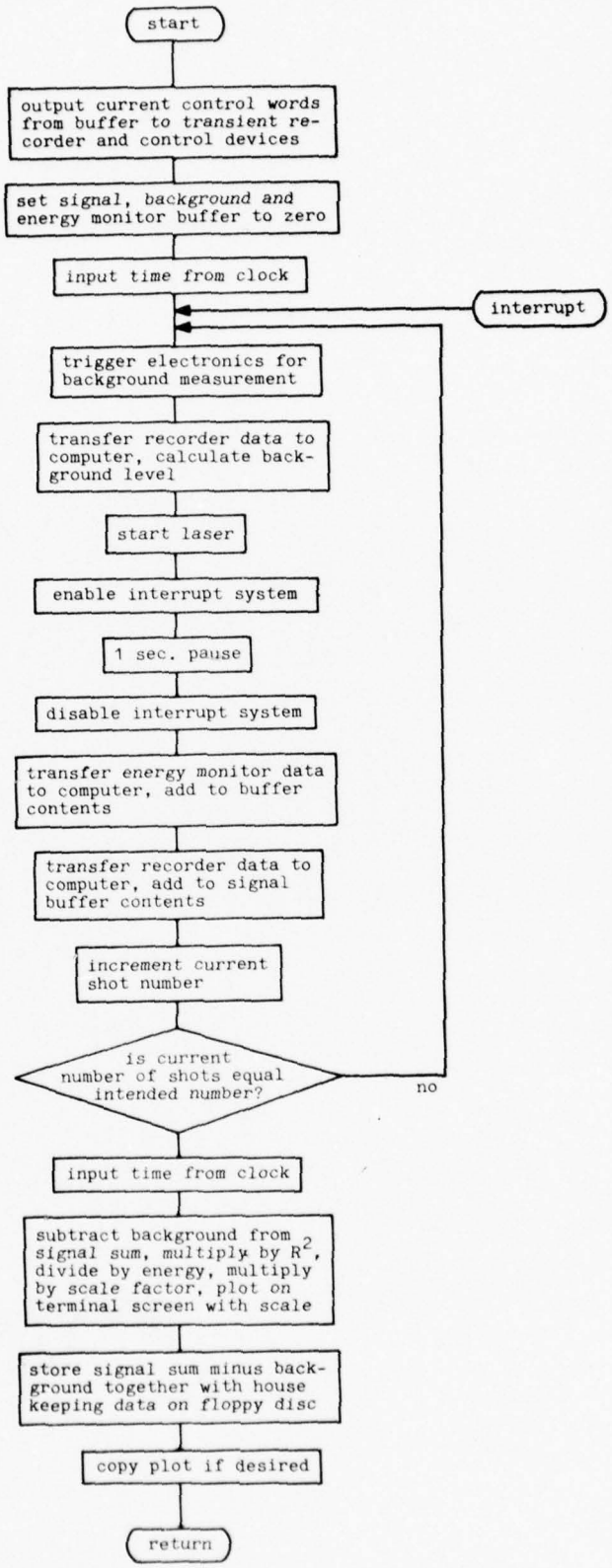
start
output current control words from buffer to transient recorder and control devices
set signal, background and energy monitor buffer to zero
input time from clock
interrupt
trigger electronics for background measurement
transfer recorder data to computer, calculate background level
start laser
enable interrupt system
1 sec. pause
disable interrupt system
transfer energy monitor data to computer, add to buffer contents
transfer recorder data to computer, add to signal buffer contents
increment current shot number
is current number of shots equal intended number?
no
input time from clock
subtract background from signal sum, multiply by R^2, divide by energy, multiply by scale factor, plot on terminal screen with scale
store signal sum minus background together with house keeping data on floppy disc
copy plot if desired
return

Fig.II.3b

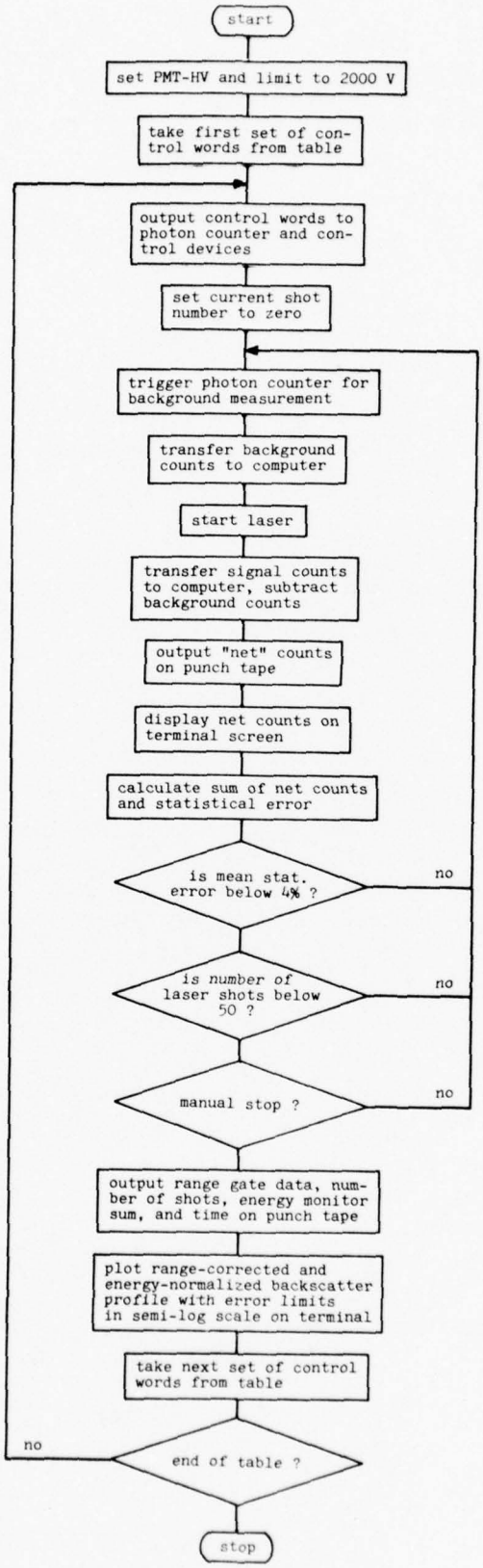
start
set PMT-HV and limit to 2000 V
take first set of control words from table
output control words to photon counter and control devices
set current shot number to zero
trigger photon counter for background measurement
transfer background counts to computer
start laser
transfer signal counts to computer, subtract background counts
output "net" counts on punch tape
display net counts on terminal screen
calculate sum of net counts and statistical error
is mean stat. error below 4% ?
no
is number of laser shots below 50 ?
no
manual stop ?
no
output range gate data, number of shots, energy monitor sum, and time on punch tape
plot range-corrected and energy-normalized backscatter profile with error limits in semi-log scale on terminal
take next set of control words from table
no
end of table ?
stop

Fig.II.4

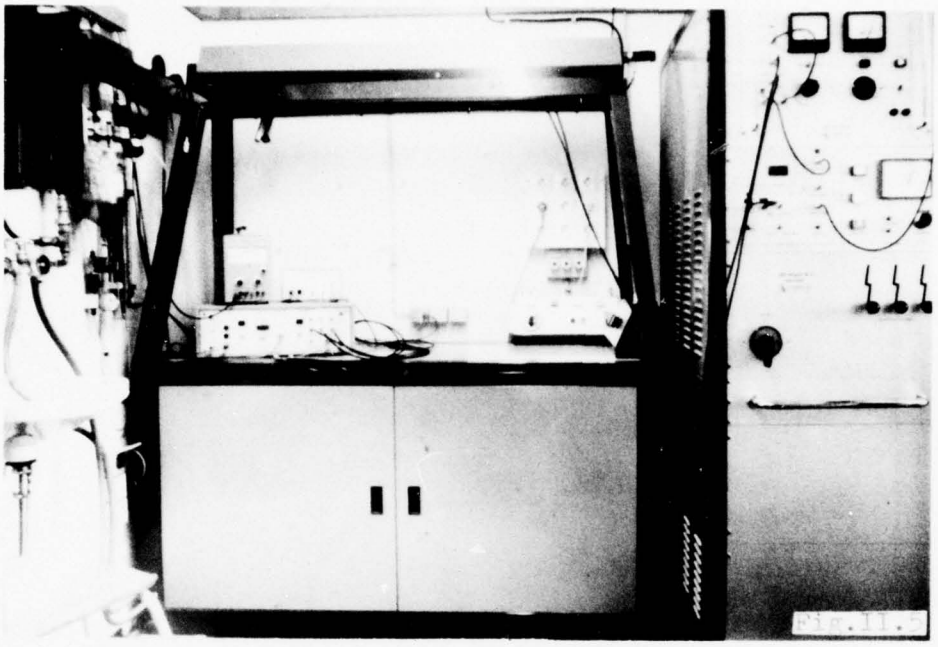

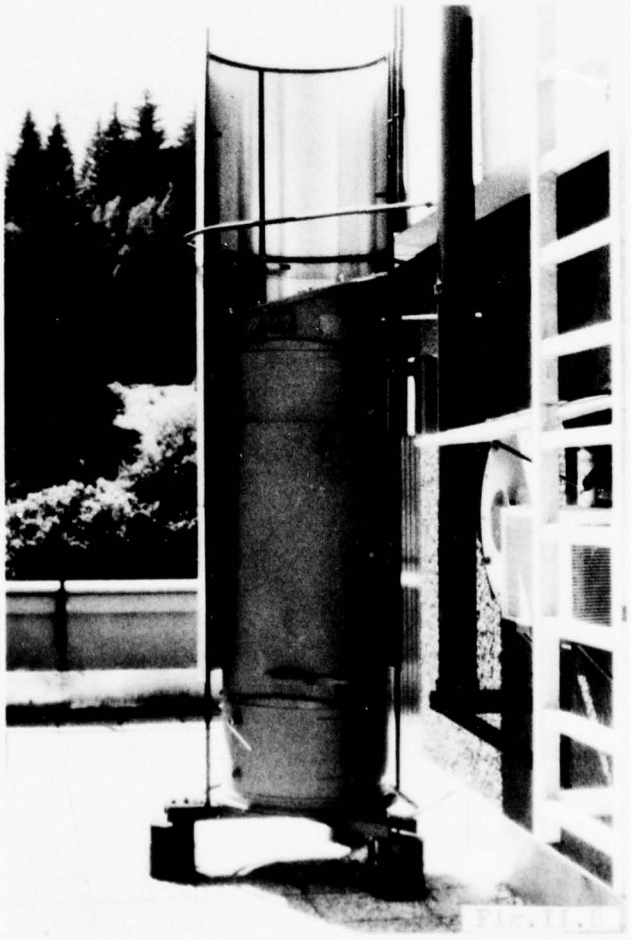

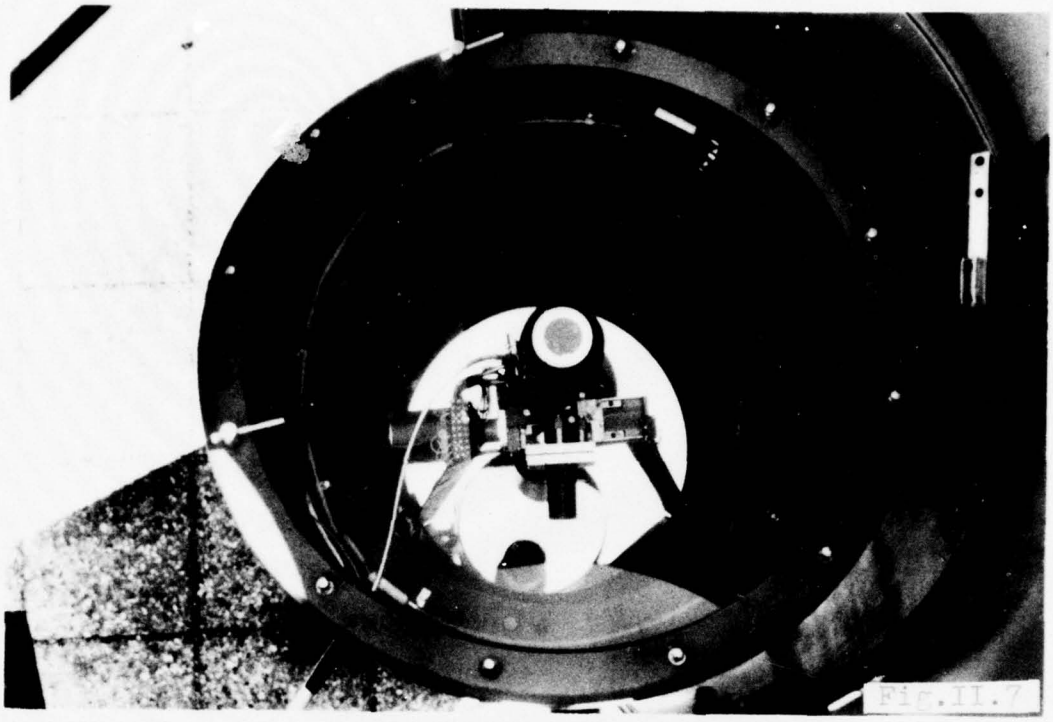

Fig. II.7

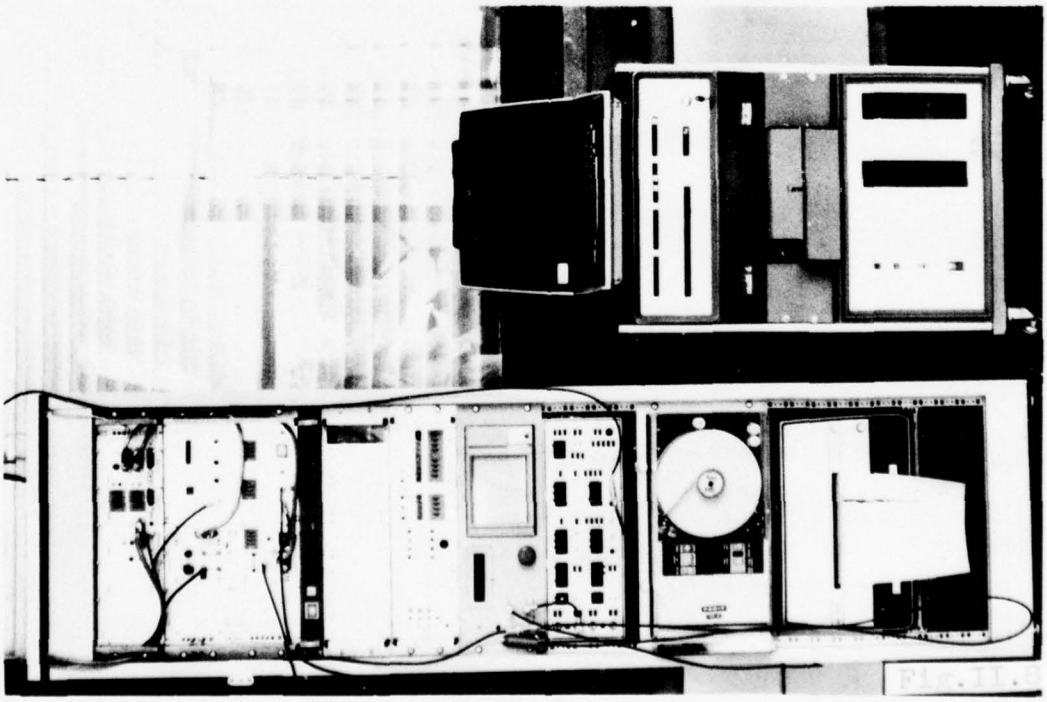

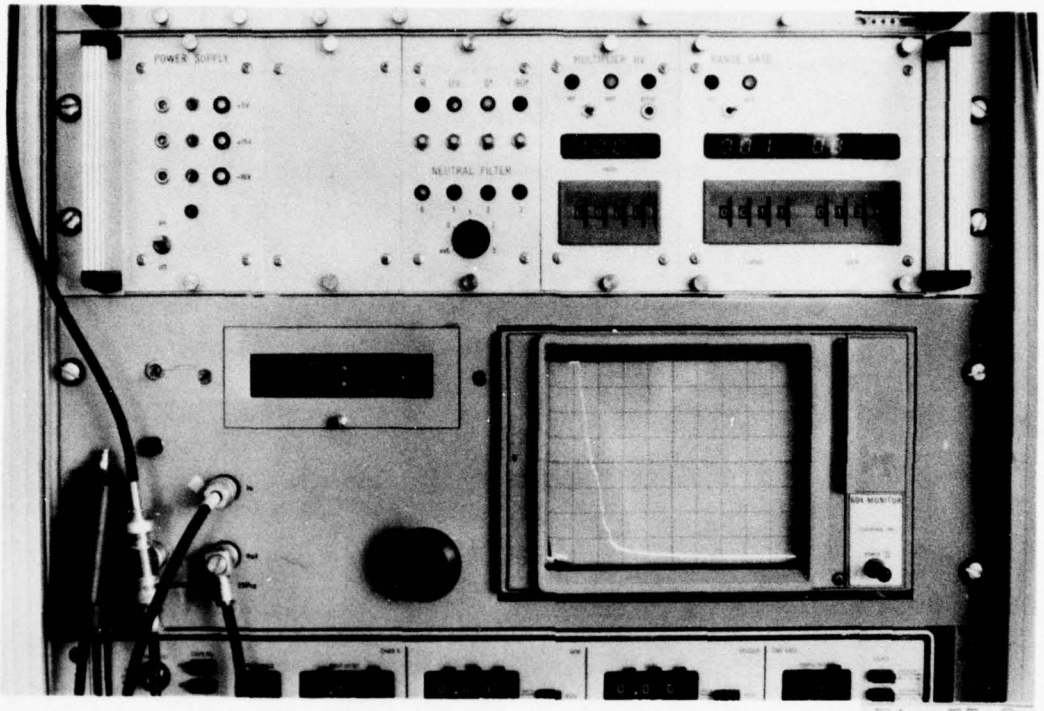

Fig.II.9

Fig.II.10

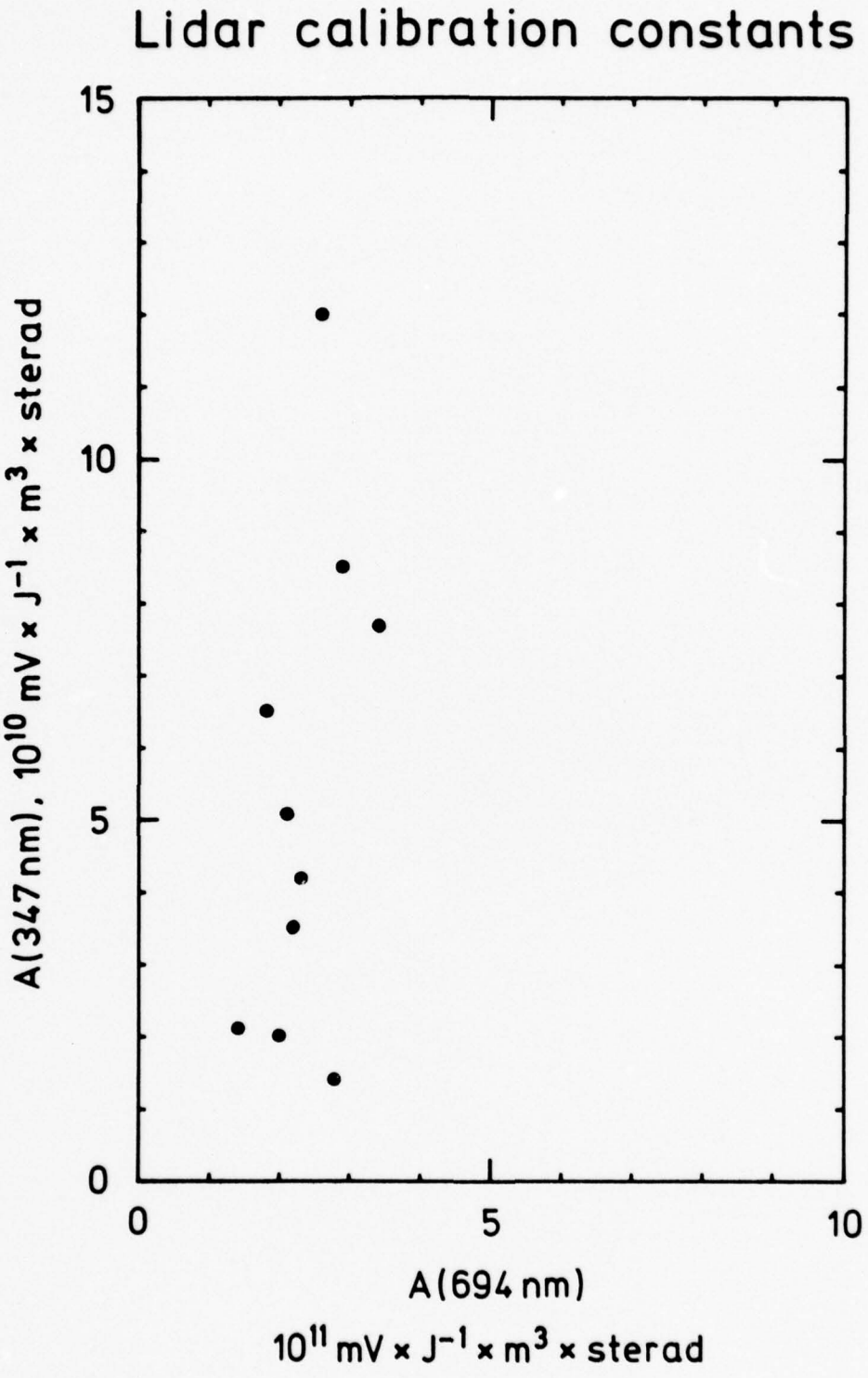
Lidar calibration constants
15
10
5
0
0
5
10
A(347 nm), 10^{10} mV × J^{-1} × m^3 × sterad
A(694 nm)
10^{11} mV × J^{-1} × m^3 × sterad

Fig. III.1

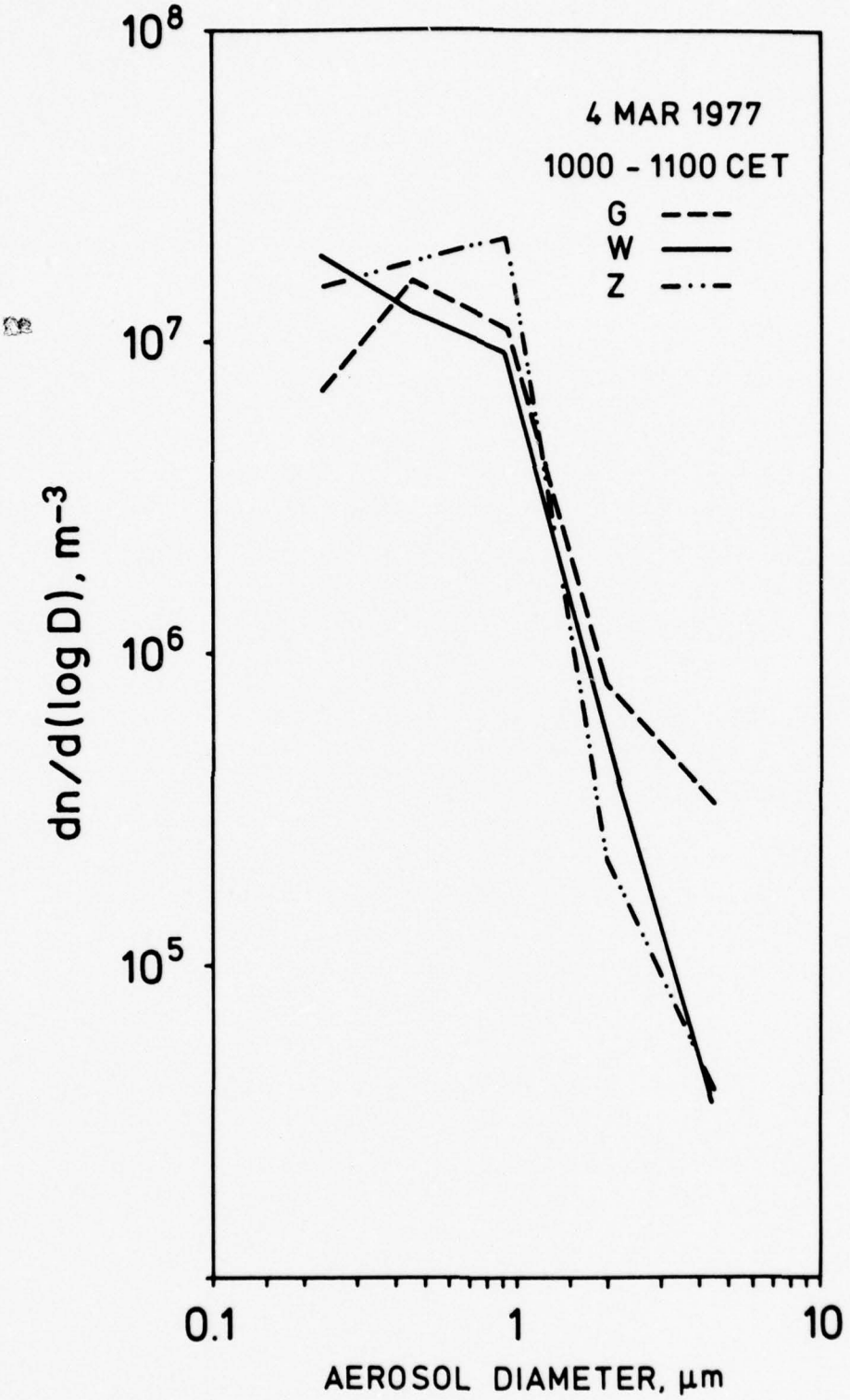
4 MAR 1977
1000 - 1100 CET
G
W
Z
10^8
10^7
10^6
10^5
dn/d(log D), m^{-3}
0.1
1
10
AEROSOL DIAMETER, µm

Fig. III.2

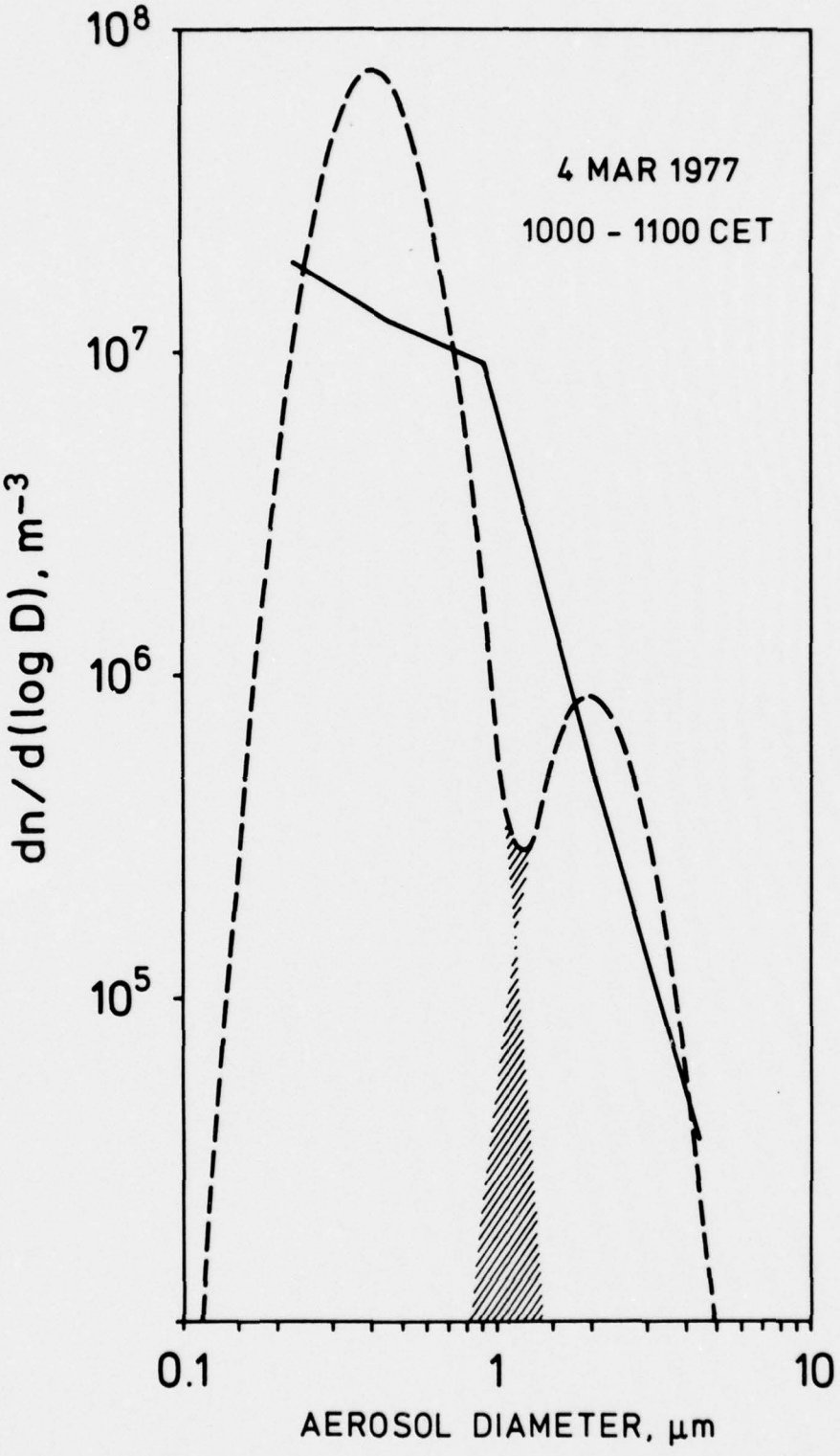
4 MAR 1977
1000 - 1100 CET
10^8
10^7
10^6
10^5
dn/d(log D), m^{-3}
0.1
1
10
AEROSOL DIAMETER, µm

Fig. III.3

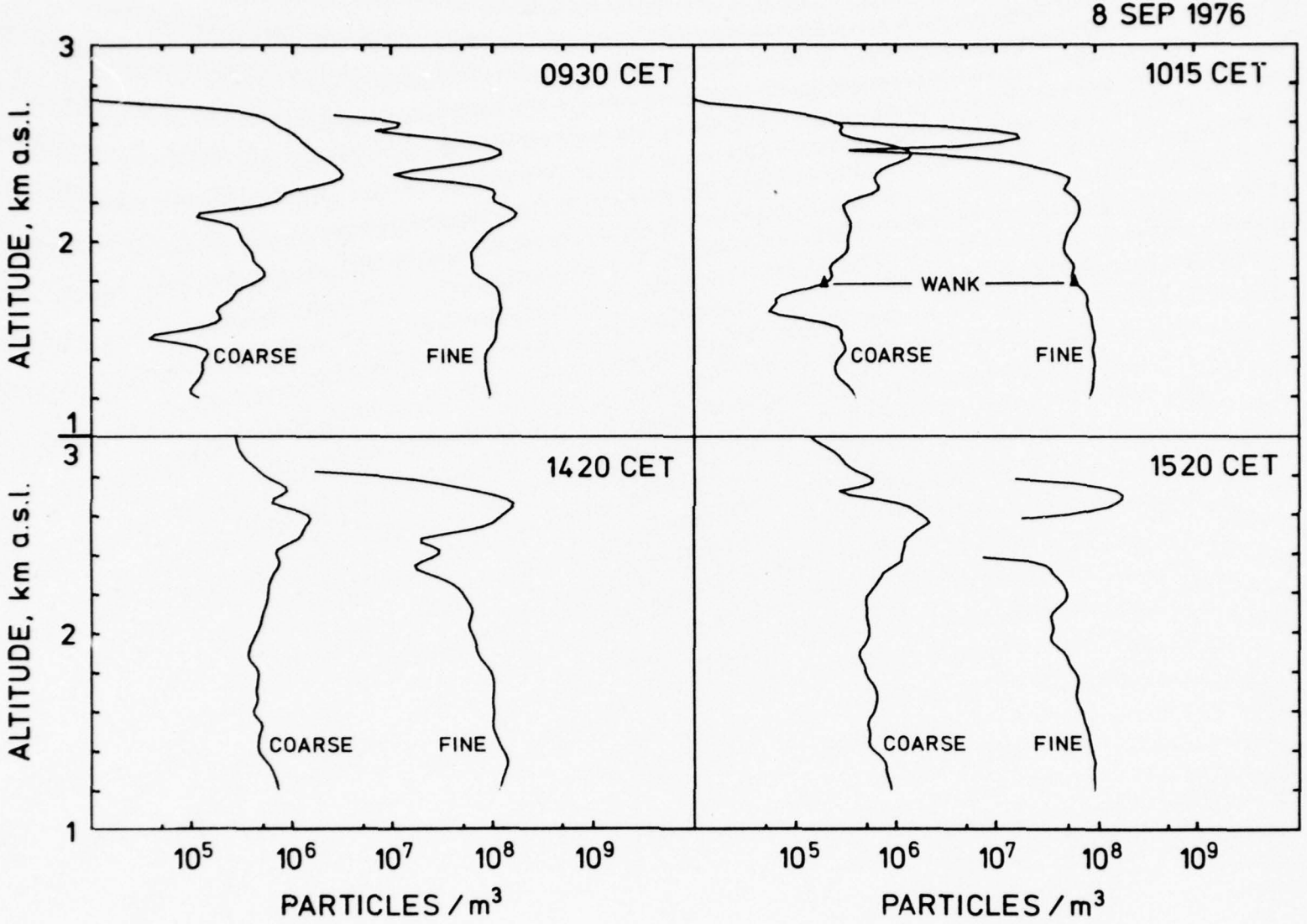
8 SEP 1976
0930 CET
1015 CET
1420 CET
1520 CET
WANK
COARSE
FINE
ALTITUDE, km a.s.l.
3
2
1
10^5
10^6
10^7
10^8
10^9
PARTICLES / m^3

Fig. IV. 1a

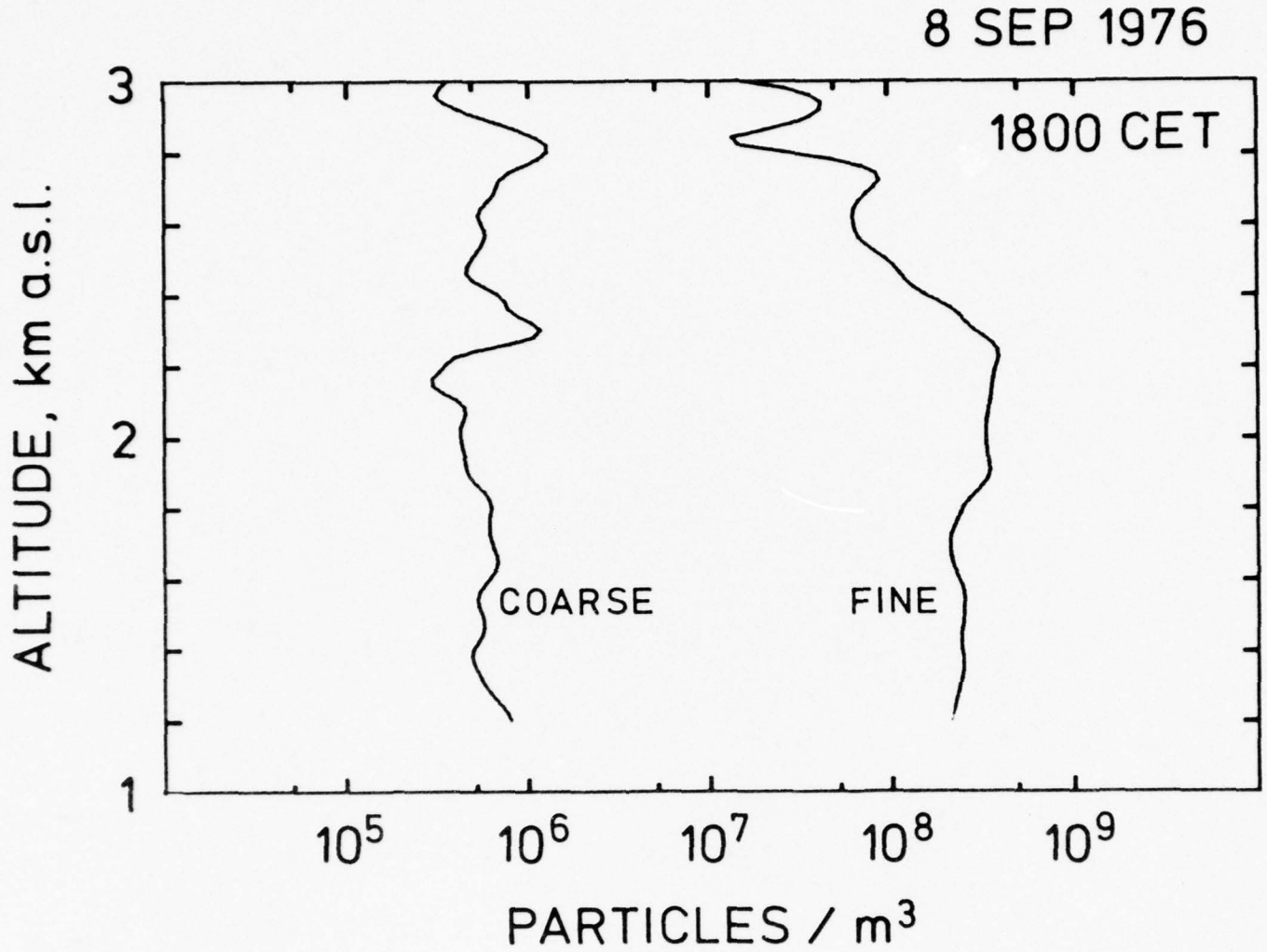
8 SEP 1976
1800 CET
ALTITUDE, km a.s.l.
3
2
1
COARSE
FINE
10^5
10^6
10^7
10^8
10^9
PARTICLES / m^3

Fig.IV.1b

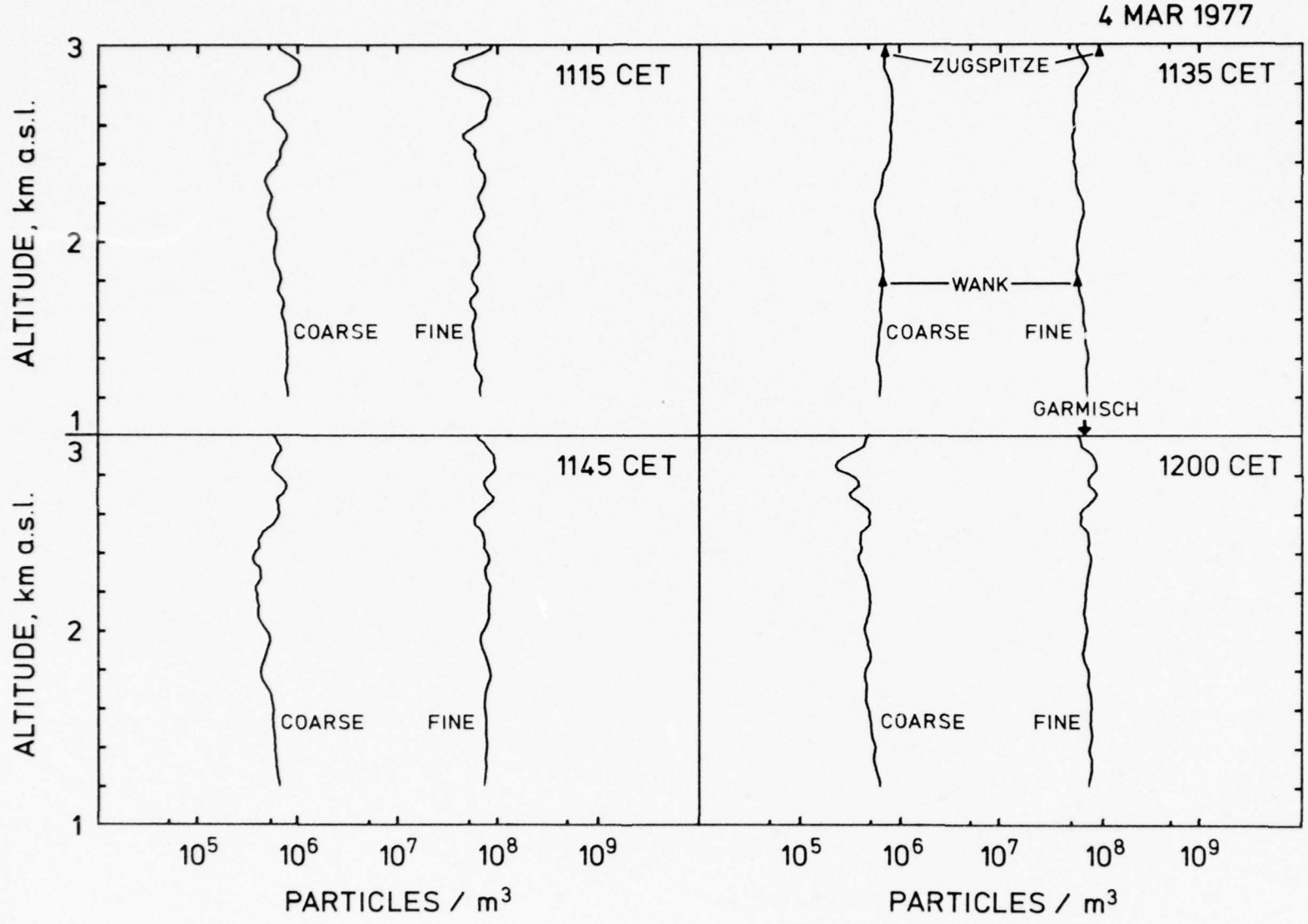
4 MAR 1977
1115 CET
1135 CET
1145 CET
1200 CET
ZUGSPITZE
WANK
GARMISCH
COARSE
FINE
ALTITUDE, km a.s.l.
3
2
1
10^5
10^6
10^7
10^8
10^9
PARTICLES / m^3

Fig. IV. 2a

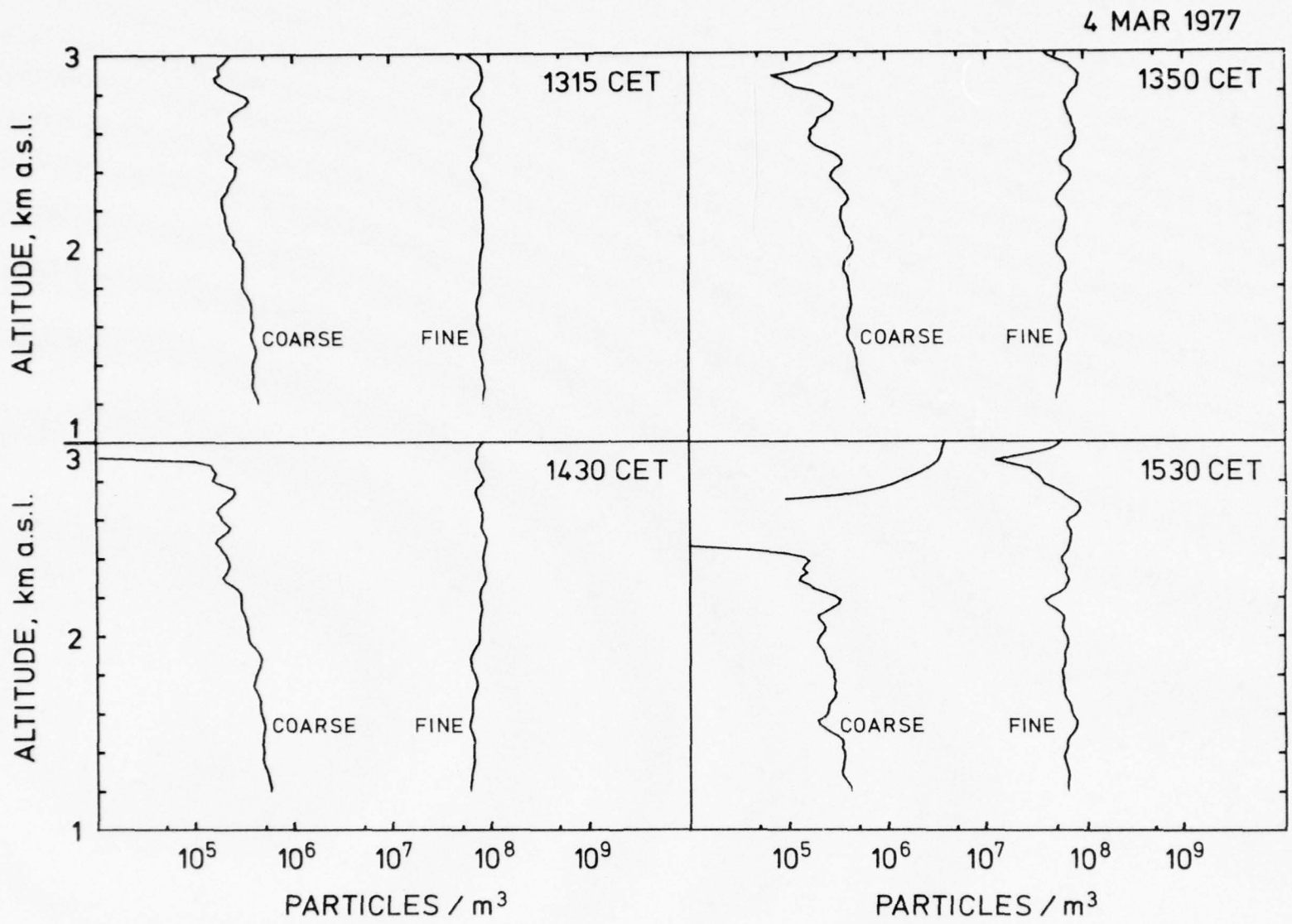
4 MAR 1977
1315 CET
1350 CET
1430 CET
1530 CET
COARSE
FINE
ALTITUDE, km a.s.l.
3
2
1
10^5
10^6
10^7
10^8
10^9
PARTICLES / m^3

Fig. IV. 2b

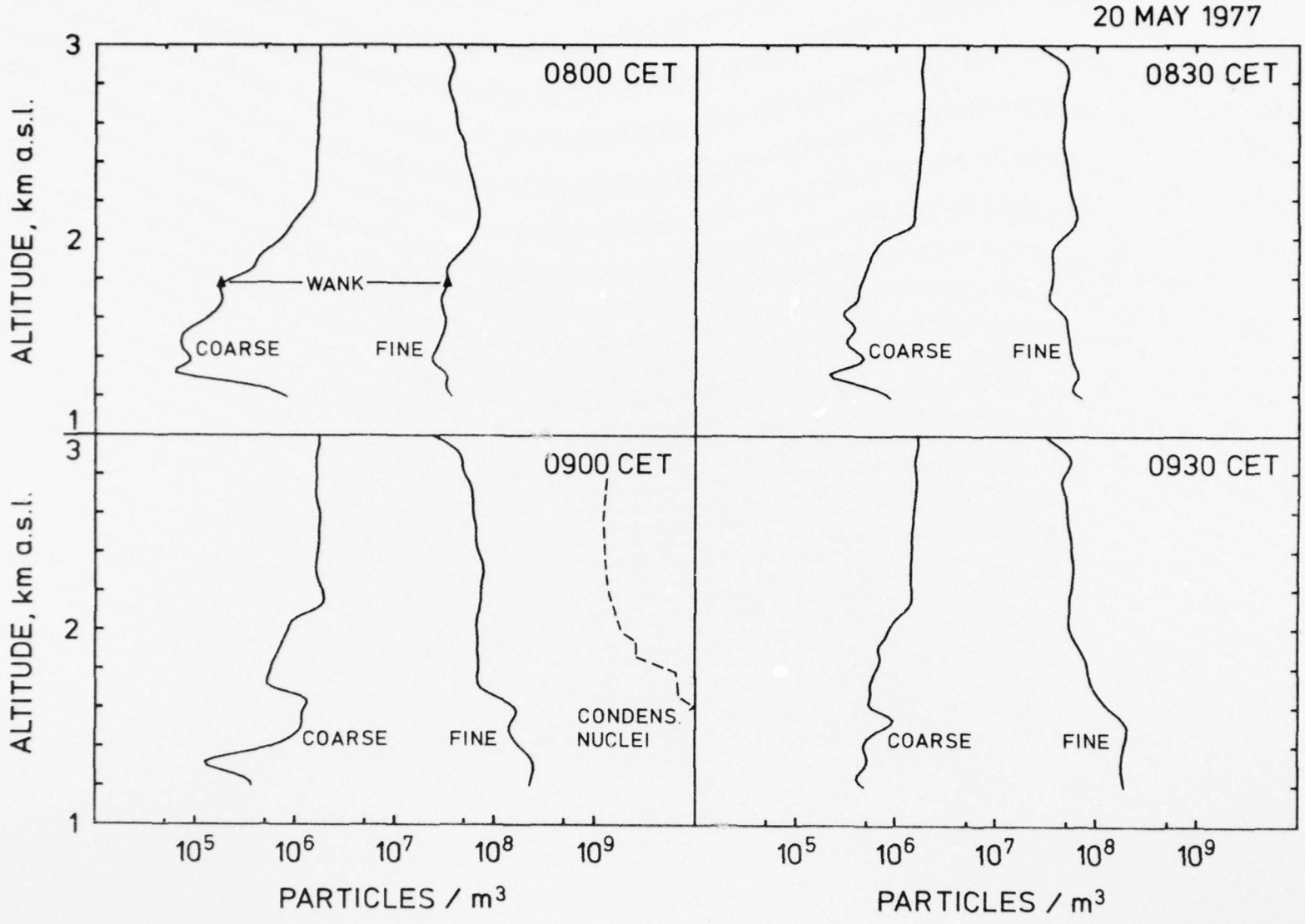
20 MAY 1977
0800 CET
0830 CET
0900 CET
0930 CET
WANK
COARSE
FINE
CONDENS. NUCLEI
ALTITUDE, km a.s.l.
3
2
1
10^5
10^6
10^7
10^8
10^9
PARTICLES / m^3

Fig. IV. 3a

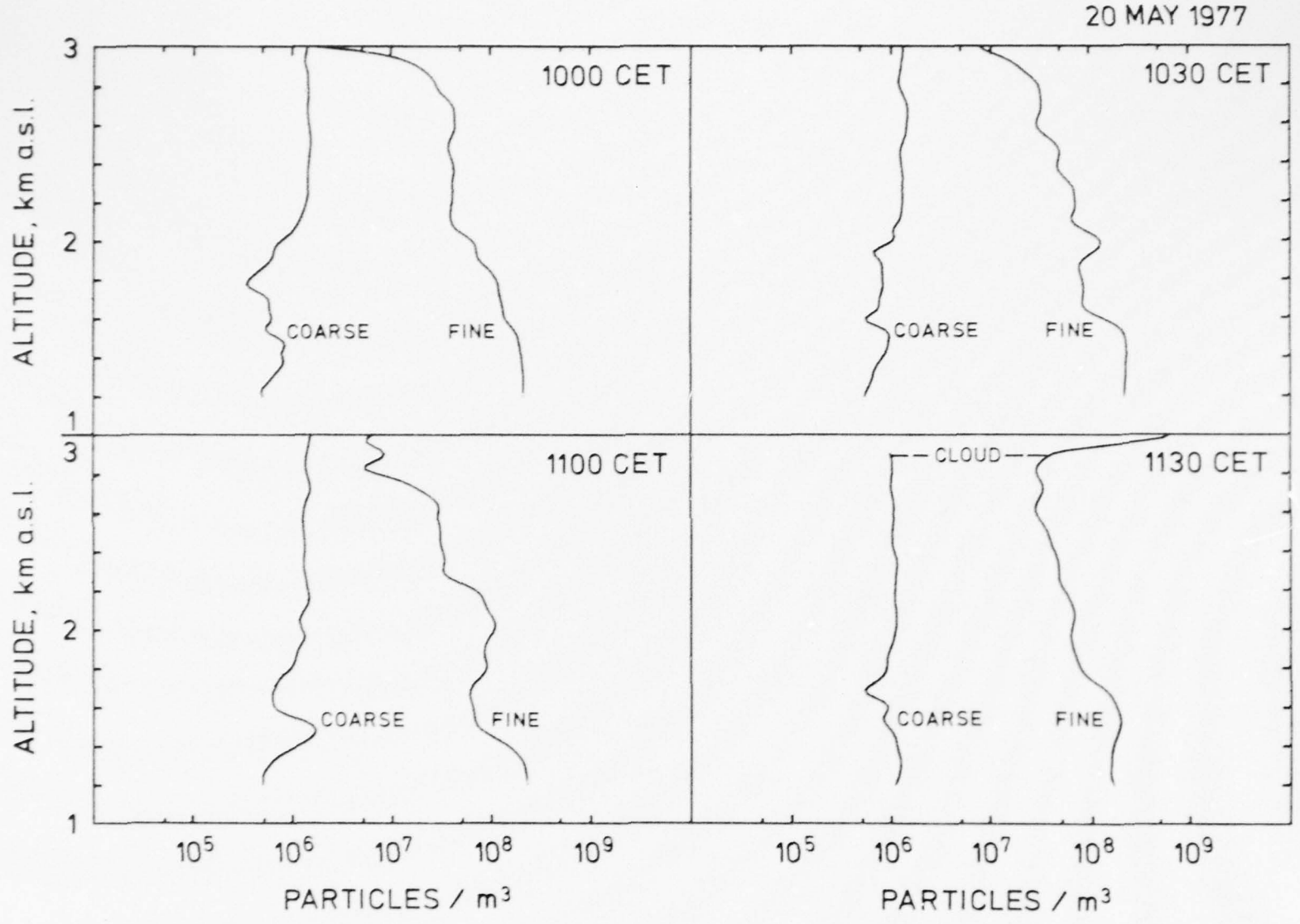
20 MAY 1977
1000 CET
1030 CET
1100 CET
1130 CET
COARSE
FINE
CLOUD
ALTITUDE, km a.s.l.
3
2
1
10^5
10^6
10^7
10^8
10^9
PARTICLES / m^3

Fig. IV. 3b

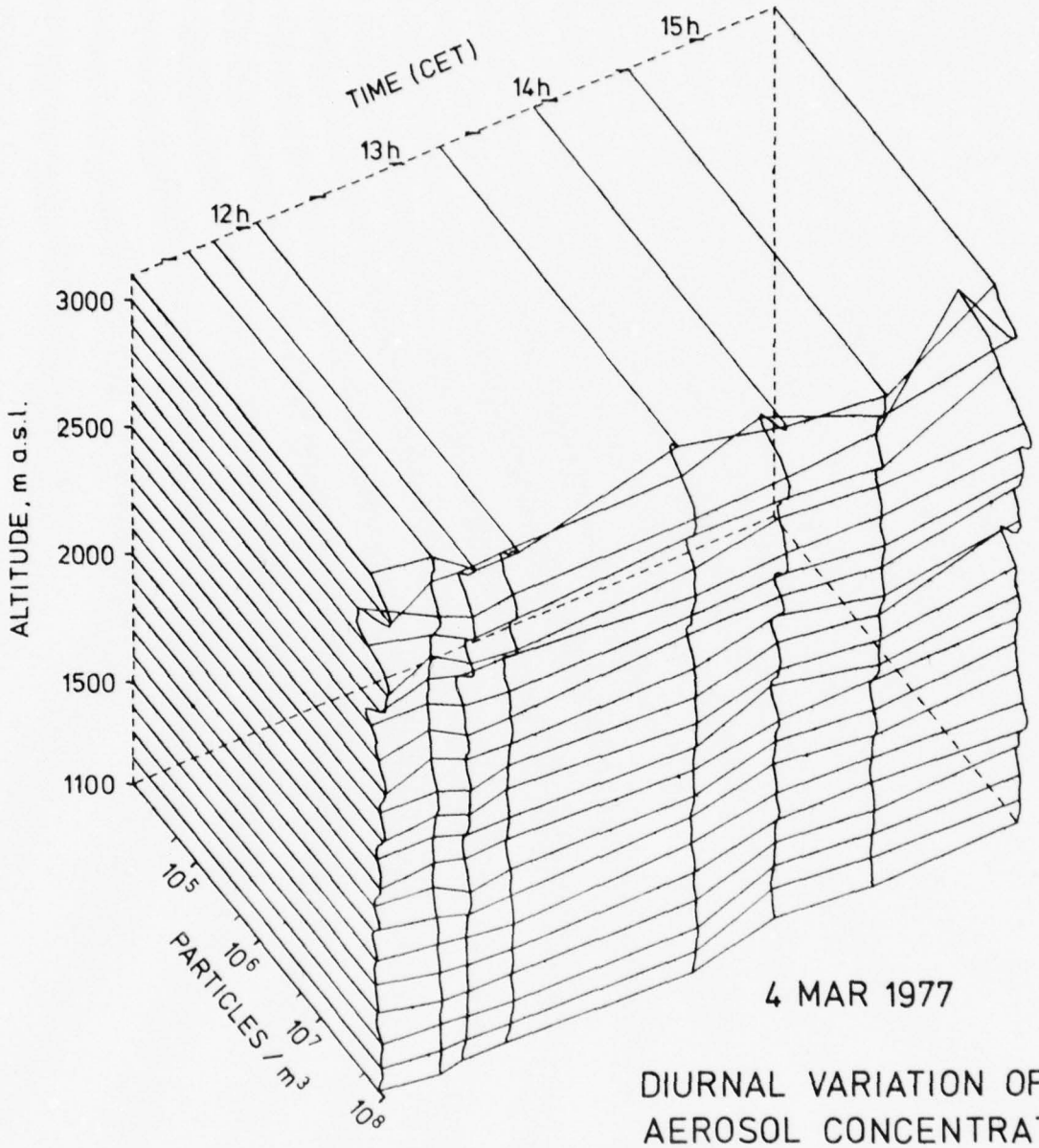

4 MAR 1977

DIURNAL VARIATION OF
AEROSOL CONCENTRATION
(FINE AEROSOL, 0.4 µm)

Fig. IV. 4a

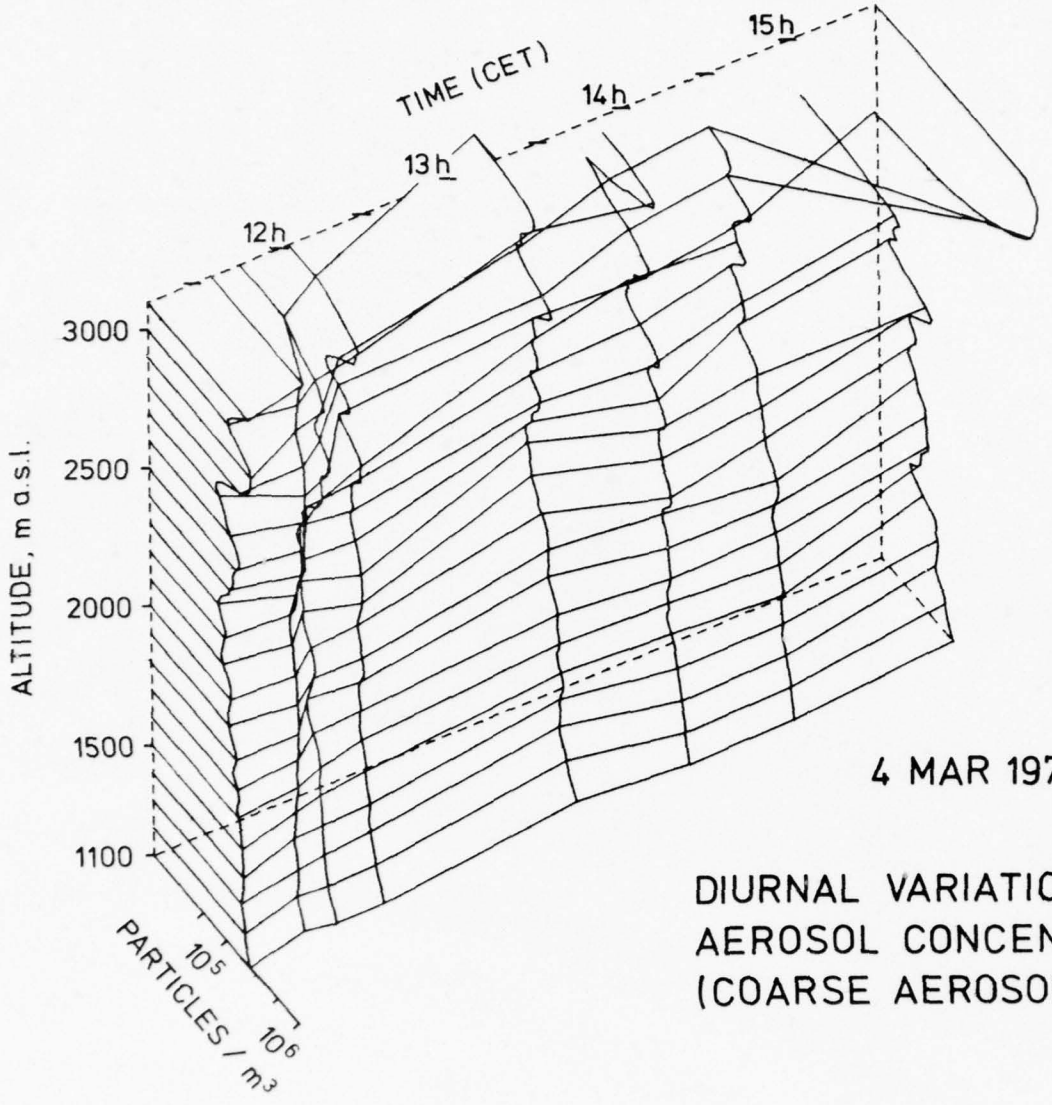

4 MAR 1977

DIURNAL VARIATION OF
AEROSOL CONCENTRATION
(COARSE AEROSOL, 2.0 µm)

Fig. IV. 4b

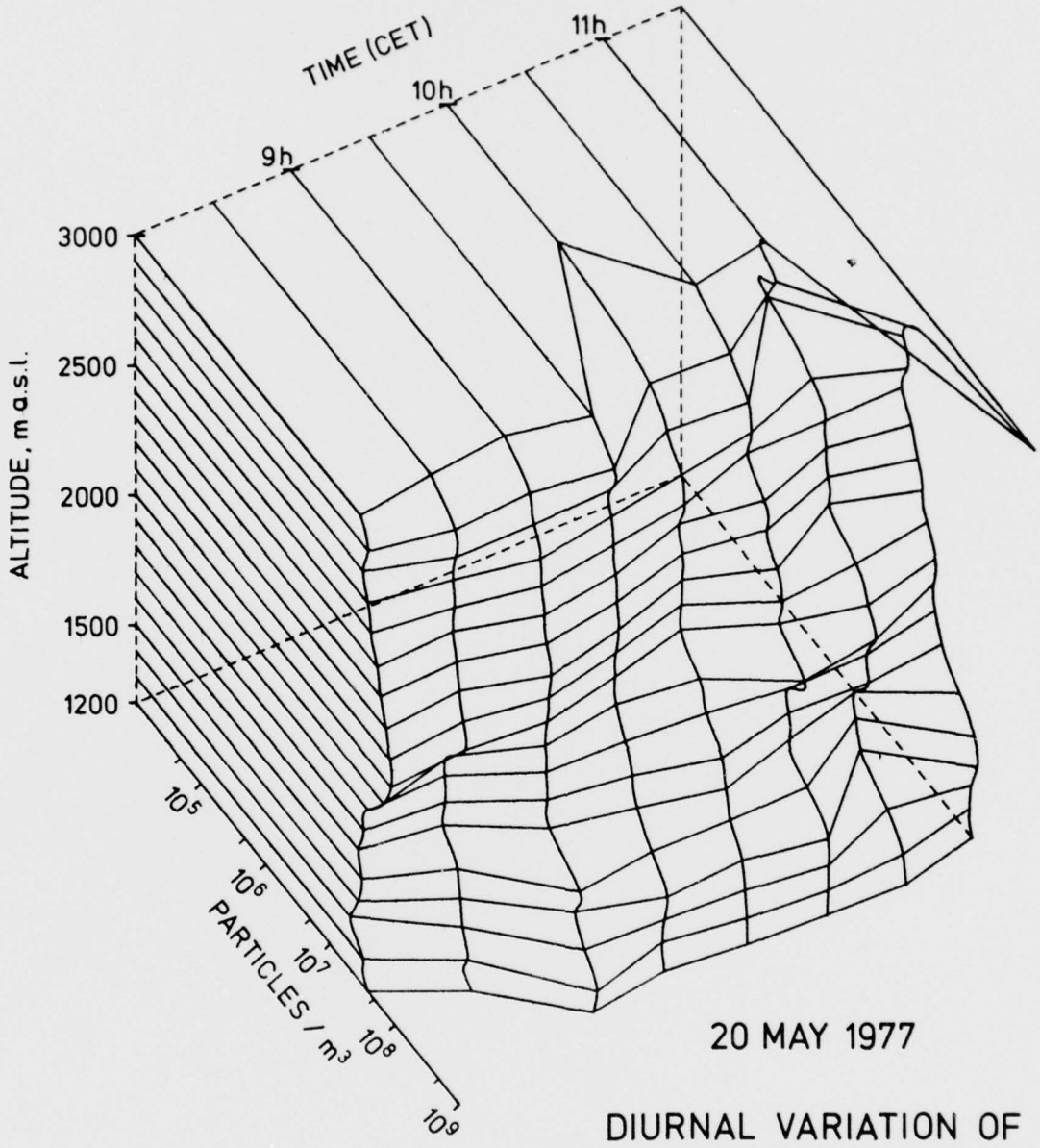

20 MAY 1977

DIURNAL VARIATION OF
AEROSOL CONCENTRATION
(FINE AEROSOL, 0.4 μm)

Fig. IV. 5a

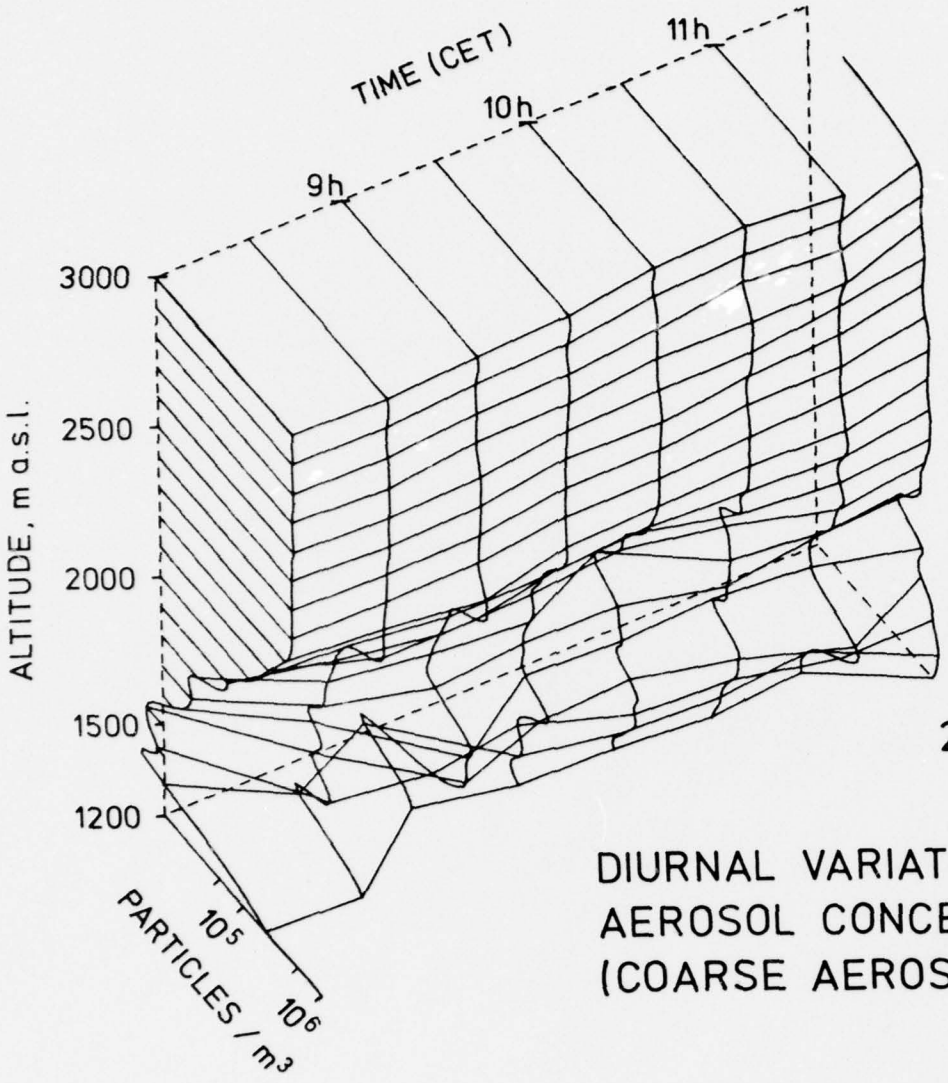

20 MAY 1977

DIURNAL VARIATION OF
AEROSOL CONCENTRATION
(COARSE AEROSOL, 2.0μm)

Fig. IV. 5b

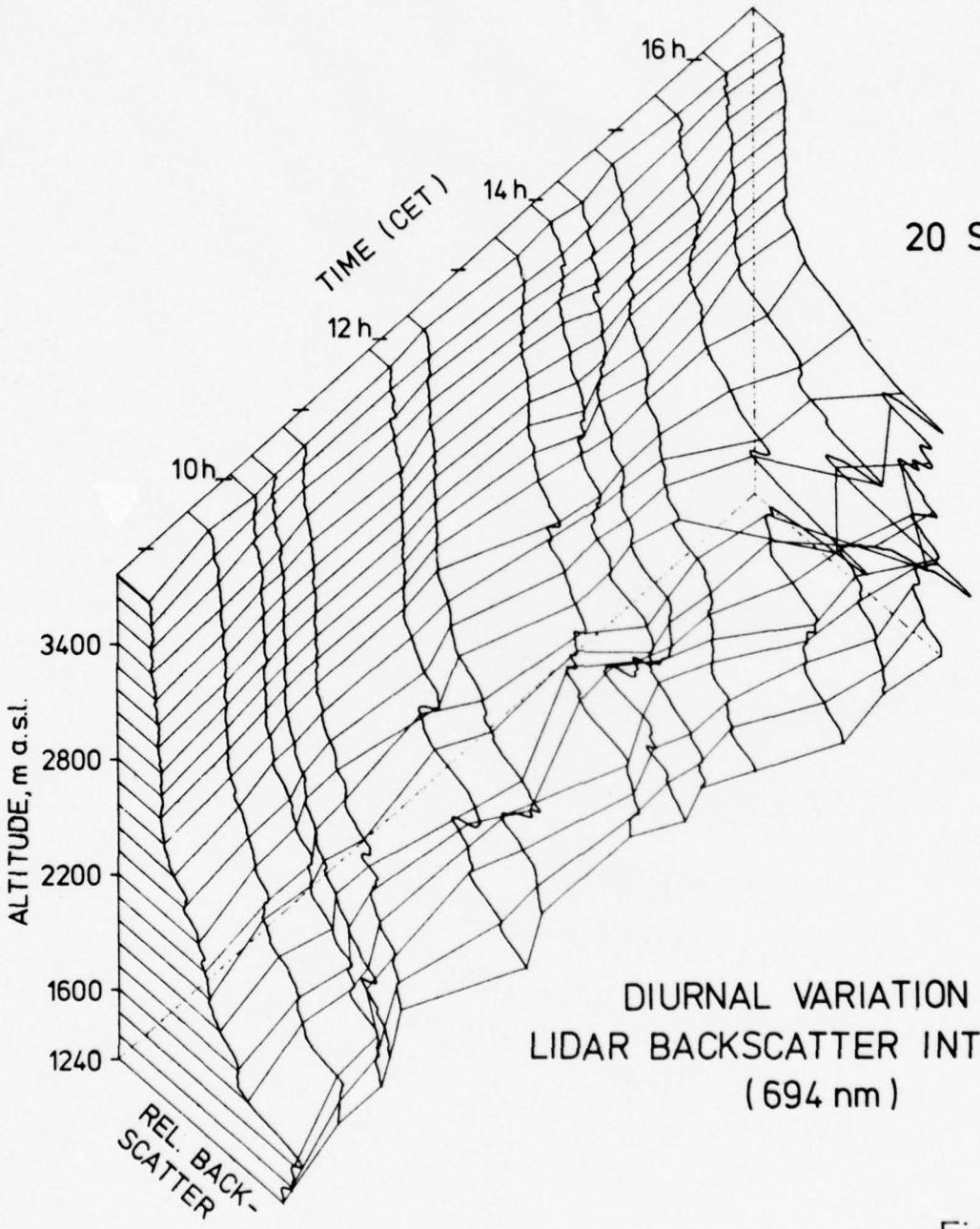

DIURNAL VARIATION OF
LIDAR BACKSCATTER INTENSITY
(694 nm)

Fig. IV. 6a

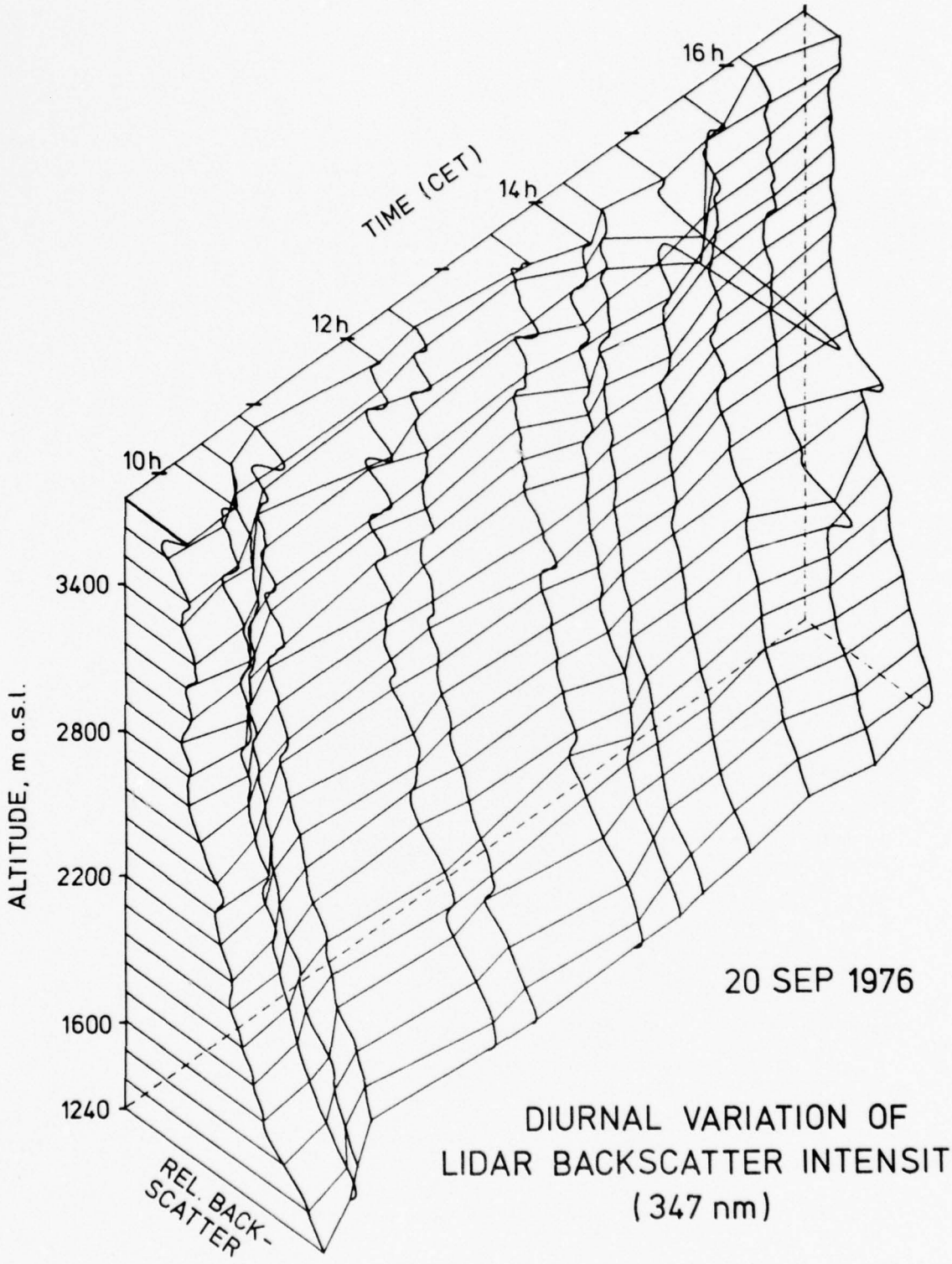

DIURNAL VARIATION OF
LIDAR BACKSCATTER INTENSITY
(347 nm)

Fig. IV. 6b

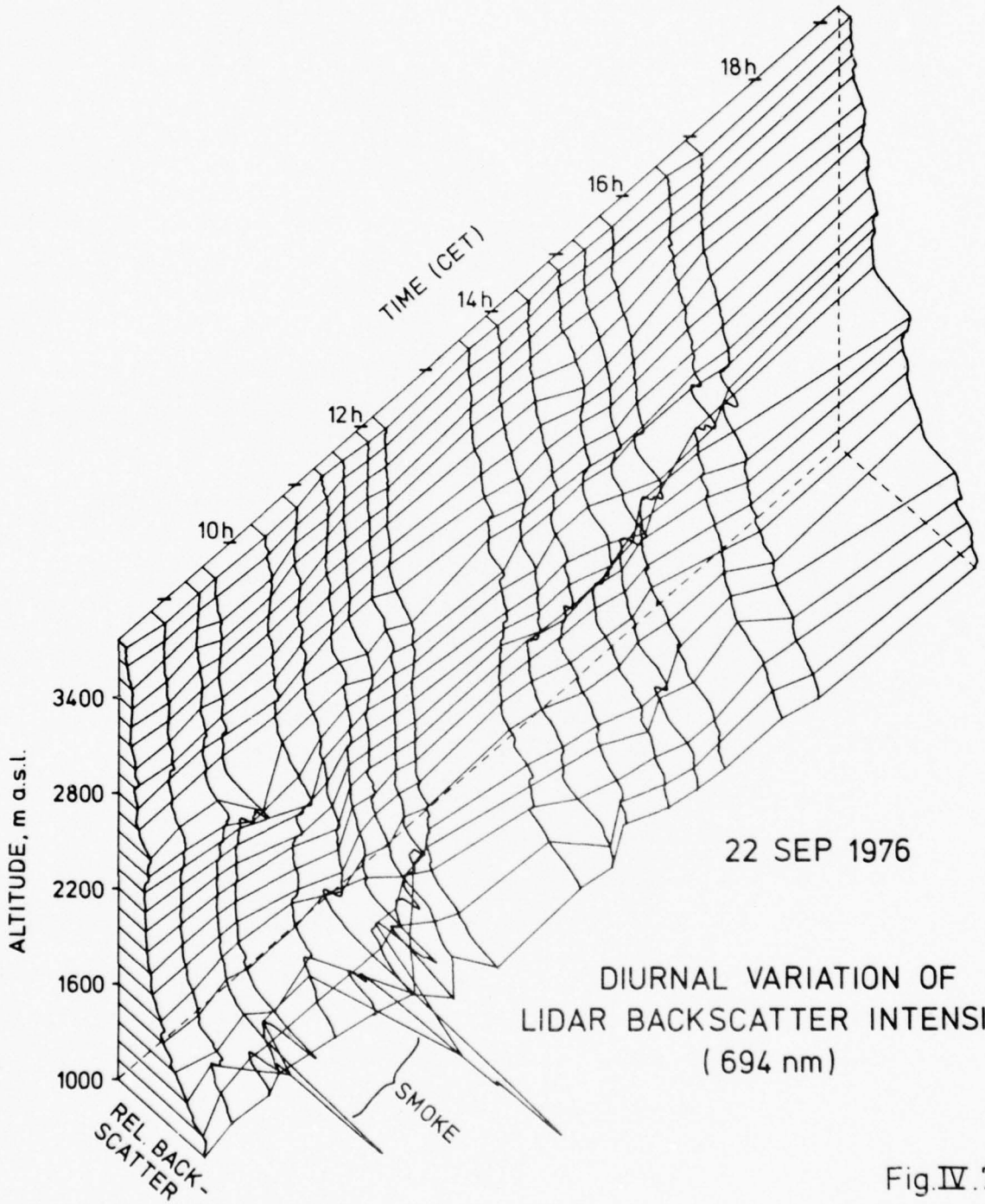

DIURNAL VARIATION OF
LIDAR BACKSCATTER INTENSITY
(694 nm)

Fig.IV.7a

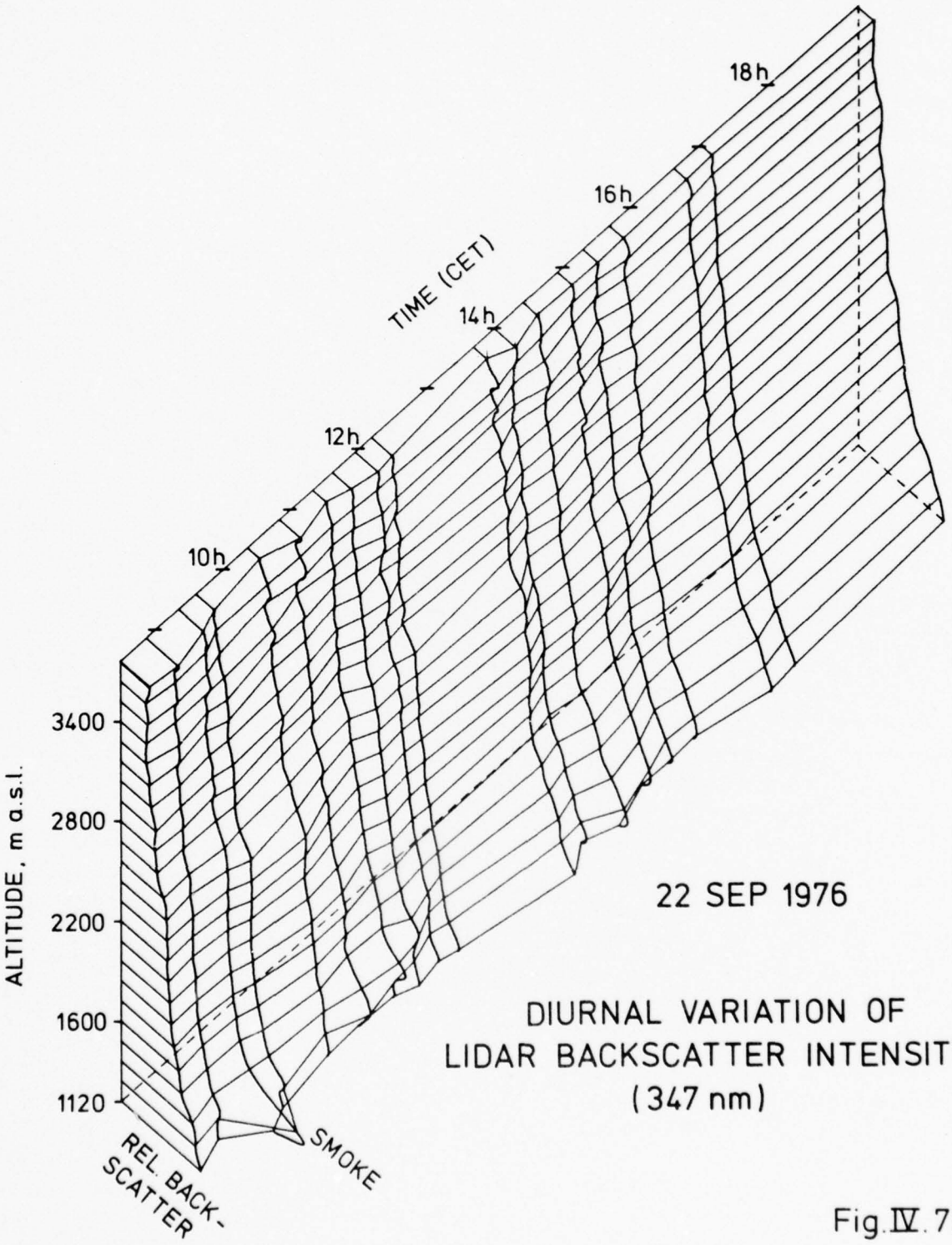

22 SEP 1976

DIURNAL VARIATION OF
LIDAR BACKSCATTER INTENSITY
(347 nm)

Fig. IV. 7b

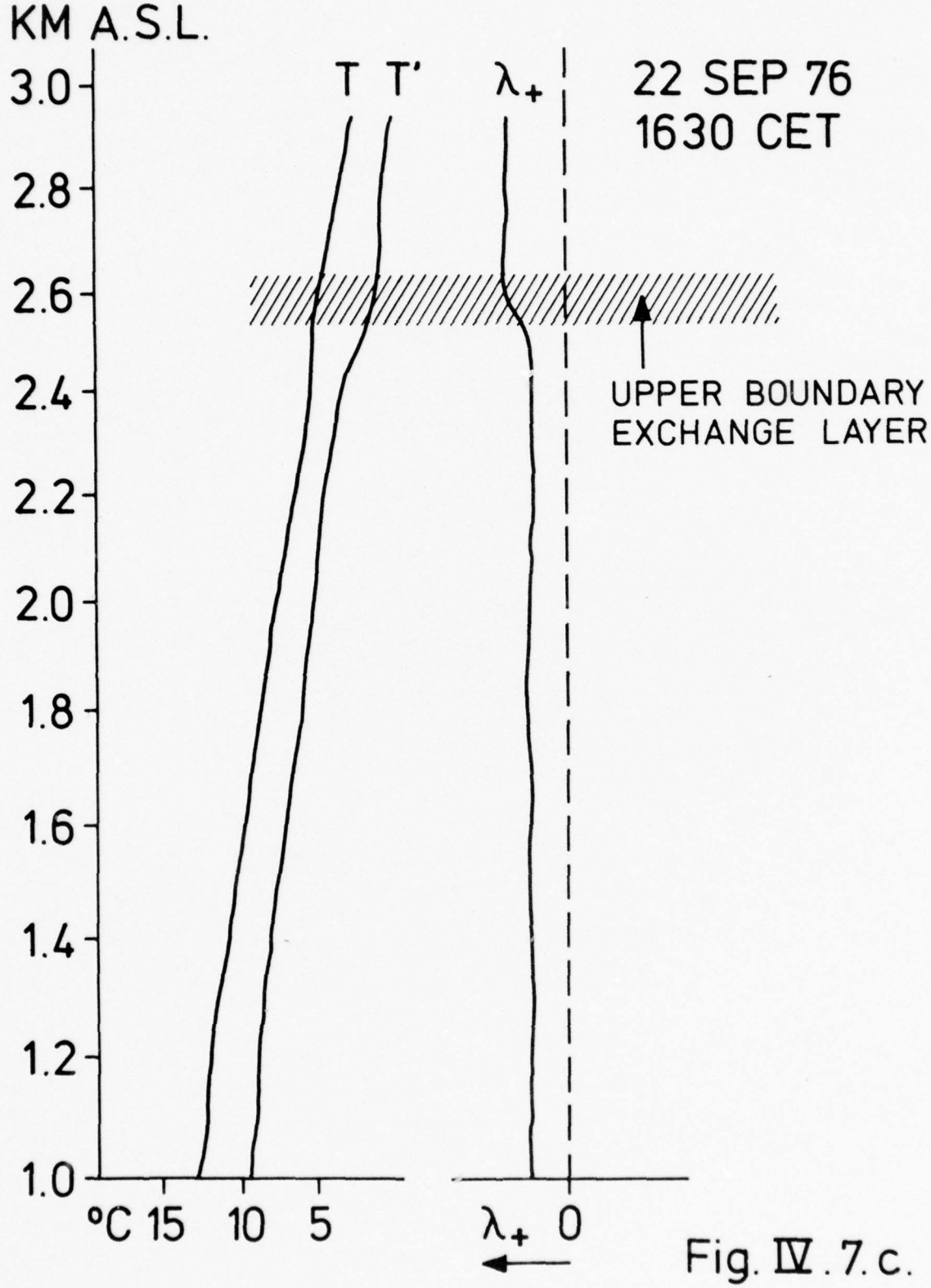
KM A.S.L.
3.0
2.8
2.6
2.4
2.2
2.0
1.8
1.6
1.4
1.2
1.0
T T'
λ+
22 SEP 76
1630 CET
UPPER BOUNDARY
EXCHANGE LAYER
°C 15 10 5
λ+ 0

Fig. IV.7.c.

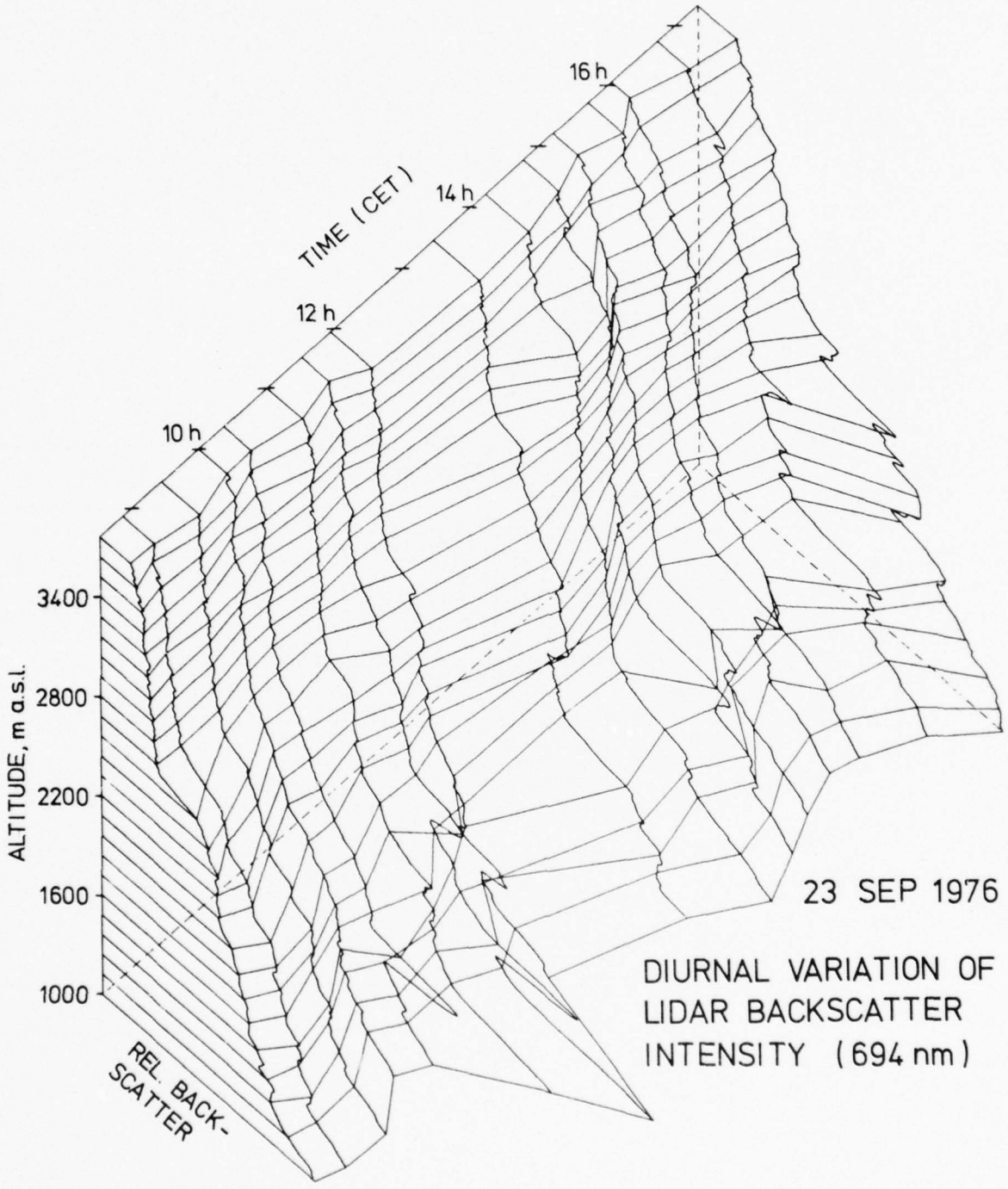
16 h
TIME (CET)
14 h
12 h
10 h
3400
2800
2200
1600
1000
ALTITUDE, m a.s.l.
REL. BACK-
SCATTER
23 SEP 1976
DIURNAL VARIATION OF
LIDAR BACKSCATTER
INTENSITY (694 nm)

Fig. IV. 8

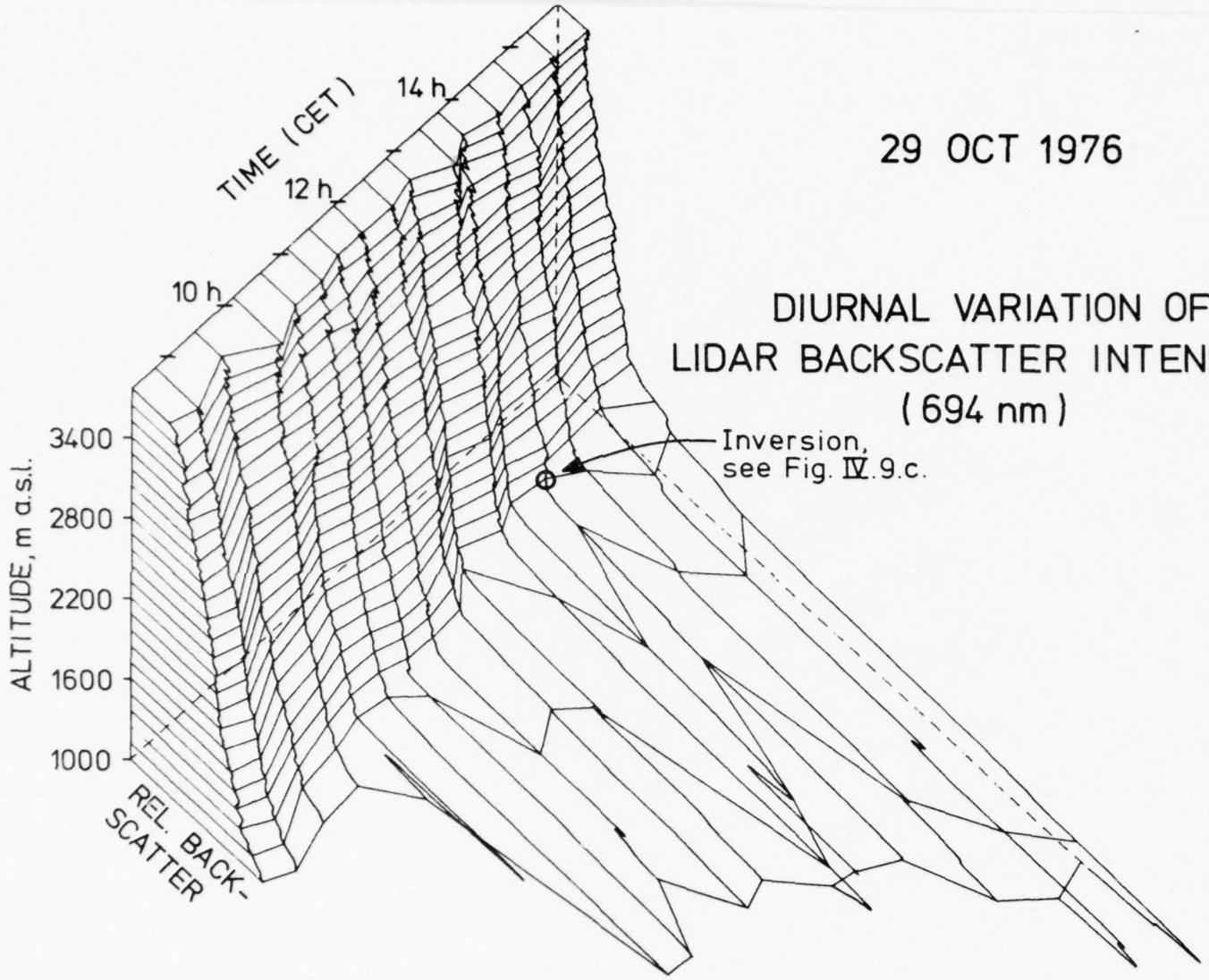
29 OCT 1976
DIURNAL VARIATION OF
LIDAR BACKSCATTER INTENSITY
(694 nm)
TIME (CET)
10 h
12 h
14 h
ALTITUDE, m a.s.l.
3400
2800
2200
1600
1000
REL. BACK-
SCATTER
Inversion,
see Fig. IV.9.c.

Fig.IV.9a

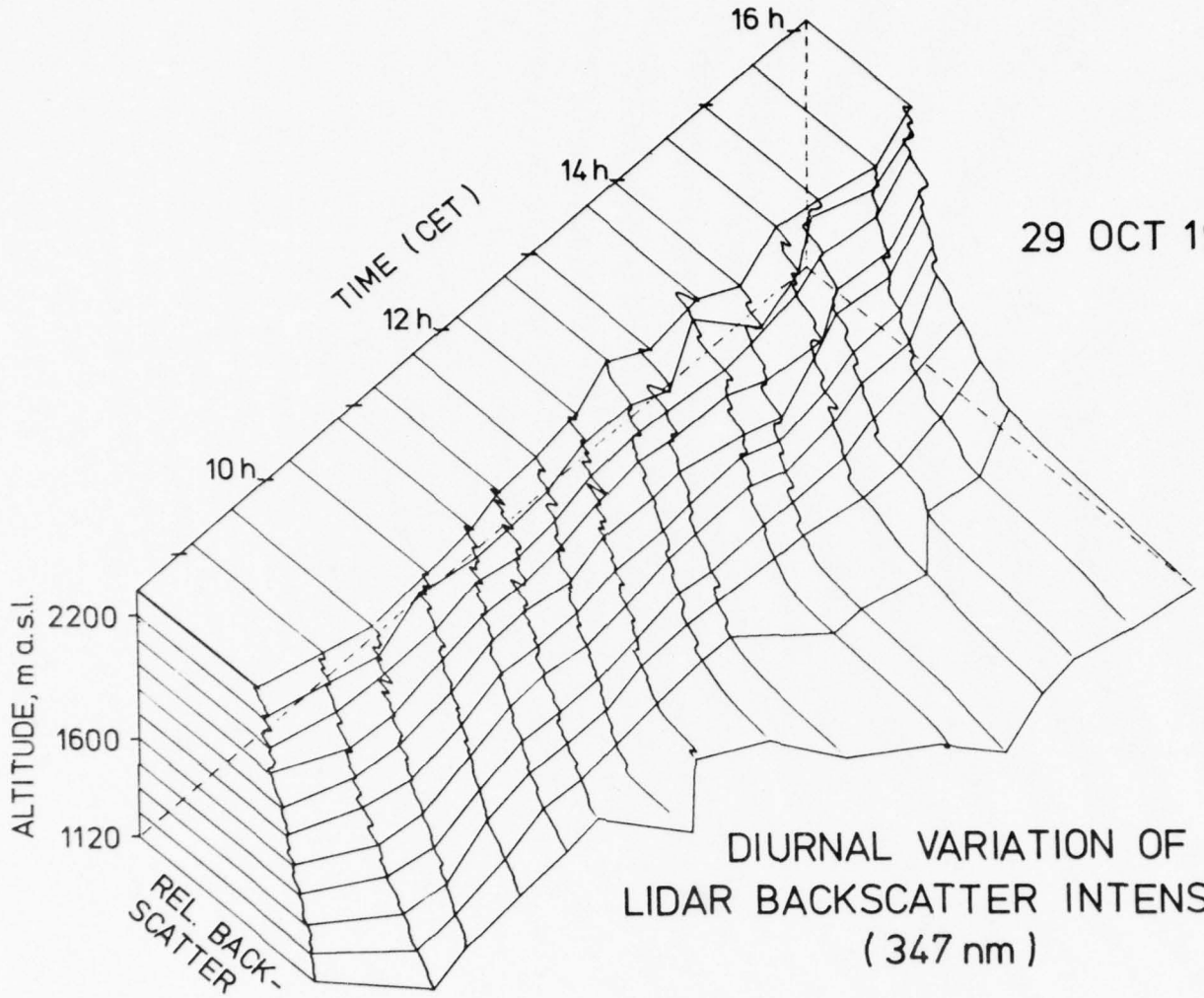

DIURNAL VARIATION OF
LIDAR BACKSCATTER INTENSITY
(347 nm)

Fig. IV.9b

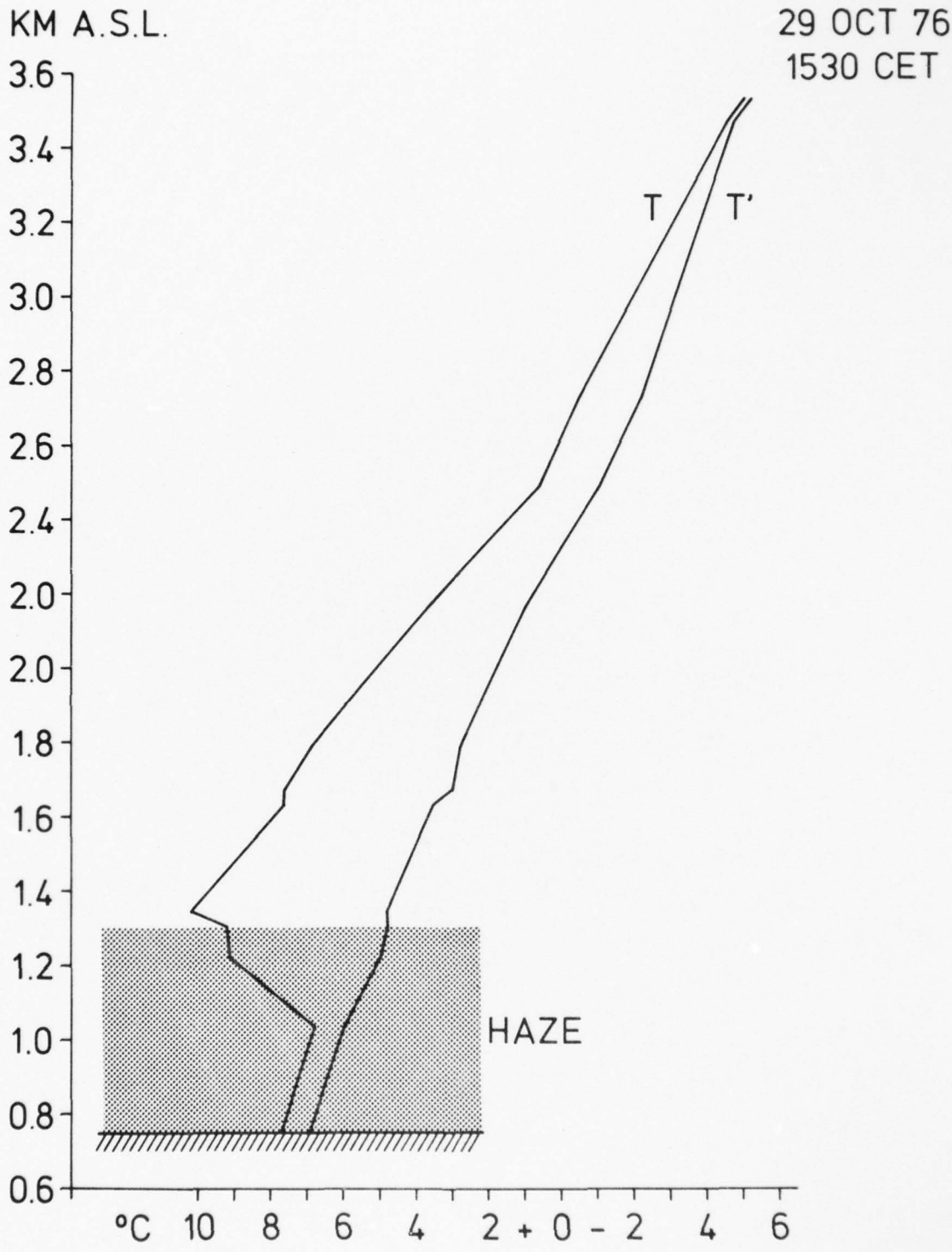
KM A.S.L.
29 OCT 76
1530 CET
3.6
3.4
3.2
3.0
2.8
2.6
2.4
2.0
2.0
1.8
1.6
1.4
1.2
1.0
0.8
0.6
T
T'
HAZE
°C 10 8 6 4 2 + 0 - 2 4 6

Fig. IV.9.c.

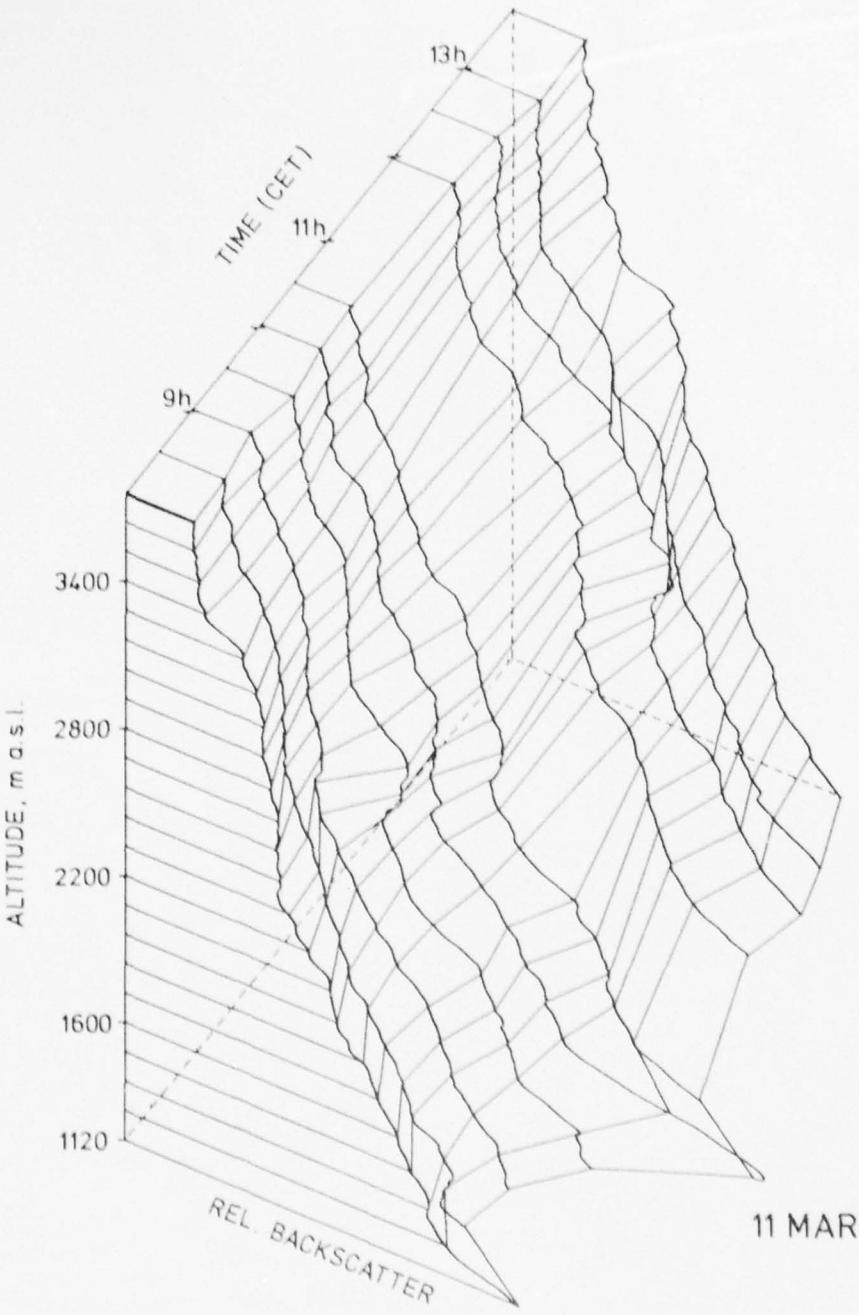

11 MAR 1977

DIURNAL VARIATION OF
LIDAR BACKSCATTER INTENSITY
(694 nm)

Fig. IV. 10a

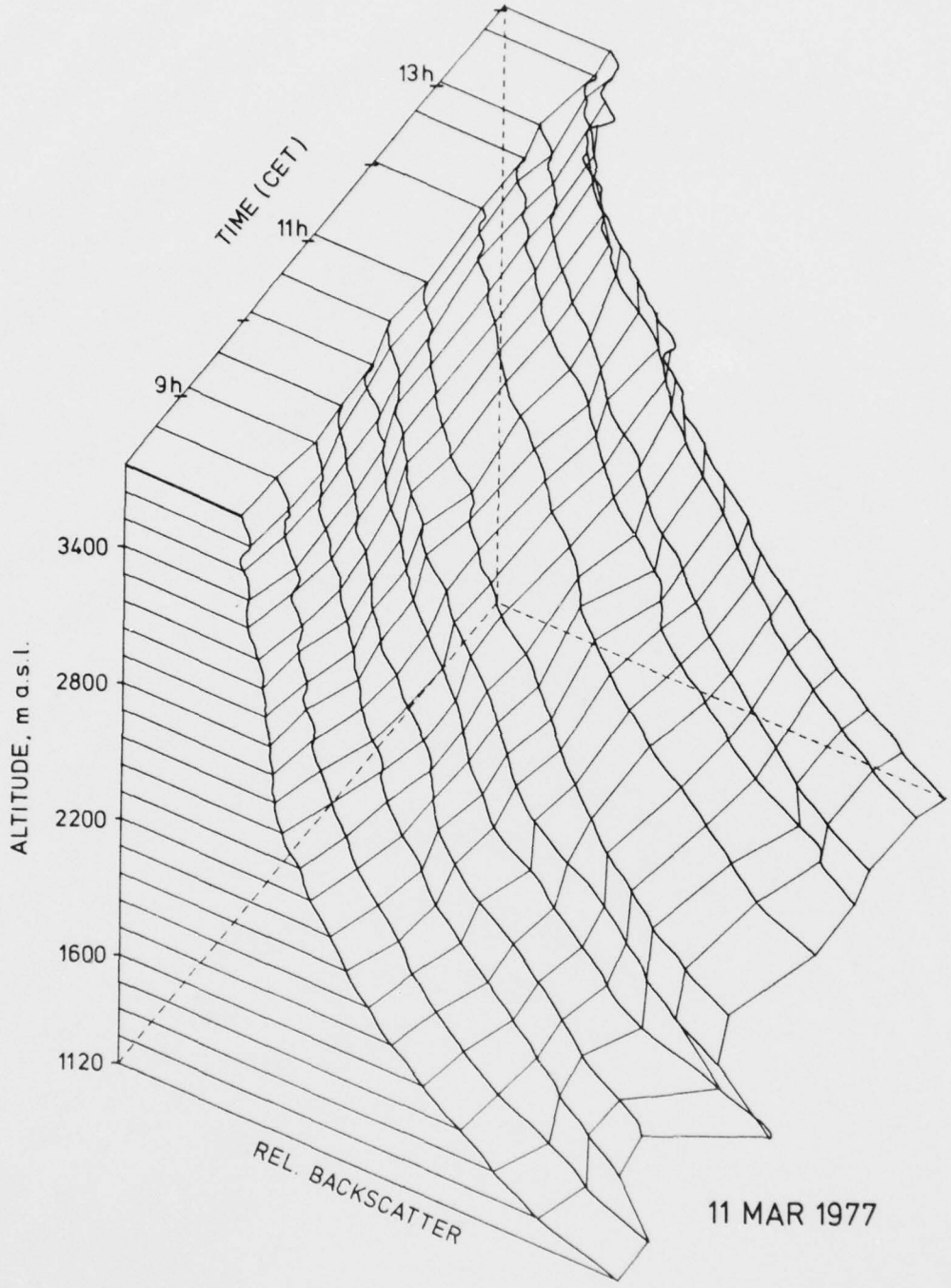

DIURNAL VARIATION OF
LIDAR BACKSCATTER INTENSITY
(347 nm)

Fig. IV. 10b

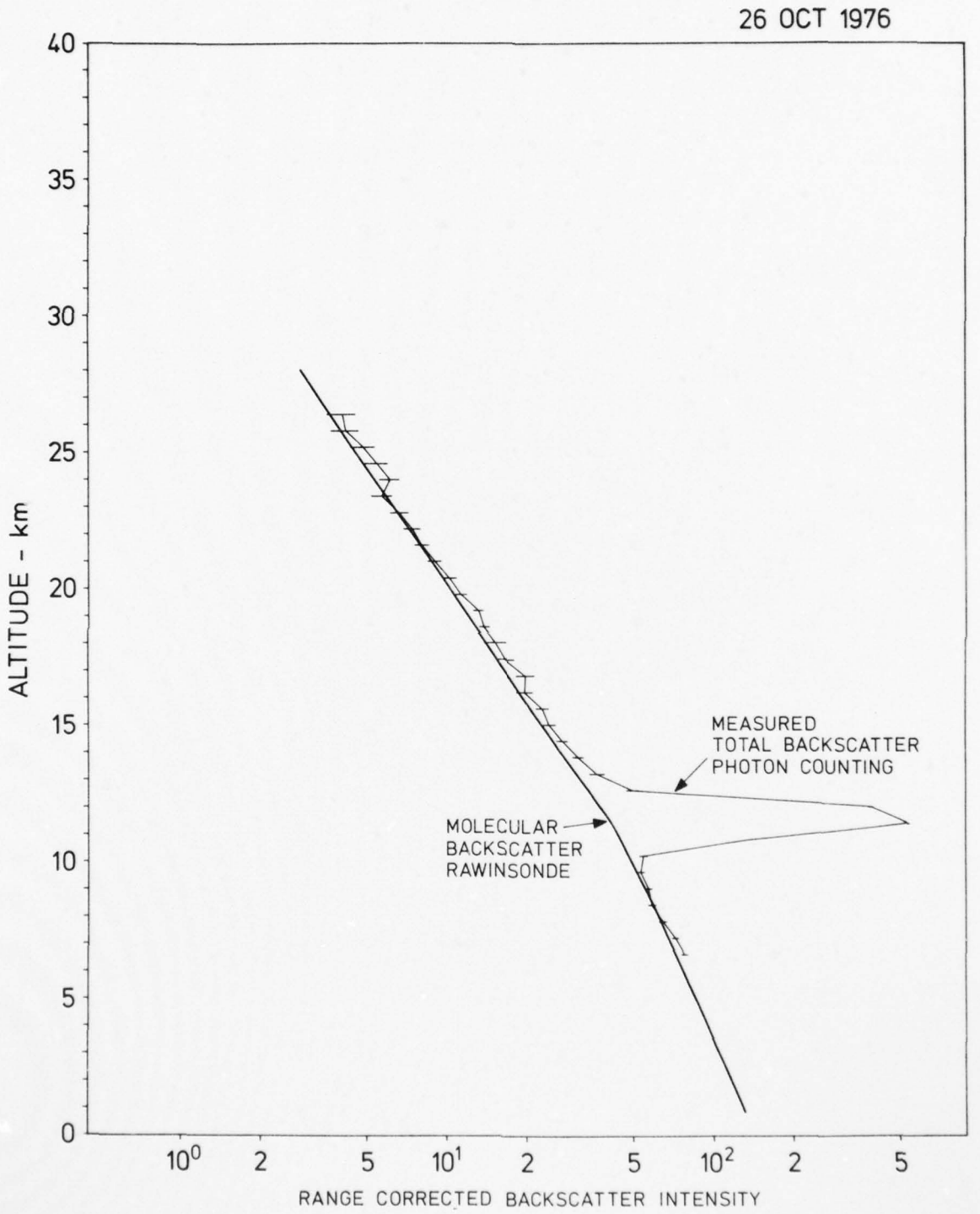
LIDAR BACKSCATTER PROFILE AND COMPUTED MOLECULAR RETURN
26 OCT 1976
ALTITUDE - km
40
35
30
25
20
15
10
5
0
MEASURED
TOTAL BACKSCATTER
PHOTON COUNTING
MOLECULAR
BACKSCATTER
RAWINSONDE
10^0
2
5
10^1
2
5
10^2
2
5
RANGE CORRECTED BACKSCATTER INTENSITY

Fig.IV.11

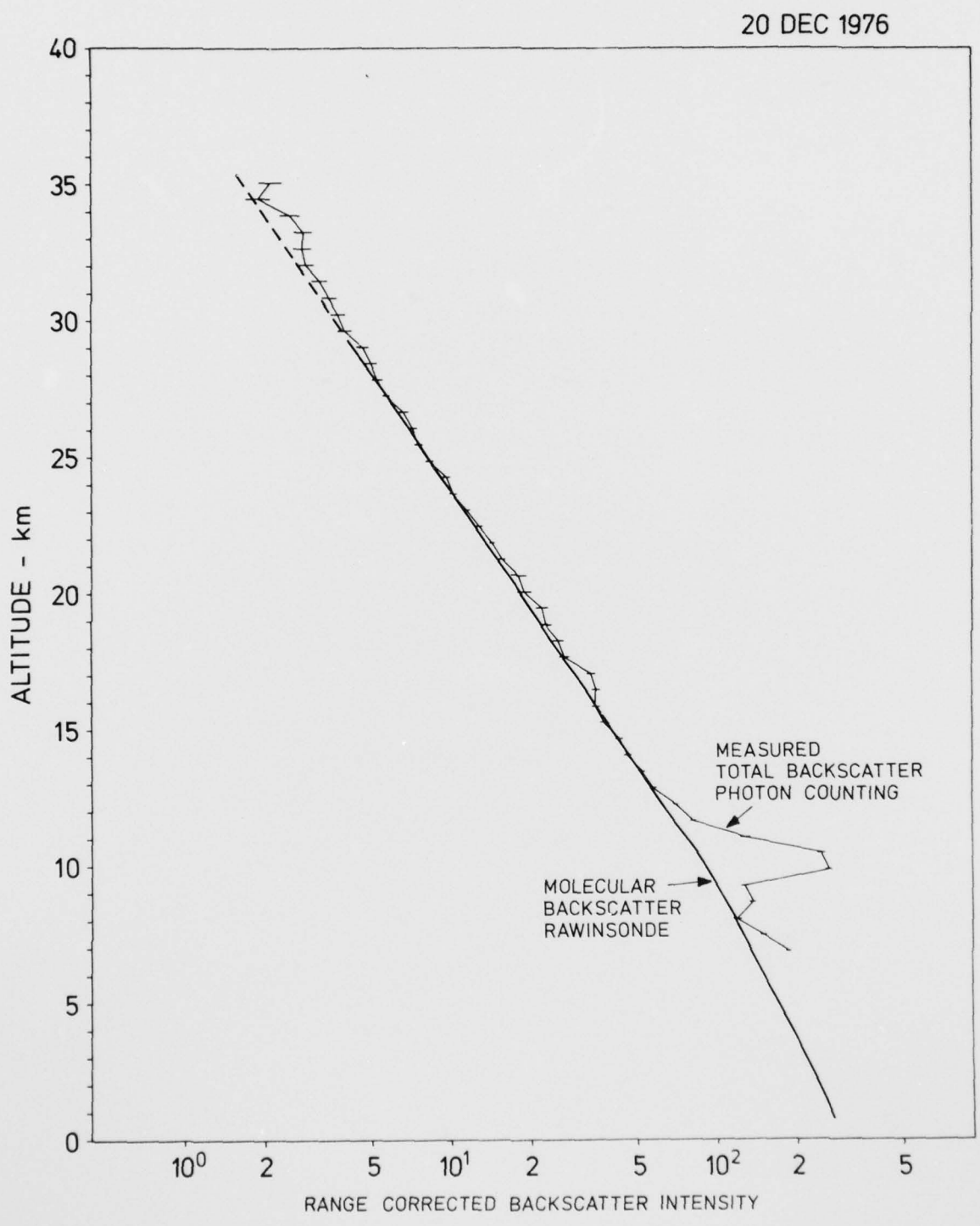
LIDAR BACKSCATTER PROFILE AND COMPUTED MOLECULAR RETURN
20 DEC 1976
ALTITUDE - km
40
35
30
25
20
15
10
5
0
MEASURED
TOTAL BACKSCATTER
PHOTON COUNTING
MOLECULAR
BACKSCATTER
RAWINSONDE
10^0
2
5
10^1
2
5
10^2
2
5
RANGE CORRECTED BACKSCATTER INTENSITY

Fig.IV.12

LIDAR BACKSCATTER PROFILE AND COMPUTED MOLECULAR RETURN

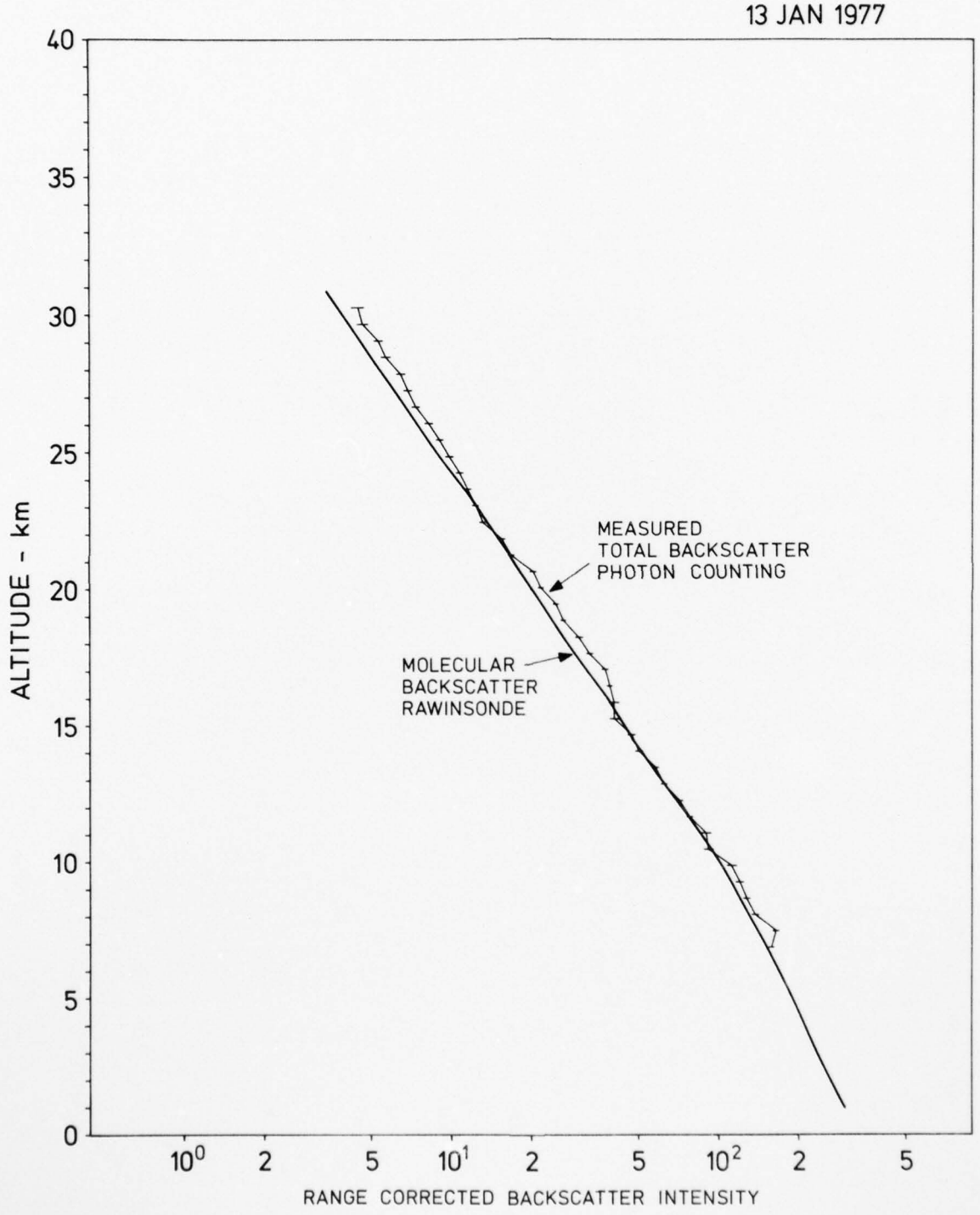

Fig.IV.13

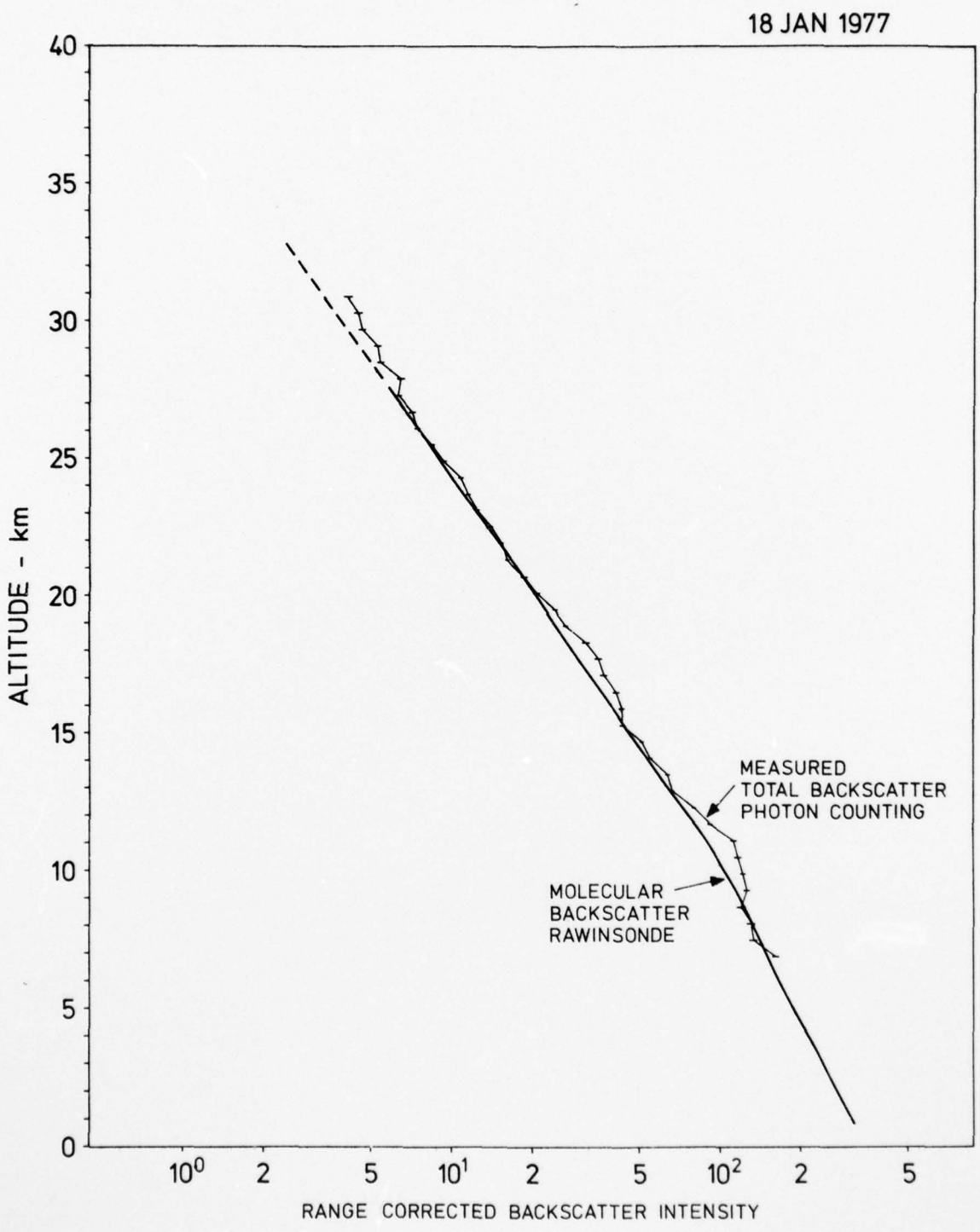
LIDAR BACKSCATTER PROFILE AND COMPUTED MOLECULAR RETURN
18 JAN 1977
ALTITUDE - km
40
35
30
25
20
15
10
5
0
MEASURED
TOTAL BACKSCATTER
PHOTON COUNTING
MOLECULAR
BACKSCATTER
RAWINSONDE
10^0
2
5
10^1
2
5
10^2
2
5
RANGE CORRECTED BACKSCATTER INTENSITY

Fig.IV.14

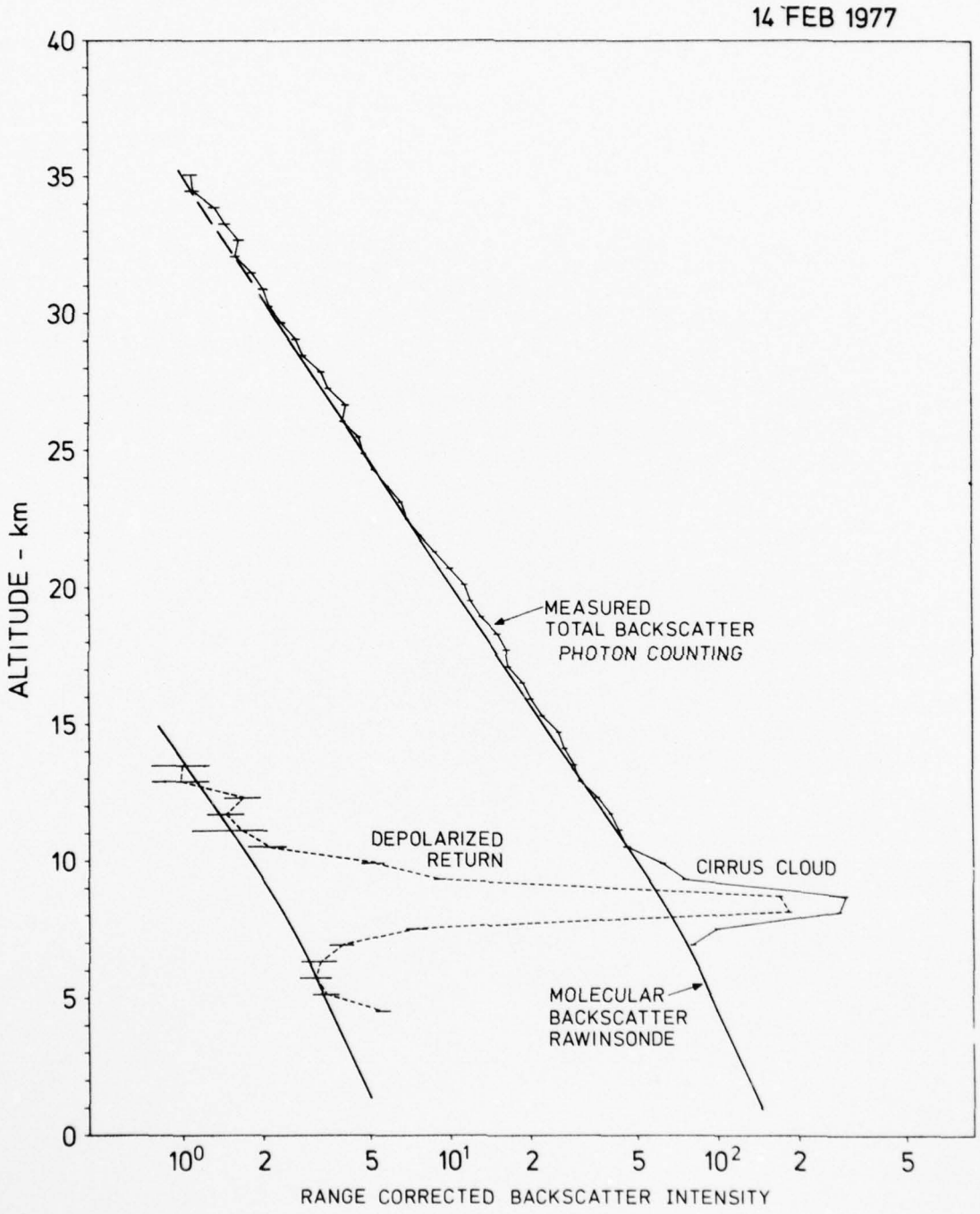
LIDAR BACKSCATTER PROFILE AND COMPUTED MOLECULAR RETURN
14 FEB 1977
ALTITUDE - km
40
35
30
25
20
15
10
5
0
MEASURED
TOTAL BACKSCATTER
PHOTON COUNTING
DEPOLARIZED
RETURN
CIRRUS CLOUD
MOLECULAR
BACKSCATTER
RAWINSONDE
10^0
2
5
10^1
2
5
10^2
2
5
RANGE CORRECTED BACKSCATTER INTENSITY

Fig.IV.15

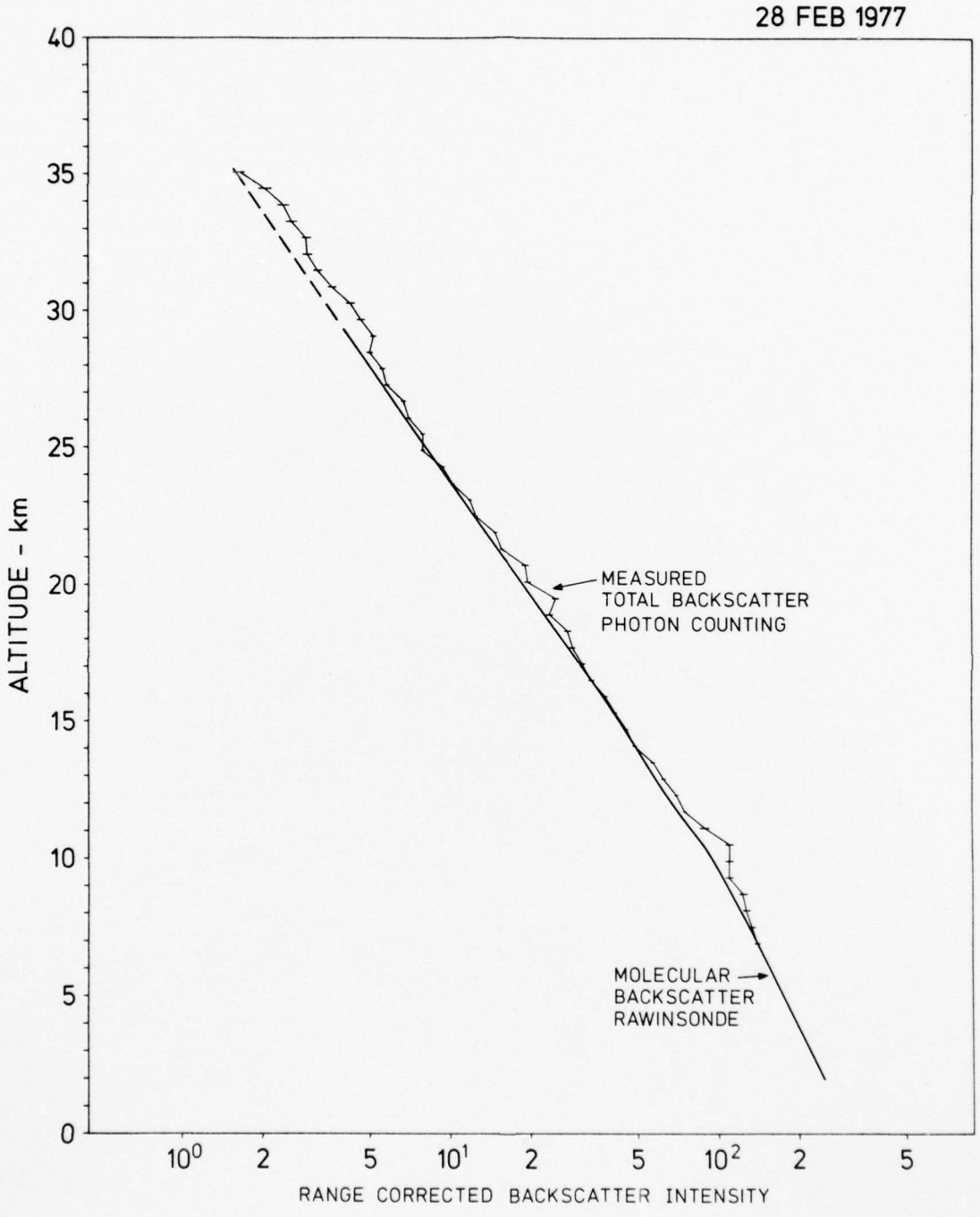
LIDAR BACKSCATTER PROFILE AND COMPUTED MOLECULAR RETURN
28 FEB 1977
ALTITUDE - km
40
35
30
25
20
15
10
5
0
MEASURED
TOTAL BACKSCATTER
PHOTON COUNTING
MOLECULAR
BACKSCATTER
RAWINSONDE
10^0 2 5 10^1 2 5 10^2 2 5
RANGE CORRECTED BACKSCATTER INTENSITY

Fig.IV.16

LIDAR BACKSCATTER PROFILE AND COMPUTED MOLECULAR RETURN

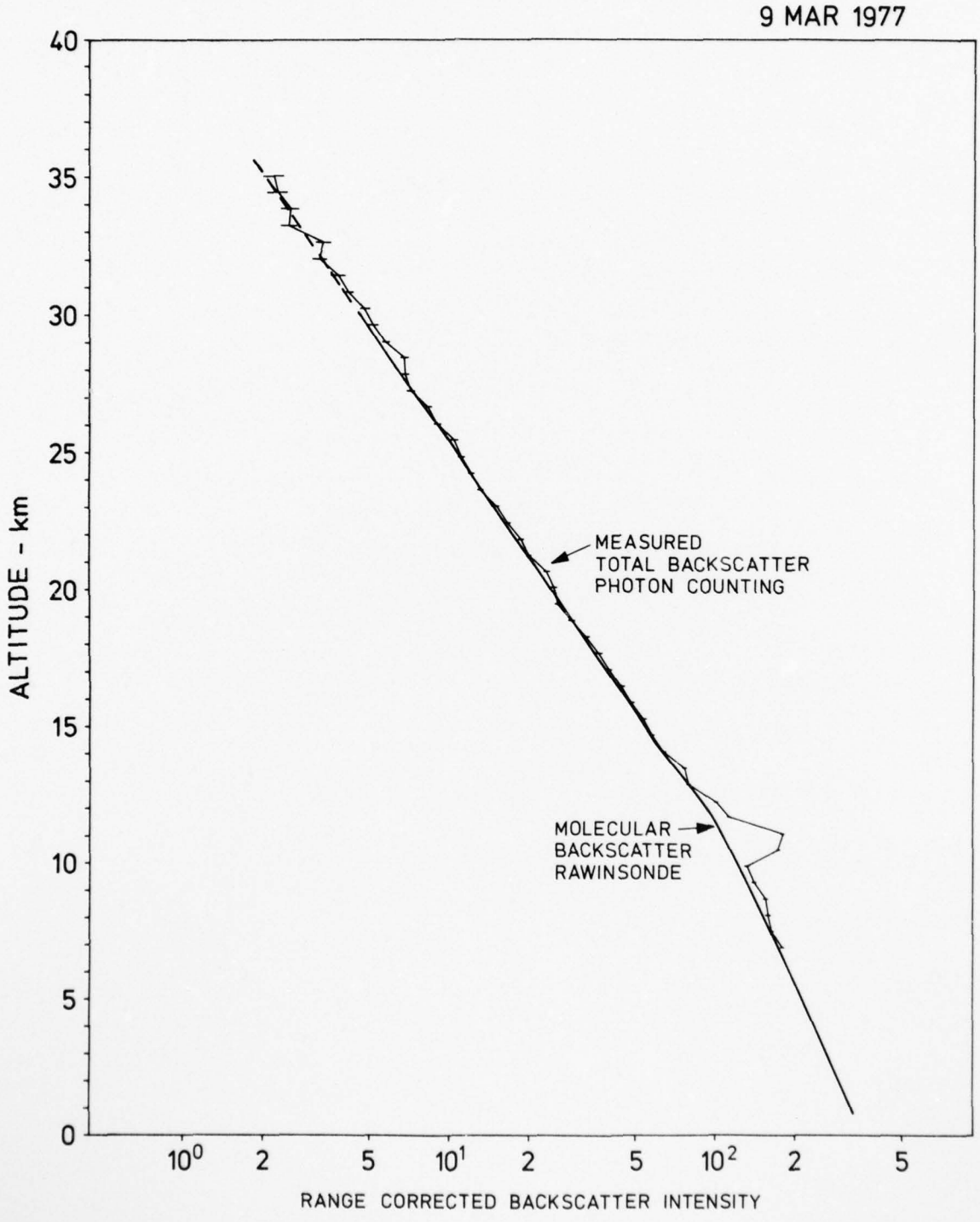

Fig.IV.17

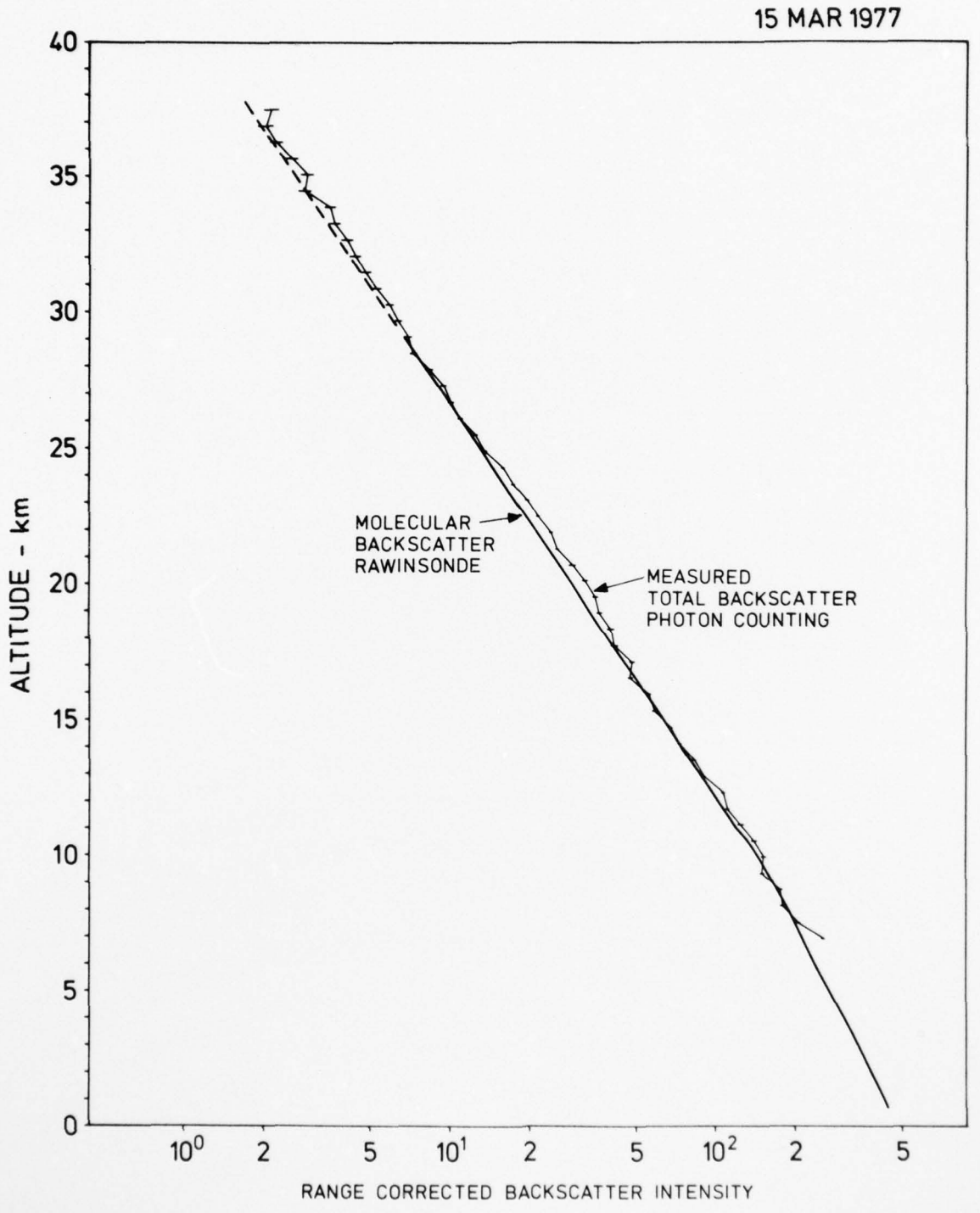
LIDAR BACKSCATTER PROFILE AND COMPUTED MOLECULAR RETURN
15 MAR 1977
ALTITUDE - km
40
35
30
25
20
15
10
5
0
MOLECULAR
BACKSCATTER
RAWINSONDE
MEASURED
TOTAL BACKSCATTER
PHOTON COUNTING
10^0
2
5
10^1
2
5
10^2
2
5
RANGE CORRECTED BACKSCATTER INTENSITY

Fig.IV.18

LIDAR BACKSCATTER PROFILE AND COMPUTED MOLECULAR RETURN

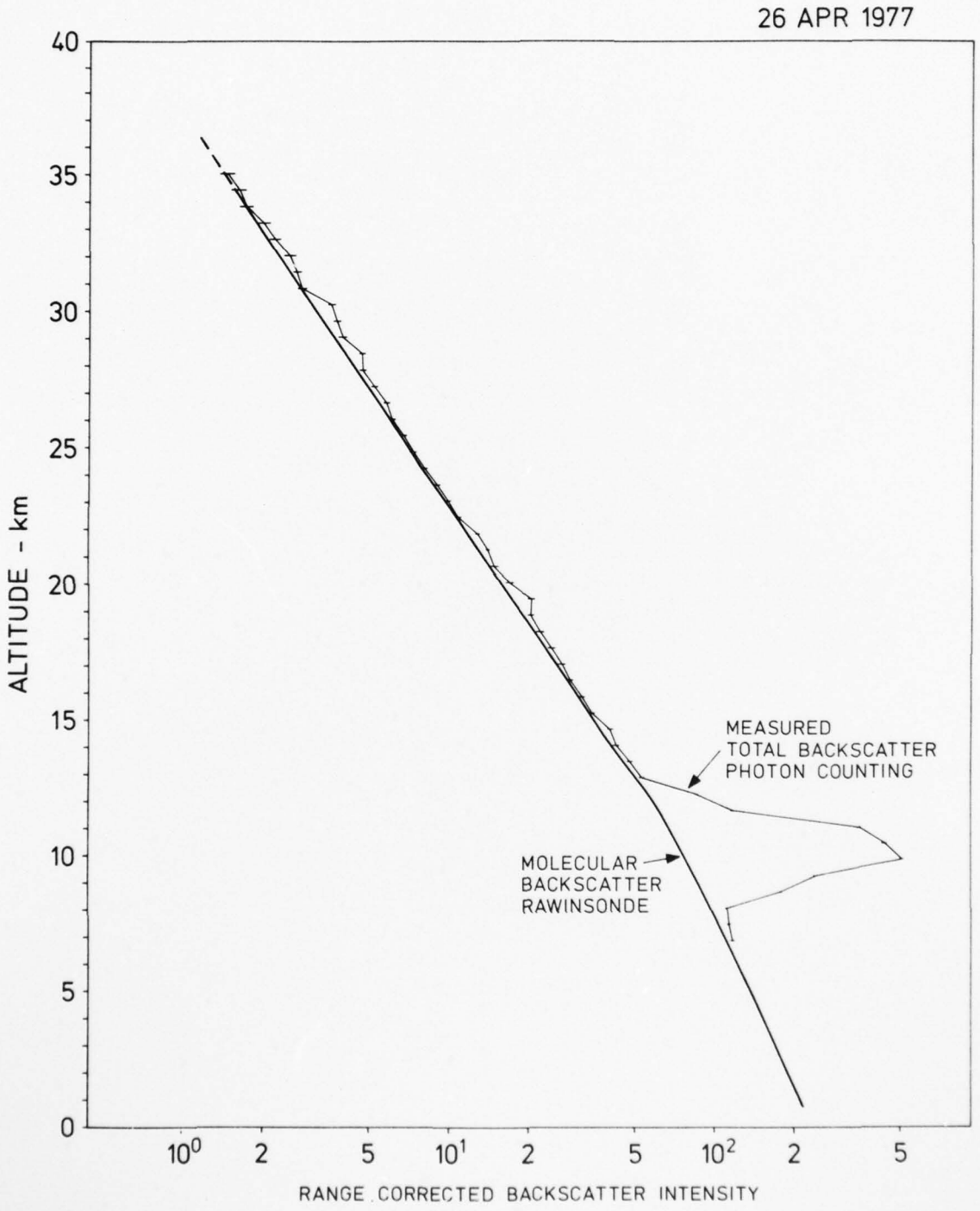

Fig.IV.19

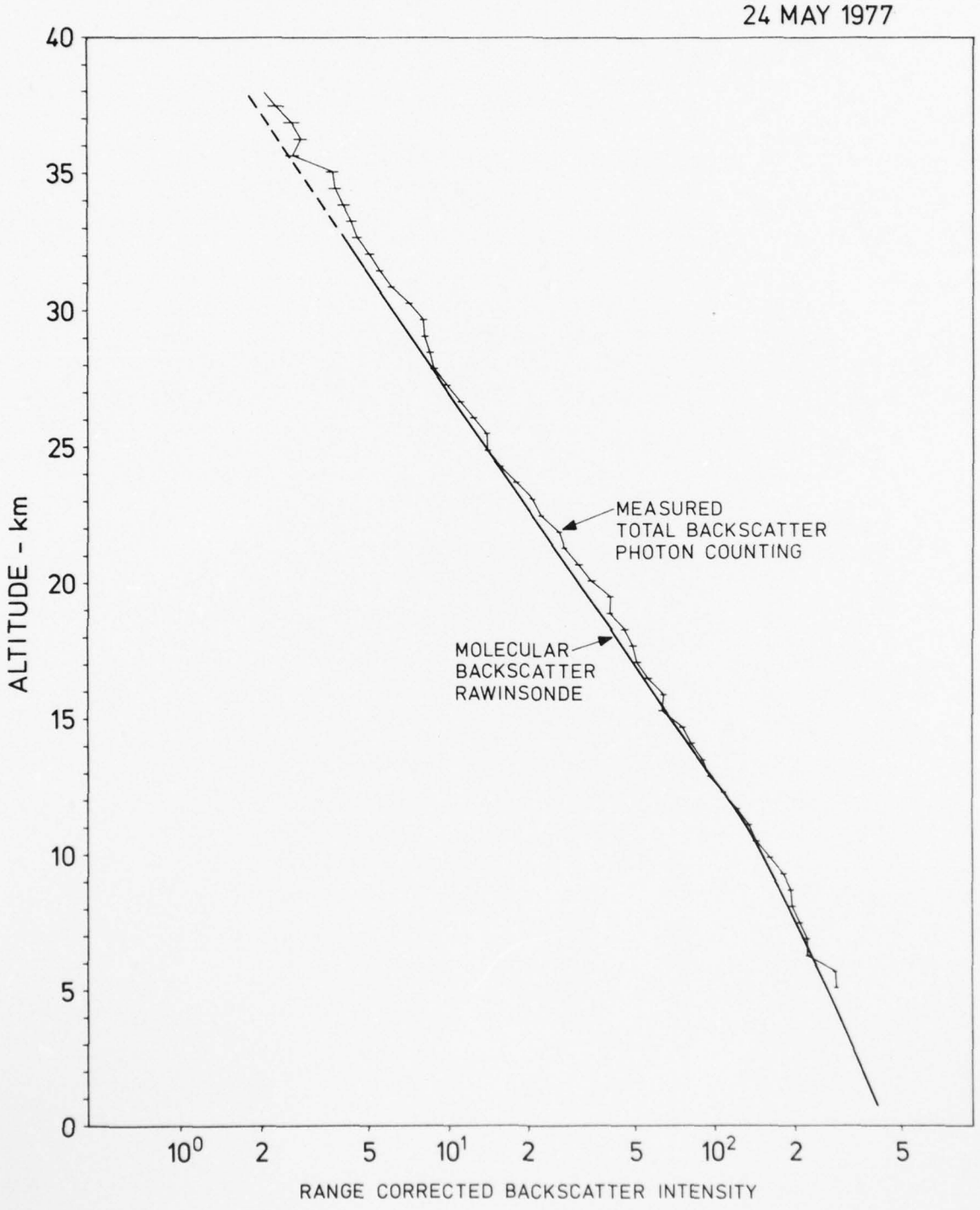
LIDAR BACKSCATTER PROFILE AND COMPUTED MOLECULAR RETURN
24 MAY 1977
ALTITUDE - km
40
35
30
25
20
15
10
5
0
MEASURED
TOTAL BACKSCATTER
PHOTON COUNTING
MOLECULAR
BACKSCATTER
RAWINSONDE
10^0
2
5
10^1
2
5
10^2
2
5
RANGE CORRECTED BACKSCATTER INTENSITY

Fig.IV.20

LIDAR BACKSCATTER PROFILE AND COMPUTED MOLECULAR RETURN

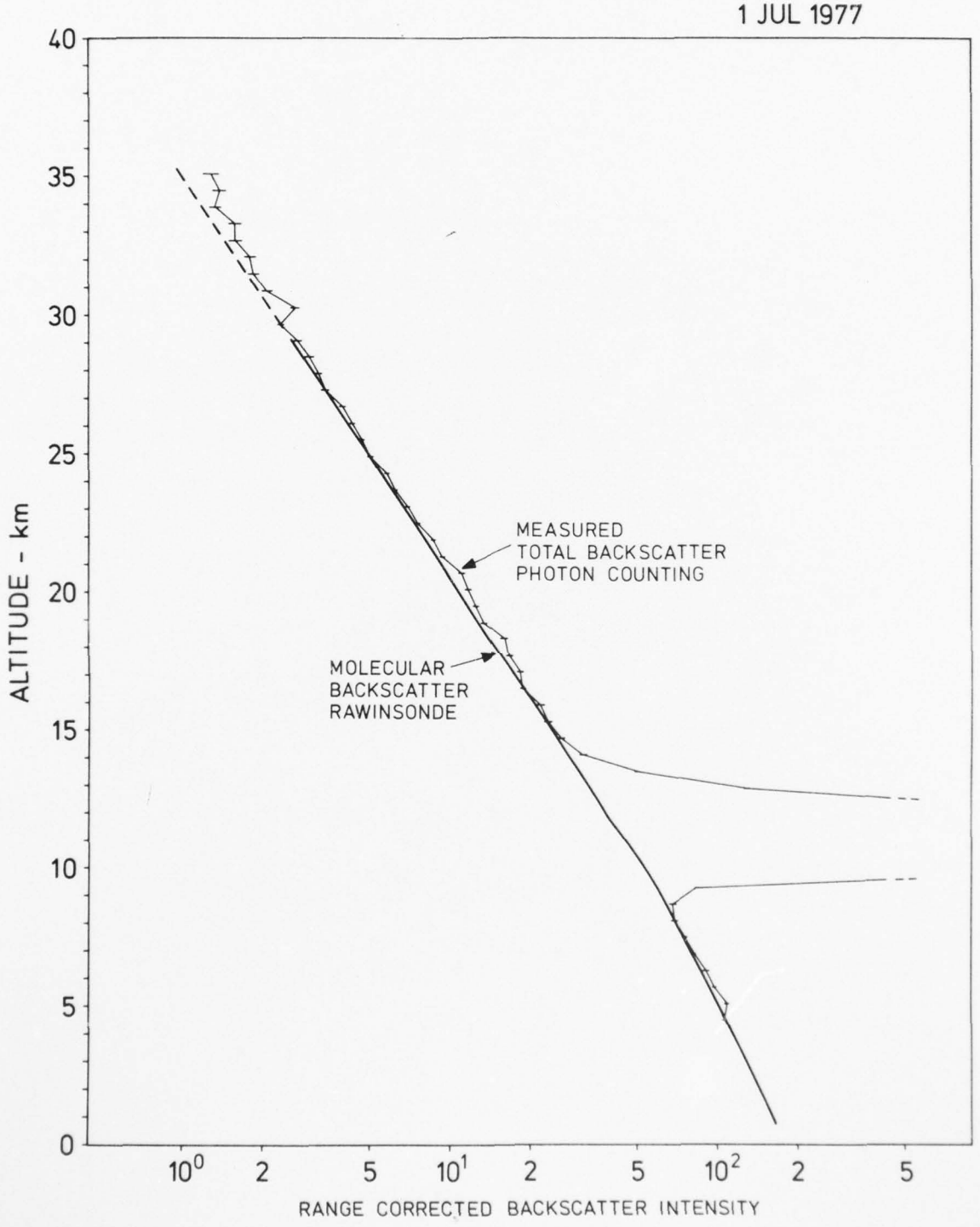

Fig.IV.21

RATIO OF MEASURED TOTAL BACKSCATTER TO CALCULATED RAYLEIGH BACKSCATTER